A Body with Active Aerodynamics for a D-I-S Race Car

AALBORG UNIVERSITY
STUDENT REPORT

A Body with Active Aerodynamics for a D-I-S Race Car

Damian Cieplak
Electro-Mechanical System Design
Aalborg University

May 2023

AALBORG UNIVERSITY
STUDENT REPORT

Department of Materials and Production
Machine and Production
Fibigerstræde 14
9220 Aalborg Ø
https://www.mp.aau.dk/

Title:

A Body with Active Aerodynamics for a D-I-S Race Car

Project:

Master Thesis

Project period:

February 2023 - June 2023

Project group:

EMSD 4 - group 6

Participants:

Damian Cieplak

Supervisor:

Henrik Sørensen

D-I-S contact person:

Jan Ørnhøj Jørgensen

Number of pages: 60
Number of pages in appendix: 7
Finished 31.05.2023

Synopsis:

This thesis regards the design and evaluation of a vehicle body with active aerodynamics for a DIS1 racecar. The key focus of the design is the active rear wing of the car, for which support brackets and actuation mechanism are designed. The car body deign is based on the premise that it should exhibit minimal drag and airflow disruptions. The rear wing is designed so it can generate sufficient downforce for the car to handle a corner as quickly as specified. As a part of the wing design, simulations for NACA 4412 airfoil based wing are performed to attain relations between aerodynamic coefficients and angle of attack. A 'Scorpion Tail' wing bracket is invented for the purpose of supporting the wing, as this bracket type exhibits desirable criteria to be incorporated in the design. The actuation of the rear wing consists of a servo-motor, flexible shaft and a worm drive. A simple control scheme is developed, presenting how the active aerodynamics should be controlled. When benchmarking, optimistic results are obtained suggesting that achieving the goals set for the car by DIS is plausible. Some simulations exhibit a negative drag acting on the rear wing, whose root cause remains unidentified. The objective of the project is considered to be realized, as the design and evaluation of the car body with active aerodynamics is deemed complete within the project scope.

Preface

This thesis has been written using LaTeX. Sources are referred to with the usage of the Harvard Method.

Damian Cieplak

Summary

This thesis regards the design of a vehicle body with active aerodynamics for a DIS1 racecar, as well as the evaluation of the design. The key focus of the design is the active rear wing of the car, for which support brackets and actuation mechanism are designed. The motivation behind this is incorporation of electro-mechanical system design in the development of aerodynamic components, as well as demonstrating multidisciplinary expertise. The project is done in collaboration with D-I-S, which provided with a car model and data used for the design and evaluation in question of the project.

Since aerodynamics have a meaningful impact on a vehicle's performance, as well as oftentimes downforce needs to be compromised if low drag is desired and vice-versa; active aerodynamics should yield a solution where a vehicle's performance is substantially improved with minimal compromises. Each design phase of the design consists of applicable simulations and/or calculations to ensure that the designed component is capable of delivering the expected performance. The design starts with developing the car body based on the premise that it should exhibit minimal drag and airflow disruptions, effectively having negligible effects on later incorporated active aerodynamic elements on it. The car body underwent two iterations, as the iterative process stopped when a satisfactory result was obtained. Thereafter, the rear wing is designed so it can generate sufficient downforce for the car to handle at least as much lateral acceleration as the current Nurburgring lap-record holder likely did at its peak during the record breaking lap, which is presumed to occur at the compression part of the 'Foxhole' corner at the track. As a part of the wing design, simulations for NACA 4412 airfoil based wing are performed to attain relations between lift and drag coefficients and angle of attack. The obtained aerodynamic coefficients differ from the ones used to initially determine the wing size, which leads a reiteration of the wing design. A 'Scorpion Tail' wing bracket is invented for the purpose of supporting the wing, as this bracket type exhibits desirable criteria to be incorporated in the design. It was chosen to be implemented after numerous structural and aerodynamic simulations, that compared it to two other wing bracket types; swan neck and reverse swan neck brackets. The actuation of the rear wing consists of a servo-motor, flexible shaft and a worm drive, which set in motion the shaft mechanically coupled with the wing. This solution is considered superior to conventional wing actuation techniques for this application, as this is a compact and light solution, that is able to adjust to the designed geometry. A simple control scheme is developed, presenting how the active aerodynamics should be controlled. The scheme uses steering wheel angle and vehicle velocity as inputs; suspension compression to determine the error to be corrected; and servo motor position as the output.

When benchmarking, optimistic results are obtained suggesting that achieving the goals set for the car by DIS is plausible. Some simulations exhibit a negative drag acting on the rear wing, it is concluded that it is probably related to the downwards curvature at the rear of the car, yet the root cause remains unidentified, which is presumed to be related to the simulation settings. In the end, the overall objective of the project is considered to be realized, as the design and evaluation of the car body with active aerodynamics is deemed complete within the specified project scope.

Nomenclature

α_{turn}	Turn banking angle
η_{mag}	Downforce magnification coefficient
η_{wing_r}	Rear wing downforce bias coefficient
μ	Friction coefficient
ρ	Air density
ρ_{fluid}	Fluid density
σ_y	Yield strength
τ_w	Wall shear stress
θ	Angle of attack
A_b	Body surface area
A_{car}	Car reference area
A_{fcar}	Car frontal area
A_{ref}	Reference area
A_{wing}	Wing reference area
C_D	Drag coefficient
$C_{l_{car}}$	Car lift coefficient
$C_{l_{wing}}$	Wing lift coefficient
C_{lcar}	Car lift coefficient
C_{lwing}	Wing lift coefficient
C_L	Lift coefficient
C_M	Pitching moment coefficient
C_{rr}	Rolling resistance coefficient
$d_{NormalStress}$	Shaft diameter based on normal stress theory
d_{range}	Range distance
$d_{ShearStress}$	Shaft diameter based on normal shear theory
E_{tot}	Total energy capacity

$F_{D_{add}}$	Drag force acting on active aerodynamic components
F_D	Drag force
F_{grip}	Lateral grip force
F_{grip}	Lateral grip force
F_L	Lift force
F_{res}	Resistive force
F_{rr}	Rolling resistance
F_{w_h}	Force acting from the wing on the shaft
g	Gravitational acceleration
G_c	Other lateral acceleration contributions
G_{flat}	Car lateral acceleration on a flat surface
G_l	Lateral acceleration
L_c	Cord length
L_{shaft}	Shaft length
m	Mass
M_b	Bending moment
m_{car}	Car mass
M_{pitch}	Pitching moment
N	Normal force
n_s	Safety factor
P	Pressure stress
P_{cont}	Continuous power
R_b	Bearing reaction force
r_{ground}	Ground sag radius
r_{turn}	Turn radius
S_{wing}	Wingspan
T_s	Axial torque
v	Object's velocity
v_{max}	Maximum velocity
v_{req}	required velocity
v_{turn}	Turn velocity
z	Distance from the left side of the shaft

Table of Contents

Chapter 1
Introduction

This thesis is made in collaboration with D-I-S, as part of development of their race car. This implies that D-I-S supplied necessary car data and resources needed to complete this project.

1.1 Historical Overview of Automotive Aerodynamics and State of The Art

In order to get a grasp of the premise of this project, the importance of and state of the art of aerodynamics should be presented.

Aerodynamics of a car have a major impact on many of its characteristics, particularly affecting its energy usage, handling, stability, cooling and speed. Two notable aerodynamic attributes are drag and downforce. Drag is the force acting against movement of the body as a result of it moving through a fluid, it is proportional to the body's shape, size and velocity squared. Due to that aerodynamic drag tends to be the dominant resisting force against car's motion when moving at higher velocities. Consequently, drag is the main culprit behind why vehicles possessing certain amount of power reach a certain top speed and highway mileage. Therefore, decreasing drag correlates with higher achievable top speeds and increased range of a vehicle.

As of the downforce, it is a force acting downwards on a vehicle, due to deflection of the fluid through which the body of interest is moving. This force aids in increasing traction of a car, since this causes additional force to be put upon car's tyres. This additional force put on the tyres enhances their grip, thus allowing a vehicle to corner faster.

Optimizing the aerodynamic design for energy usage and speed, as well as for handling has very prominent visual implications; whereas for the former the car's body will end up being very smooth and streamlined to minimize drag; and for the latter case it will most likely be equipped with numerous spoilers and wings to maximize downforce. Oftentimes maximizing downforce correlates with increase in drag, thus a streamlined body tends not to yield a terrific downforce production. Based on this, it can therefore be implied that often designing a vehicle body causing low drag is likely to trade-off the amount of downforce produced by that body, and vice versa. As a result of this, in most applications a vehicle's body tends to be designed so it reaches a compromise between the two traits from an aerodynamic point of view. Clearly, it should be mentioned that a vehicle body's design is inclined to take into account other traits, such as aesthetics or ergonomics.

Looking back, when it comes to land vehicles drag was the primary concern aerodynamically speaking. Streamlining vehicles was somewhat fashionable already in 19th century, finding its application in train design. An 'air resisting train' has been patented as soon as 1865. As of cars, drag reduction became a prominent feature in cars chasing the land speed record at the end of eighteen hundreds, aiding in breaking the 100 km/h automobile speed record by La Jamais Contente in 1899, which as most land speed record cars of the time, was an electric vehicle. It was not until 1920s that a passenger car's drag reduction had a positive influence, particularly by Rumpler's Tropfenwagen (depicted in Subfigure 1.1a), which then influenced a number of race cars in the proceeding years, thus being a start of an era of teardrop-like shape design in the automotive industry, which was motivated by increasing stretches of highways allowing cars to move at higher velocities for longer distances. It should be noted that the shape of cars of each era is also highly influenced by the aesthetic trends, manufacturing methods and other practical aspects of a vehicle of the time; leading to cars not necessarily improving aerodynamics-wise as the years went on. (1) (2)

It was not until 1957, when G.E. Lind-Walker facilitated the understanding of downforce, especially with regards to race cars. First instances of aerodynamic features to intentionally generate downforce could be observed in 1960s on Chaparral racers, giving them remarkable advantage. These cars featured front and rear spoilers, which a few years later, in 1966 led to employment of a rear wing on Chaparral 2E, that is visible in Subfigure 1.1c. (3) This led to development of front and rear wings on Formula 1 cars in 1968 (4), and also significantly influenced NASCAR racers observed by the sudden appearance of spoilers on most of them. The impact of trends in motorsport became noticeable on sports cars of the coming years, as new sport vehicles started employing spoilers. At this point it has been observed that even though the straight line speeds of some racers decreased as a cost of increased drag due to downforce generation, the trade-off paid off as lap times got faster due to increased cornering speed. At some point wings were considered to be banned, as a result of mechanical failures of their support. The next leap in car aerodynamics came in 1970s, where the ground effect was utilized, which is based on the downforce generation by creating low pressure under the car, effectively 'sucking' it to the ground. This has been achieved in a number of ways, for instance by making the gap between the underside of the car and the ground small; by implementing 'side-skirts', which restrict the air from the underside of the car escaping through the side gaps; or by using motorized fans to suck the car to the ground, as it has first been implemented in Chaparral 2J, featured in Subfigure 1.1d. (5) Another important upswing in aerodynamic development came in form of rear 'diffusers', whose first resemblance could be observed in the underfloor of Lotus 78 Formula 1 racer (visible in Subfigure 1.1b), (6) and that in the next decade started becoming an aerodynamic staple in motorsport. (7)

Yet another pivotal innovation is active aerodynamics, which in principle is controlling an aerodynamic feature according to desired outcome. An instance of this is changing the position of a wing so it generates more downforce when cornering, and then changing it so the drag is minimized on the straights. The first documented resemblance of that idea could be observed in Mercedes Benz T80 in 1939, a concept car meant to break the land speed record, which had movable aerodynamic elements and whose completion did not fulfill, thus resulting in it never hitting the road. (8) In 1952 an instance of active aerodynamic braking could be observed on Mercedes 300SL Prototipo, with manually employable wing, thus leading to increased drag and downforce, aiding in slowing the car down when braking. The first documented case of active aerodynamics being used in motorsport was by Michael May, an enthusiast who implemented a movable wing on his Porsche 550 Spyder racecar, which is depicted in Subfigure 1.1e. After a practice for a race at Nurburgring in 1956, Porsche forced the organizers to revoke May's car entry, which likely was due to the thread posed by the car to Porsche factory team, as during the practice the car's lap times were outstanding. (9) The previously mentioned Chaparral 2C featured a movable tailgate (essentially moving the rear spoiler), operated by a dedicated pedal, being the first car with active aerodynamics to compete in motorsport. The first instance of automatically controlled active aerodynamics was done by Porsche in the 908 25 series. In this instance, the car was equipped with movable flaps on the rear of the car linked to its rear suspension, where a flap would lift when the suspension would experience decompression due to body roll or pitch, thus counteracting that action by producing downforce and drag. Active aerodynamics have been banned in many motorsport series, due to safety hazards related to their failures, leading to unpredictable or reduced grip, as well as instability of the car, consequently being a potential cause of accidents. However, this technology found its purpose in production vehicles. The 1986 Lancia Thema (seen in Subfigure 1.1f) was the first production car to feature a retractable spoiler that would employ at a certain speed or manually to reduce the lift (by increasing downforce) of the rear of the car, thus making it more stable at high speeds. (10) Mclaren F1, a speed record breaker from 1990s, who's record persist to this day for a naturally aspirated production car; featured a much more sophisticated active aerodynamics apparatus. In this case, there were a rear wing and front splitter, whose angle was adjusted so the car stayed balanced under braking. What is more, the aforementioned fan suction downforce generation under the car resembling he one in Chaparral 2J was utilized; whereas here it was a manually activated mode that enabled enhanced downforce upon user's desire. (11) Another speed record breaker, particularly popular in 2000s, Bugatti Veyron, featured controllable rear wing and spoiler, flaps for the front diffuser, along with adjustable ride height and angle; which were controlled according to the car's velocity and mode. (12) (13)

(a) Rumpler's Tropfenwagen (1)

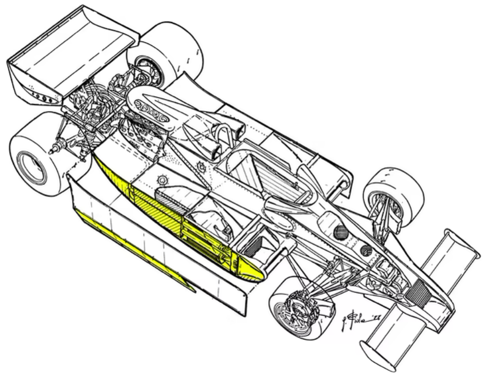

(b) Lotus 78 (6)

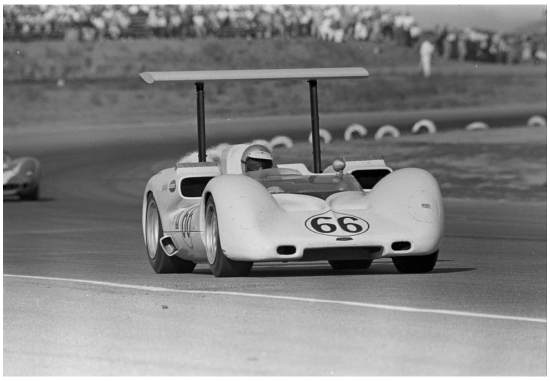

(c) Chaparral 2E (5)

(d) Chaparral 2J (5)

(e) Michael May's Porsche 550 Spyder (9)

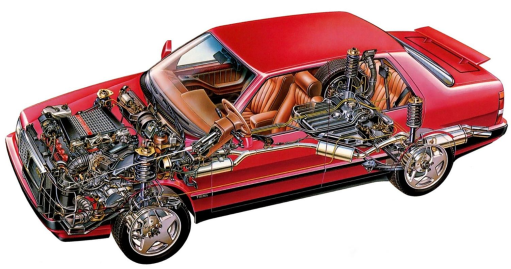

(f) Lancia Thema(10)

Figure 1.1. Depictions of exemplary aerodynamic breakthrough cars throughout the history.

Regarding the recent state of the automotive aerodynamic technology, most of it are improvements upon the aforementioned technologies. Production cars nowadays incorporate deployable spoilers and wings, many of whom also adjust their angle according to the mode or desired outcome, whereas their control is more sophisticated and adjustable than before. Additionally, active aerodynamics are being applied to more elements and in new ways, an example of that is an active rear diffuser. (14) Another innovative instance of that can be observed in Bugatti's active dimple airscoop (visible in Subfigure 1.2a), which has gradually bulging out dimples on its top, which aid the in making the airflow attached to the car's body, thus reducing drag and directing more air towards the rear wing of the car, therefore also increasing downforce with minimal compromises. (15) Due to improvements in Computational Fluid Dynamics (CFD) and computational power, the aerodynamics of cars can be optimized in much more detail, therefore leading to car shapes ending up being more optimized than before. In motorsport, vehicles use plenty of features, such as vortex generators to direct the air, so it produces the desired result. Moreover, in recent years some supercar manufacturers started incorporating unique technologies to achieve improved cornering characteristics, by generating different amounts of downforce on one side of the car than the other. Examples of that are: Zenvo's tilting rear wing (Subfigure 1.2b);(16) or Lamborghini's Aerodinamica Lamborghini Attiva (ALA), which features flaps that open or close to redirect the air through vents placed on both sides of the car, in a way that either maximizes downforce or minimizes drag; as each vent has its corresponding flap, they can be controlled independently, achieving aerovectoring, that is different drag and downforce characteristics between the sides of the car. (17) (18)

(a) Active rooftop dimples by Bugatti (15)

(b) Tiltable wing by Zenvo (16)

Figure 1.2. Images of exemplary state of the art active aerodynamics solutions.

1.2 D-I-S Racecar

The premise of this thesis is designing a body for a DIS1 racecar, whose initial design can be seen on Figure 1.3, along with aerodynamic features that would bring it closer to achieving its goals. The body is intended to be designed in a way that would optimize drag and downforce characteristics according to the desired outcome; that is minimal drag when moving at constant or increasing speed on straights, necessary amount of downforce to provide the car with necessary grip for the desired cornering, maximal drag and balance assistance when breaking. This is meant to be achieved with the usage of existing technology (Mentioned in Section 1.1) and perhaps with new innovations invented when working on this project. Therefore, it has been decided that implementation of active aerodynamics would be an advisable idea, which would also appropriate and relatable to the study of Electro-Mechanical System Design.

Even though DIS/CREADIS is an engineering consulting firm, it has an internal project where a racecar is being developed. The main goal of the car is being a demonstration of engineering innovation that D-I-S is capable of. Despite the fact that the car is mainly built for the racetrack, it is also desired for it to be road legal. The car is designed to be propelled by four electrical motors, each driving its corresponding wheel. The energy for these motors is stored in the batteries present on the car, as well as it can be provided from a combustion engine driving a generator providing the energy to the batteries. It has been decided to implement this hybrid arrangement in order to save the weight of the vehicle and allowing for a greater range. The car is not aimed to compete in any motorsport competitions, therefore it is not bound to follow any specific regulations. However, the car is targeted to do time trials on racetracks. Additionally, it is intended to appear at Sportscar Event, which allocates its profits to benevolent causes, such as Børnecancerfonden (Danish children cancer fund); at the event guests can take a look at cars and be driven around as passengers around a racetrack.

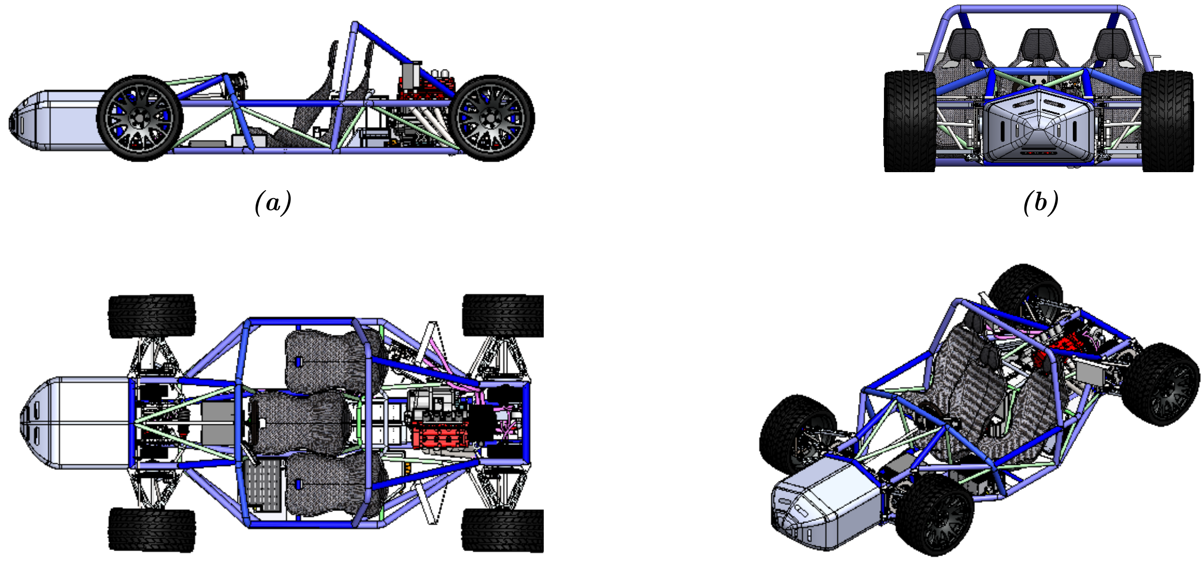

(a) *(b)* *(c)* *(d)*

Figure 1.3. Depictions of the initial DIS1 car design, seen from the right side, front, top and isometric view.

The car's chassis and its components are already designed, as well as manufactured to a certain extent. The body design is supposed to integrate with what has been done hitherto; however, some of what has been outlined thus far may be due to change. It should be noted that the car is still in its developing stage, and the design made for this project is likely to be due to change, as the underlying structure for which it is designed is probable to be altered as well.

Chapter 2
Problem Description

2.1 Focus, Motivation, Delimitation and Requirements

As stated previously the goal of this project is designing a body with active aerodynamics for the DIS1 racecar, so the car achieves as close to optimum performance as possible. Based on that, it should be stressed that the focus is on the holistic design and the process itself, rather than attempting to optimize a particular part of the design or particular process within the design procedure. Therefore, processes such as modeling and simulation are not going to be attempted to be done with supreme accuracy, instead these processes should be attempted to be as accurate as necessary without major sacrifices in time and resource consumption. Clearly, the optimization of the design will occur; however, this will be done in an iterative process until a satisfactory result is obtained. As stated earlier, the remaining design of the car has already been finalized for its first iteration (which this project is also supposed to be focused on), yet minor changes can be done, especially if they are likely to enhance the performance of the body of the car and the car overall. Nonetheless, the intent is to design a body for the car as it has been designated for this project, apply minor changes only if doing so manifests an evident advantage; otherwise, changes should be suggested after the body would be designed. Therefore, the body has to be designed so it can be integrated and perform well with the existing design. As the aerodynamic performance is the main objective of the body's design, cooling and other secondary effects related to the airflow will not be addressed in detail. Cooling-wise, it is assumed that as long as the lateral radiators on the car receive direct airflow, the airflow should be satisfactory. Brake cooling will also be considered to be outside of the project scope. The active aerodynamic components to be designed are front wing and the rear wing, where the rear wing design being the predominant focus. Resultantly, components supporting the rear wing, as well as its actuation mechanism should be developed. Additionally, the overall performance of the design should be evaluated and a basic control scheme should be developed.

Accordingly, the main project focus is as follows:

To design and evaluate a body for a DIS1 racecar, featuring active aerodynamic components, with the rear wing being the uttermost central component of focus.

The motivation behind this is the incorporation of electro-mechanical system design into aerodynamic design, which will be done by implementation of actuated elements in form of active aerodynamics. This will also serve as a proof of mulitdisciplinarity the project, as it will be a combination of the fields of mechanical, electronic, industrial and graphical design.

It should be noted that many of the goals for the DIS racecar provided by DIS, which are available in Appendix A, are independent of the work done in this project and some of the susceptible aspects may not be directly affectable. The susceptible goals are:

- Be build on innovative solutions
- Accelerate 0-100 in less than 2,0 sec
- Accelerate and decelerate 0-200-0 in 10 seconds or less
- Range of 50 km on the racetrack
- Range of 400 km for road use

- Focus on performance rather than comfort
- Be the fastest car ever on the TopGear test track
- Be the fastest car around the Nürburgring – Nordschleife
- Be able to achieve the above mentioned on road legal tires

Still, these goals are highly dependent on the existing design, and the design that is the premise of this project has only partial influence on the realization of these goals. The realization of these goals can be questionable, nevertheless, it is targeted to approach their attainment as close as feasible. Additionally, there are also desires for the car to be functional in its usage, for instance being able to see what is behind the car from inside the car, which can be attained by incorporating mirrors. Also, the car is preferred to be road legal and be aesthetic to a certain extent. Despite these desires, they will not be prioritized in exchange for the engineering and innovative goals of the vehicle. Moreover, as the car is not targeted to compete in any specific competition, it is not intended to fulfill any specific regulations; yet, the car is deigned with safety in mind and some parts of its design follow some regulations, which is done in order to meet certain standards, an example of that is the crumble zone at the front of the car.

2.2 Details About The Car

The car in question is a series hybrid; it features an engine that is there solely to generate power for the battery pack, whose power is used by the electric motors. The engine in use is a Hayabusa gasoline engine, with 300 HP and featuring a 20 L tank. It is coupled with two EMRAX 268 generators charging a battery pack, whose total available energy capacity is 18.3 kWh. The wheels are powered with two EMRAX 228 and EMRAX 268 motors, in front and rear respectively, offering a total continuous power of 384 kW and total peak power of 668 kW. (19) (20)

The car without a body is expected to weight approximately 700 kg including the driver, with an even weight distribution between the front and the rear. The ground clearance of the vehicle is 77 mm without any rake angle present, which can be observed along with the rest of the dimensions on Figure 2.1. The tyres present on the DIS1 racecar, are identical to the ones used in Dodge Viper ACR; 295/25R19 in the front and 355/30R19 in the rear, for whom friction and rolling resistance coefficients are not widely available. Due to fact that these are high performance tyres and the car is mainly designed to drive on dry asphalt, the aforementioned coefficients can be assumed based on these facts, thus yielding friction and rolling resistance coefficient values as 1.3 and 0.013 respectively. (21)

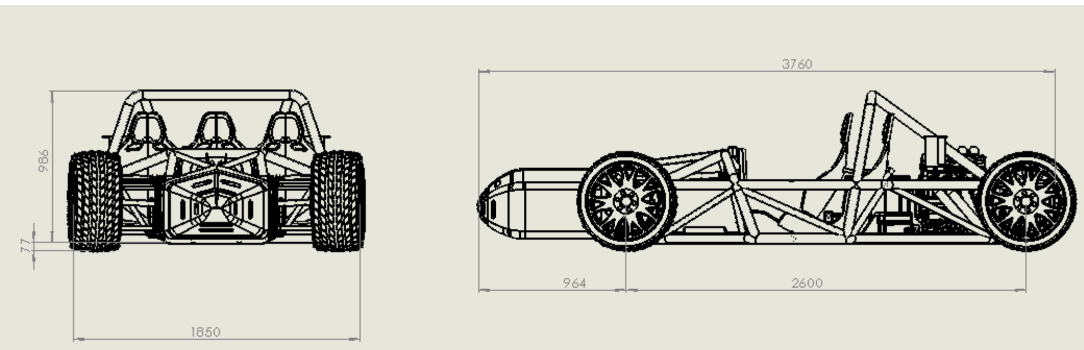

Figure 2.1. Blueprints of the DIS1 car in its initial state, showing its basic dimensions

Using the aforementioned information, more useful data can be extrapolated from it. To begin with it is the case for total energy capacity of the vehicle. Knowing that the fuel tank can contain 20 L of gasoline, and that its energy density is 8.43 kWh/L, (22) as well as assuming that the efficiency of the combustion engine and the generator are 25 % (23) and 95 % (20); it can be inferred that there is additionally 40 kWh of energy available to charge the battery pack, thus potentially yielding the total energy capacity of the car to be 58.3 kWh. The provided and extrapolated data from this section are summarized in Table 2.1.

Car weight (including driver)	700 kg
Weight distribution (front/rear)	50/50
Battery total energy capacity	18.3 kWh
Car total energy capacity	58.3 kWh
Total peak power	668kW
Total continuous power	384kW
Tyre friction coefficient	1.3
Tyre rolling resistance coefficient	0.013

Table 2.1. A table summarizing car data provided by DIS and extrapolated based on that information

2.3 Theoretical Framework

As there is a relative motion between a body and the fluid it is embraced within, there are forces acting between these entities. These forces are called aerodynamic forces, and can be separated into drag and lift force; where drag acts against the direction of the moving object; while lift acts in a direction perpendicular to drag and pointing away from the ground, whereas downforce is essentially the same force acting in the opposite direction. The aerodynamic forces are a result of pressure stresses and sheer stresses acting on the object in question, which is described by Equation 2.1 and 2.2 for drag F_D and lift F_L respectively. Figure 2.2 may assist in visualizing the descriptions in this paragraph related to these equations. Pressure stress P, which is acting in a perpendicular direction to the surface of the body A_b, is due to pressure distribution around the object. That is to say, pressure difference between one side of the object and the other, will cause a net force in the pressure negative gradient direction; in essence, a higher pressure at the front of the object and lower at the rear will cause drag, as there is net force from higher pressure area in the front to the lower pressure area in the back. These pressure differences occur in a number of ways, where most are related either to flow separation or difference in fluid velocity over the body's surface. As a mean of understanding the flow separation, it is of substance to understand the boundary layer behaviour. The boundary layer as the name may suggest is an intermediate layer of fluid flowing along the body with varying velocity, where the velocity is zero at the surface due to no-slip wall conditions and approaches the velocity of the bulk flow the further it is from the surface. Sufficiently strong curvature of the surface causing a relative negative pressure, is likely to cause flow separation, due to the bulk flow being further away from the surface and lowered pressure making the velocity of the flow close to the surface to reverse direction to fill the 'void', thus resulting in swirls. This is one the main contributors to drag in cars, as the rear of most cars has an abrupt change in surface curvature, causing flow separation, thus a very prominent low pressure region behind the car. If decreasing the change in curvature is not viable, another way to prevent this is turning the fluid flow along the surface from being laminar to being turbulent, as a turbulent boundary layer is more apt to follow the curvature of a surface. This can be done using vortex generators, often implemented on airplane wings or in Formula 1 cars; or by having dimples on the surface right before the strong curvature occurs, that is the reason why golf balls have dimples, as well as why it was implemented in one of the aforementioned aerodynamic solutions by Bugatti. As of the pressure distribution related to fluid velocity over the surface, due to Bernouli's principle the faster a fluid moves in a confined zone the lower pressure it is going to yield. This is one of the main rationales behind why airplane wings create lift, as the air on the top surface of the wing has to travel further than on the bottom surface and the flow that separates in front of the wing seeks to rejoin at its rear, the flow on the top side travels faster than the one on the bottom, thus causing lower pressure at the top and higher at the bottom, resulting in lift. A racecar wing works analogously, as to put it simply it is similar to an overturned airplane wing, thereby creating downforce instead. Another instance of that can be observed in cars using ground effect, as mentioned in 1.1; due to the same principle, since automotive underfloor devices aim to limit the cross sectional area under the vehicle, it causes the air to accelerate in that region, thus due to increased air velocity under the vehicle, a substantial downforce generation can be obtained. Diffusers further exploit that to create an even larger pressure drop under the rear of the vehicle.

$$F_D = \int_{A_b} (-P \cdot cos(\theta) + \tau_w \cdot sin(\theta))dA_b \tag{2.1}$$

$$F_L = \int_{A_b} (-P \cdot sin(\theta) - \tau_w \cdot cos(\theta))dA_b \tag{2.2}$$

Regarding the wall shear stresses τ_w, they are caused by frictional forces acting tangentially to the surface of the body as the fluid moves along that surface. Therefore, the larger and the rougher the area being perpendicular to the direction of the movement of the object, the larger the wall shear stresses and drag associated with them. Due to that, dealing with lift it can be said that shear stresses can be neglected for its generation, as a fluid seldom moves along the surface of an object for sufficiently long in the direction that is perpendicular to the object's movement, without also moving in the opposite direction. Based on the above, it can be concluded that a streamline body, such as a wing despite experiencing little drag due to pressure stresses, it is likely to attribute a significant part of the drag to the wall shear stresses and virtually all of its lift due to the pressure stresses. The angle of attack θ, meaning the angle between the chord line of a body and the incoming fluid, where the chord line is an imaginary line from the leading to the trailing edge of the body; can be adjusted to obtain certain characteristics. This is essentially what is done when changing the angle of an aeroplane wing flap (as it changes the chord line angle, due to change in trailing edge position) or a sportscar rear wing angle. Often the increase in lift due to increase of angle of attack may result in increased drag; however, during stall, which happens when a certain angle of attack is exceeded, the lift generated is decreasing with the increase in angle, yet the drag may not correlate as previously with the lift, thus it may keep on increasing up to a certain angle that is different than the stall angle.

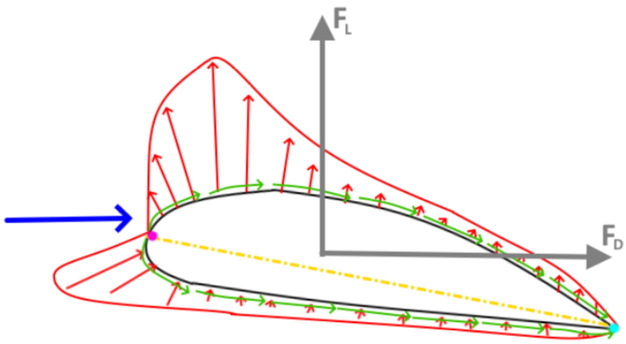

Figure 2.2. An illustration aiding in the understanding of equations 2.1 and 2.2; where pressure stress distribution is shown in red, wall shear stress in green, fluid flow direction in blue, chord line in orange, leading edge in pink and trailing edge in cyan. Pressure arrows pointing towards the surface represent higher pressure, while pointing away from the surface represent lower pressure.

Due to the fact that pressure stresses P and wall shear stresses τ_w are usually unknown and the whole surface area of the body can be difficult to determine, a different set of equations, outlined by Equation 2.3 and 2.4 is applied in practice to determine drag and lift forces respectively. These equations concern a body who's relative velocity v to the fluid makes it so the fluid particles move from the front to the back of the body; stated differently, the body would have higher pressure at the front than the back, which in air it would manifest itself as the body experiencing headwind. It can be observed that these equations are identical, with the difference lying in the drag C_D and lift C_L coefficients. These coefficients stem from the fact that they are defined as a ratio between the aerodynamic force (drag or lift); and a product of half object's velocity relative to the fluid v to the power of two, object's reference area A_{ref} and density of the fluid ρ_{fluid}. Thereby, it can be implied that the coefficients are a metric of how well the object's geometry is utilized to produce the aerodynamic force of interest. It should be noted that the reference area is in some measure an arbitrary concept, by convention in automotive design it is referring to the frontal area of the vehicle, while in aeronautics it is referring to the planform (top-down) area of an aeroplane wing.

$$F_D = \frac{1}{2} \cdot \rho_{fluid} \cdot v^2 C_D \cdot A_{ref} \tag{2.3}$$

$$F_L = \frac{1}{2} \cdot \rho_{fluid} \cdot v^2 C_L \cdot A_{ref} \tag{2.4}$$

Another important concept to address is the center of pressure, which can be described as a point on a body where if a singular pressure force would be applied, it would be equivalent to the sum pressure fields acting on that body. This is analogous to the center of mass, which represents the same phenomenon, that is rather regarding the mass distribution than pressure distribution on the body. The center of pressure force tends to act around the center of mass point, thus acting at a moment arm around that point, essentially applying torque on the object. From an automotive design and engineering standpoint it is important that the sideways center of pressure is behind the center of gravity, as if the sideways center of pressure would be in front of center of gravity it would cause the vehicle to be yaw unstable. This is due to the fact that side winds would provoke the car to steer in the same direction as the center of pressure vector, and it would increase in magnitude as the car is increasing in yaw angle. This is attributable to the fact that as the yaw angle increases, the sideways aerodynamic force component of a forward moving object gets amplified as well. Conversely, if the sideways center of pressure is behind the center of gravity, the sideways center of pressure is stabilizing the car, by increasingly applying more force returning the car to straight line motion as the yaw of the car increases. (24) This is shown in Subfigure 2.3a. With respect to longways center of pressure, illustrated in Subfigure 2.3b, it has less adverse effects on the car yaw stability, as it mainly affects the grip distribution between the axles. The further forwards the longitudinal center of pressure is, the more biased the car is to oversteer; and the further backwards it is, the more bias towards understeering. It is of importance to mention that center of pressure may change as a consequence of vehicle's aerodynamics, which can be caused for example by actively changing the angle of a component; or by increasing the rake angle of the vehicle when breaking, thus if ground effect devices be implemented both in the front and rear of the vehicle, it would cause an even stronger downforce and grip at the front axle of the vehicle, thereby changing the pressure center further forwards, biasing the vehicle towards oversteering. Furthermore, center of pressure can act as a simplification tool when modeling for structural analysis of a particular component, which can lead to a simple analytical solution of the problem. For instance a wing can be modeled as a supported beam with center of pressure acting on it as a single force vector, enabling a simple analytical solution to the problem.

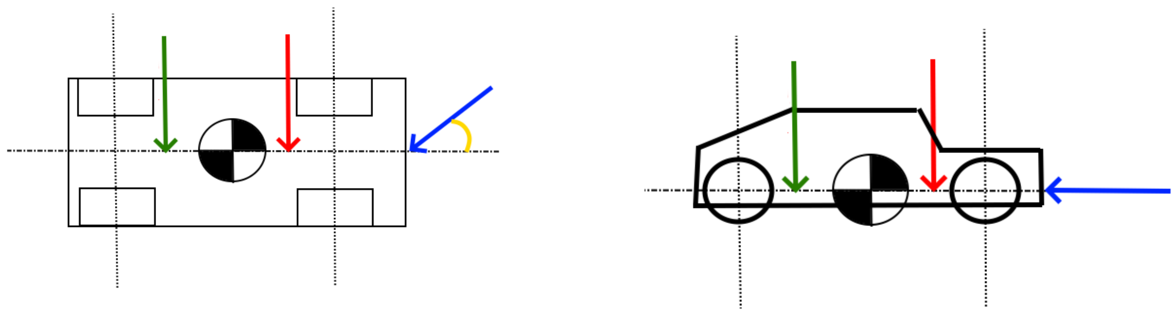

(a) An illustration of sideways center of pressure, where the vehicle is seen from above. Green arrow signifies sideways center of pressure being rearwards relatively to the center of mass of the vehicle, which is characterized as a dowel symbol, while red arrow signifies it being forwards. Blue arrow represents the fluid flow direction and the yaw angle is shown in amber.

(b) An illustration of longways center of pressure, where the vehicle is seen from the side. Green arrow signifies longways center of pressure being rearwards relatively to the center of mass of the vehicle, while red arrow signifies it being forwards and blue arrow represents the fluid flow direction.

Figure 2.3

Moving further, a concept also worth mentioning is pitching moment and its associated coefficient. The pitching moment of an airfoil is a moment or torque as a result of the aerodynamic forces acting on the airfoil as if the airfoil would be pinned at its aerodynamic center. The aerodynamic center is defined as a point on the cord line of an airfoil, where theoretically the pitching moment does not vary significantly with angle of attack; which is considered applicable only for small angles and small variations of the moment. The aerodynamic center of an airfoil tends to be situated at the quarter length away from the leading edge of most sub-sonic airfoils. The pitching moment M_{pitch} of an airfoil can be described with Equation 2.5, which is reminiscent of the simplified equations describing lift and drag forces produced by a body, whilst here a pitching moment coefficient C_M is used as a primary factor stemming from the geometry of the airfoil. Even more, the whole equation is multiplied by the airfoil cord length L_c, due to the fact that it is dealing with a moment, rather than a force; as well as the fact that it addresses the notion that the pitching moment is dependent both on the airfoil reference area

A_f and its cord length, with the pitching moment coefficient adjusting the proportionality of the obtained moment and these dimensions. Another way to state the above can be as follows: the aerodynamic center is a point at which if pinned, the pitching moment, being the total aerodynamic force applied at the center of pressure, would be almost the same as the angle of attack changes. This is due to the fact that as the angle of attack increases (within a certain range), the center of pressure moves closer to the aerodynamic center, while simultaneously the lift force increases proportionally, which is illustrated in Figure 2.4.

$$M_{pitch} = \frac{1}{2} \cdot \rho_{fluid} \cdot v^2 \cdot C_M \cdot A_{ref} \cdot L_c \tag{2.5}$$

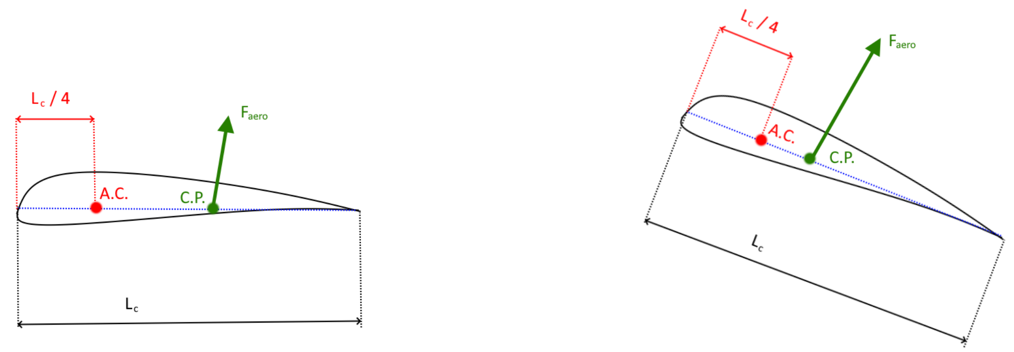

(a) *(b)*

Figure 2.4. Illustrations showing the aerodynamic center $A.C.$ and how it relates to the pitching moment being a product of the aerodynamic force vector F_{aero} applied at the center of pressure $C.P.$ when the angle of attack changes. L_c denotes the chord length, and it can be seen that the aerodynamic center is a quarter length from the leading edge of the airfoil.

Chapter 3
Body Design

As a means to start the design phase of the body and its accessories, it is wise to begin that phase with the component that the rest is strongly dependent on; the car body that is. As all the other aerodynamic components of the car are situated on the car body, they are inherently potently influenced by it, more so than they are influencing the body, primarily in terms of aerodynamics, but also regarding mechanical aspects, such as structural integrity, efficacy and so on. It is of importance to mention, that the body design described in this chapter is not meant to be perceived as the final design for the car's body, but rather an initial step meant to satisfy the criteria demanded from it.

3.1 Premise and Preliminary Design

The main premise of the car body is to create a housing and a shield for the chassis and the driver whilst posing minimal aerodynamic drag. Therefore, from an aerodynamic point of view, it has been decided that the body's main objective is to be as streamlined as possible and minimize the production of lift in the process. It is important to mark that most car body shapes tend to produce lift if they have not had been designed with ground effects in mind or other means to produce downforce, which oftentimes leads to an increase in drag. In the initial stage of the design, the ground effect will not be strongly emphasized, as that is not of particular interest for this project's design and can be further optimized at a later stage without a potent impact on the active part of the car's aerodynamics. It should be kept in mind that, the diffuser is predicted to be implemented on the car eventually, leading to its inclusion on the initial sketches, which can be seen on Figure 3.1. Despite that a sketched diffuser is present in the drawings, it will be excluded from the design, as it falls outside of the scope for this project.At this stage, the ground effect will be designed in a minimalist fashion; the underfloor is meant to pose minimal drag, thus it will be smooth and feature a slight upward curve at its end to grasp a bit of the effects one can get from a diffuser, yet without the increase in drag. The reason why downforce is much less desirable in favor of minimizing drag in the car body design in its initial stage; is due to the fact that active aerodynamics are meant to be the controlling body behind the amount of downforce and drag associated with it produced. Consequently, the body is meant to be streamlined and create as little disturbances for the aerodynamic accessories as possible; effectively acting as a base to which accessories can be added and that can be easily modified for further optimization.

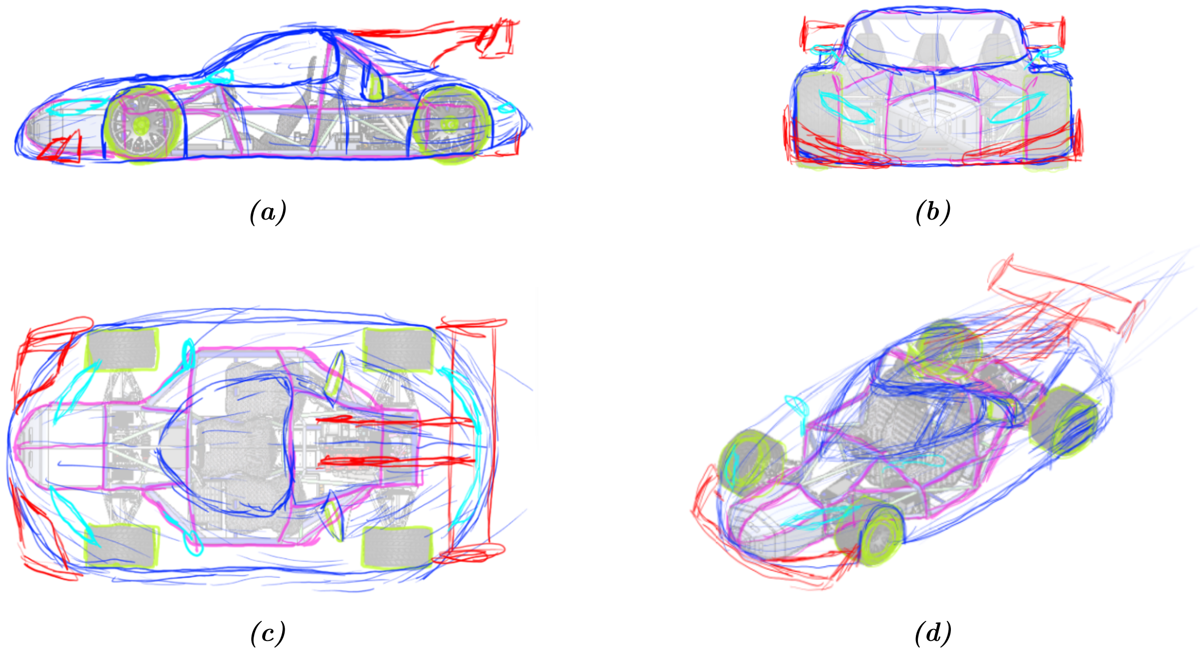
(a) *(b)* *(c)* *(d)*

Figure 3.1. Depictions of initial drawings of DIS1 car body design, seen from the right side, front, top and isometric view. These act as a starting point for the body design process. The original DIS1 car design can be seen with in the background as a somewhat transparent image. The frame has been highlighted in pink, the wheels and radiators in lime, the body in blue, wings and diffusers in red, lights and mirrors in cyan.

Another important aspect of the car body is to supply the radiators with airflow, so they can extract heat from components that require cooling. In this case, as component cooling is outside of the scope of this project, the fact that there would be inlets for the radiators is satisfactory. Optimizing for sufficient airflow to the radiator inlets can always be done at a later stage of the design, as in this case it is not expected that the cooling would be particularly concerning for this vehicle, since hybrid powered vehicles require less cooling power than pure combustion engine vehicles.

From the structural point of view, the body will not be examined in detail. It is presumed that if the structural hazards would be at play, the body could be structurally reinforced by additional components attached to the chassis or thickened in the risky spots. What is more, vehicle's bodies do not tend to be components that are particularly structurally susceptible, as other components, such as the chassis, are meant to carry most of the structural burden of the car. The lights and the mirrors are also omitted from consideration in the initial stage of the design, yet they are included on the initial sketches for the aesthetic reasons.

As the first step of the design initial sketches of the car's body have been drafted, which can be seen on Figure 3.1. The purpose of these sketches is to act as a general guidance on how to design the body, give an idea on how components would be situated on it and present the envisioned aesthetic that the car may potentially obtain. The part of the sketch that holds the most merit is the one drafted in blue, as this is the representation of the car body shape, which is the main concern at the initial stage of the design. What is worth noting is that the windshield depiction is there only to aid in visualizing the car and does not serve any other functional purpose for the initial design of the car. Second, the active aerodynamic components are drafted in red, which is meant to show: what are the active components, which in this case are thought to be the diffuser, rear and front wing; and how they are situated on the body. Drafts in cyan are there mostly for aesthetic reasons at this point, as they are regarding the lights and mirrors. Chassis is drafted in pink, to aid in visualization of the relative positioning and proportions of the body. Lastly, parts coloured in lime show where openings in the body might be necessary; therefore, wheels and radiators belong there.

3.2 Initial Design

The first iteration of the car body design is essentially a replica of the sketch presented in the previous section. However, the design had to be altered to suit the dimensions of the existing car parts and the limitations of the used CAD software. The software used for the car body design is Solidworks and the body itself was designed using the 'surface' module in the program. This feature allows for smooth surface design that can later be thickened, thus being a good representation how the real car body would look like when manufactured. Yet, it should be kept in mind that this module has its potent limitations. Namely, the inability for certain shapes and transitions between shapes to be established in the program, as even though the desired design has been previewed, the program tends to abort the operation and display errors. Besides that, not all the shapes are feasible to make, so the design is really a close approximation of the desired shape. Also, regarding the adjustment to the dimensions of the already designed car parts; the difference between the draft and the CAD design get more prominent. When drafting it is not clear how well does the sketched body wrap around the chassis or what are the dimensions of certain distances between certain features. For instance, when designing the body it turned out that the positioning of the radiators and the chassis makes it very inconvenient for the radiator inlets to be of the sketched size and positioning, thus the radiator design turned out to be significantly differing in the CAD model. Additionally, there is a discrepancy between different views displaying the sketch from different angles. Conversely, the CAD design will always be consistent between different views, therefore contributing to the deviation from the sketched design. The modeled design of the first iteration is visualized in Figure 3.2.

The main premise of the car body design is to minimize the drag associated with it. Therefore, the car body initial design is meant to closely represent a teardrop shape, within the other limitations posed on the car body. The first limitation is the chassis shape, making the car body shape close to flat at the bottom and curved at the top to efficiently encompass the chassis and other components. Furthermore, the body size is also meant to be minimal, which is due to the fact that an increment in body size corresponds to an increased frontal area and viscous drag, as well as increased complexity and weight of the body, all of which are detrimental factors to the car's performance. Moreover, the lift force is rather an undesired occurrence, which led to attempting to limit the amount of air being directed under the car, while keeping the teardrop shape. The main features of a teardrop shape moving from the front are: a gradual increase in size that is rather rounded in fashion; then continuing the same gradient towards the rear, resulting in a rather sharp end. The idea of gradual increase in size moving from the front has remained in the design, where the curvature followed the encapsulation of the existing parts; however, to limit the size of the rear of the car the teardrop end has been significantly shortened and much less gradual in the design.

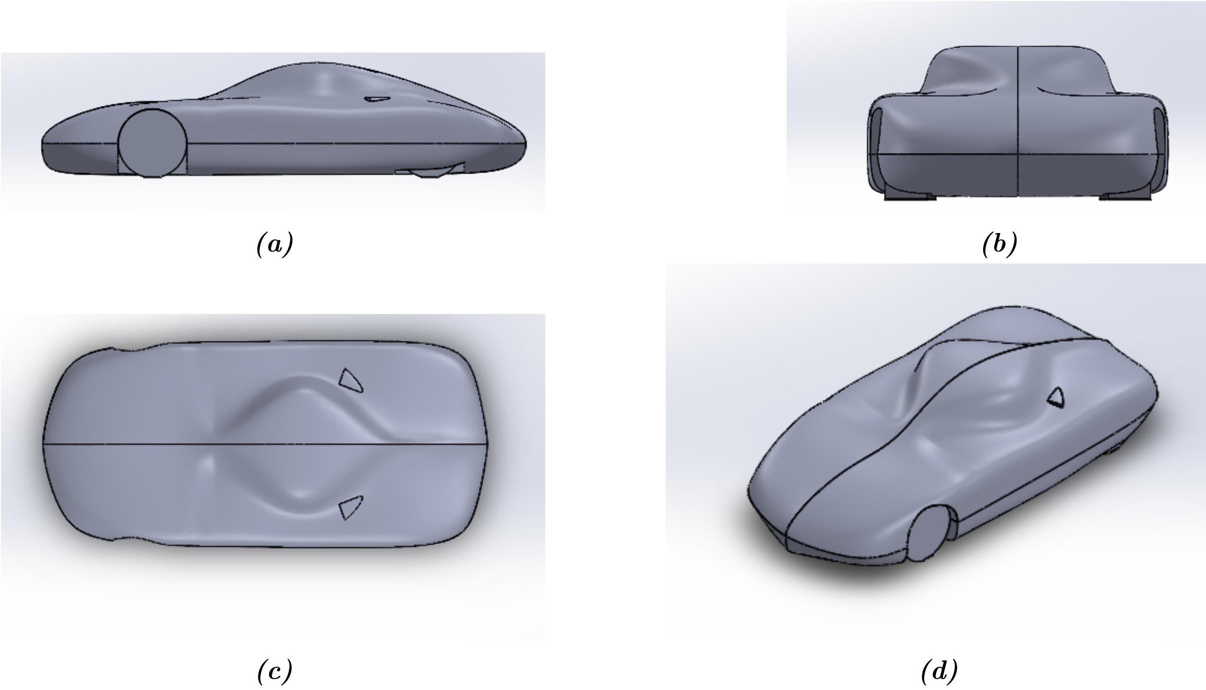

Figure 3.2. Depictions of the first iteration of the car body design. Moving from top to bottom and left to right, the body can be seen in right, front, top and isometric view respectively.

As mentioned before, the radiator intakes have been significantly resized and reshaped compared to the sketch, which is due to the radiators being positioned quite low and towards the center of the car, which is was not that apparent during the sketching phase. The idea during the design was to make the radiator inlets as big as necessary to supply direct airflow to the radiators, instead of redirecting air to them. What is more, it has been decided to seal the cavity for the rear wheels as a means to significantly reduce drag. This is meant to potently reduce the vertices and pressure differences created by the cavity within which the rear wheels are situated. Clearly, that solution has been omitted for the front wheels, as they need to turn in the yaw direction, thus making sealing the front wheel fenders unfeasible without a notable enlargement of the body size, as well as the necessity for reshaping of that area.

In order to validate the design and possibly improve upon it in the future iterations, aerodynamic simulations have been done. The main purpose of the car body simulations is to obtain useful data, such as drag and lift force, as well as visualizations of the airflow around the body. Knowing these can guide one's design decisions regarding reiteration or not, since satisfactory drag and lift forces and coefficients along with an airflow that can be considered up to par with the desired one; otherwise, a reiteration should be performed. It is worth mentioning that the drag force is of the highest importance, as this is the main factor to be minimized in the car body design. Meanwhile, the lift force and airflow are of secondary and tertiary significance respectively. The aerodynamic simulations are performed using ANSYS Fluent module, which is within the access for the work of this thesis and enables accurate simulations and insightful analyses of fluid flows. The simulations are performed in accordance with 'Aerodynamics of an FSAE car' course by ANSYS. (25) This procedure has been chosen to follow due to similar problem being solved; that is a car of similar size with aerodynamics features analyzed with regards to drag, lift and airflow. Nevertheless, due to computational limitations the procedure performed here deviated slightly from the one shown in the course. This resulted in: a coarser mesh in the bodies of influence and curvature around the car; simplifying certain considerations within the simulation that are not absolutely crucial for an accurate result, such as setting the car wheels as stationary, which for a closed wheeled car should not play a vital role; and other small changes, such as solving the problem with single-precision computation, rather than double-precision. In this case, the simulation has been performed for a flow velocity of 30 m/s, as this is a velocity at which the aerodynamic effects are significant and a velocity that is likely to be experienced during a corner on a track or a motorway. It is worth mentioning that the obtained drag and lift coefficients can be used for other velocities as well, thereby the obtained data is applicable for different conditions. The contours obtained from the simulations, showing the static pressure and velocity magnitude can be seen in Figure 3.3. It is worth stating that the simulations ran for the necessary amount of iterations to yield results where the obtained values either barely change from iteration to iteration or there is a repeating oscillatory pattern over a longer range of iterations.

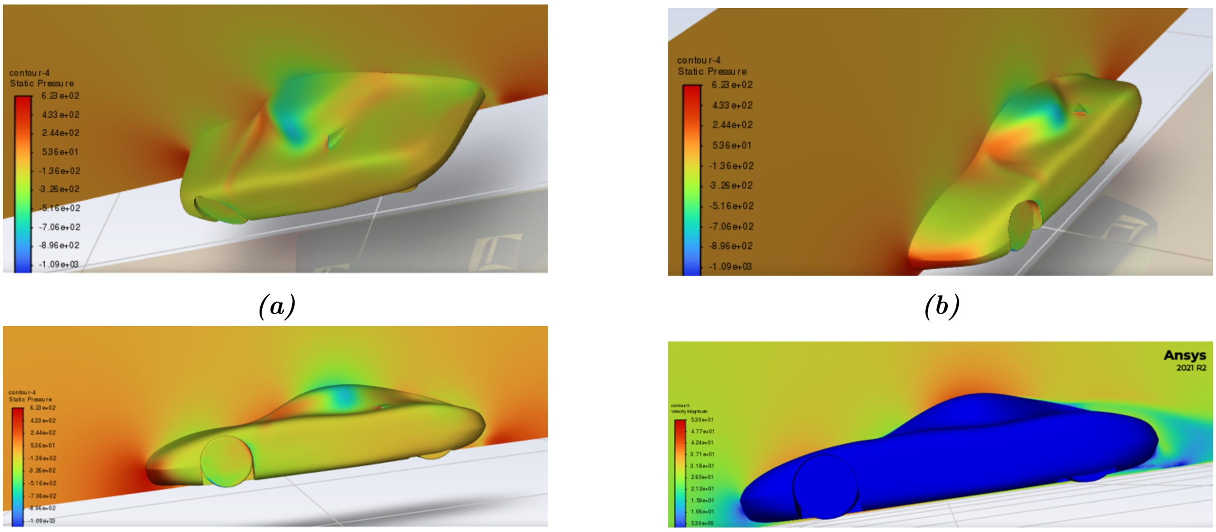

(a) *(b)* *(c)* *(d)*

Figure 3.3. Images from the aerodynamic simulation of the first iteration of the car body; showing velocity contour in the lower right corner and pressure contours from different angles on the rest of the images.

Based on the simulation results, it has been noticed that the design would benefit from reiterating, thus it has been decided that the current result is unsatisfactory and redesign must occur. Firstly, the drag coefficient value of 0.287, and the drag force of 302 N are considered satisfactory, as these are lower than most vehicles. In contrast, the lift coefficient of 0.581 and 610 N of lift force associated with it, seem to be very high and are presumed to be corrigible in a simple manner. The main culprit of the lift generation is suspected to be the shear curvature of the body; as the body has a longer path for the airflow to travel at the top than the bottom, the air that has been 'split' at the front of the body and that is directed to the top part of the body has to travel the a longer distance in the same amount of time as the air that has been directed to the bottom part of the body, in order to merge at the rear; this leads to the air flowing faster at the top of the body, thus creating lower pressure, thereby creating lift. This is an inherent feature of the car body that not much can be done about, therefore other means should be investigated. The ground effect implemented seems to have minimal effect, as attempting to create Venturi effect by narrowing the air entering the bottom of the car into a low clearance and exiting with an upward slope at the rear, does not seem to produce significant low pressure zones under the body. Some of the lift could contribute from the stagnation zone at the lower part of the front bumper of the body, which creates high pressure at the lower part of the front of the body, thus creating pressure. As of the effects of drag it can be seen that the rear of the car produces some stagnation zones and the fact that the tail of the car is somewhat long does not seem to contribute to mitigating pressure lowering at the rear of the car. What is more, it can be noticed particularly on Subfigure 3.3b that a design mistake has been made, where the rear of the front wheel fender sticks out more than the front in its upper area, thus creating a high pressure zone in the front of the rear wall of the cavity, which contributes to worsening the streamlining performance. This can be marked by significantly more red zone in the upper part of the rear wall of the fender in the aforementioned subfigure.

3.3 Car Body Reiterations

Based on the shortcomings of the first design, which were deducted from the simulations done on it, led to reiterations on it have being performed. To start that process, a new sketch of the second iteration has been done, whose right view can be seen in Figure C.1, which is the view where most changes occurred. The modelled design has its most important views depicted in Figure 3.4. The first flaw to be fixed was the front of the body, which created high pressure stagnation zones on the lower part of the front. This has been corrected by essentially extending the peak of the front part downwards, therefore featuring a minimal downwards slope at the front, which is presumed to minimize the high pressure zones responsible for the lift. Obviously, it is expected that high pressure stagnation zones will be formed at the front by the nature of the geometry; nonetheless, these should be mainly causing drag, as the direction of the pressure gradient is suspected to be close to horizontal, thus lacking significant vertical components in the mentioned zone.

Another altered feature was the rear of the car body, which in the reiterated version featured a 'Kammback' resembling tail. The point of that is to mimic the effect of the teardrop tail shape, without its impracticalities and with a minimal increase of drag as a result. The 'Kammback' tail is practically an abruptly cut rear end of the car, meant to induce a wake region behind the car, that would imitate a tapered tail to a certain extent. The reason for choosing this approach rather than attempting to extend the already existing tail, was the fact that the already existing tail provided negligible advantages, and it can be stipulated that extending it further would provide minimal aerodynamic improvements, while adding burdens from the structural and maneuverability points of view. Additionally, the aforementioned fault in the front of the rear part of the front wheel well has been fixed, simply by assuring that all the surfaces surrounding the opening are close to tangent. Moreover, overall shapes present on the car were altered; this included inclusion of flatter surfaces, change in curvatures and other minor alterations. These were done primarily to simply the geometry, which made it significantly easier to work with, as well as it is presumed that it should make it simpler in terms of manufacturing. The changes had a minuscule effect on decreasing the frontal area of the vehicle, decreasing it by $0.006\,\mathrm{m}^2$ and yielding a frontal area of $1.902\,\mathrm{m}^2$. Yet, there are certain flaws present on the body, which are clearly unintentional. Most of these regard overall shapes of certain features that deviate from what was intended, which come from the aforementioned limitations of the software used and the limited amount of time considered to be reasonable allocated to fix those issues. One potent example of these type of flaws, is particularly noticeable in the right view of the modelled design seen on Subfigure 3.4a. This is to showcase an unintentional dip at the bonnet of the car body, that then transitions into a bump close to where the windshield is expected to be, to then transition to another less notable dip right before the radiator inlets.

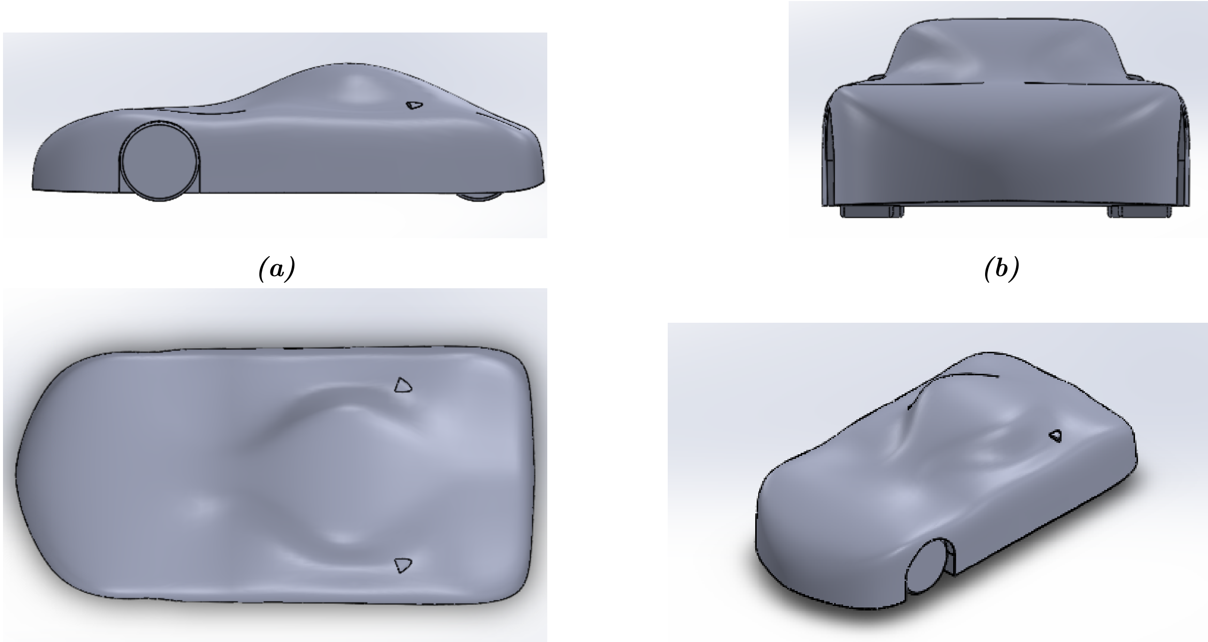

(a) *(b)*

(c) *(d)*

Figure 3.4. Views of the second iteration of the car body design. Moving from top to bottom and left to right, the body can be seen in right, front, top and isometric view respectively.

Here again, simulations with identical settings to the previous have been performed to validate the design with the same settings as before, so the results are comparable. The contours of the static pressure and fluid velocity magnitude are shown in Figure 3.5. First off, the drag force and its corresponding coefficient have stayed identical after the redesign; in fact, these have been slightly reduced, yielding 300 N of drag force and a drag coefficient of 0.286. Second, the lift force has been significantly reduced, yielding 501 N of produced lift and 0.478 in its corresponding coefficient, resulting in a 22 % decrease. It is, however, of importance to mention that due to inaccuracies in simulations, the obtained values and differences should be taken with a grain of salt. Concerning the overall car body size, it has been slightly reduced, which should contribute to lowered weight. It can be noticed that the aforementioned geometrical fault starting at the bonnet and ending by the radiator intakes, is likely to be partially responsible for a rather minuscule improvement in drag; as a increased pressure in front of it can be noticed; and it can be stipulated that it might produce some additional turbulence that could potentially be detrimental to the aerodynamic performance.

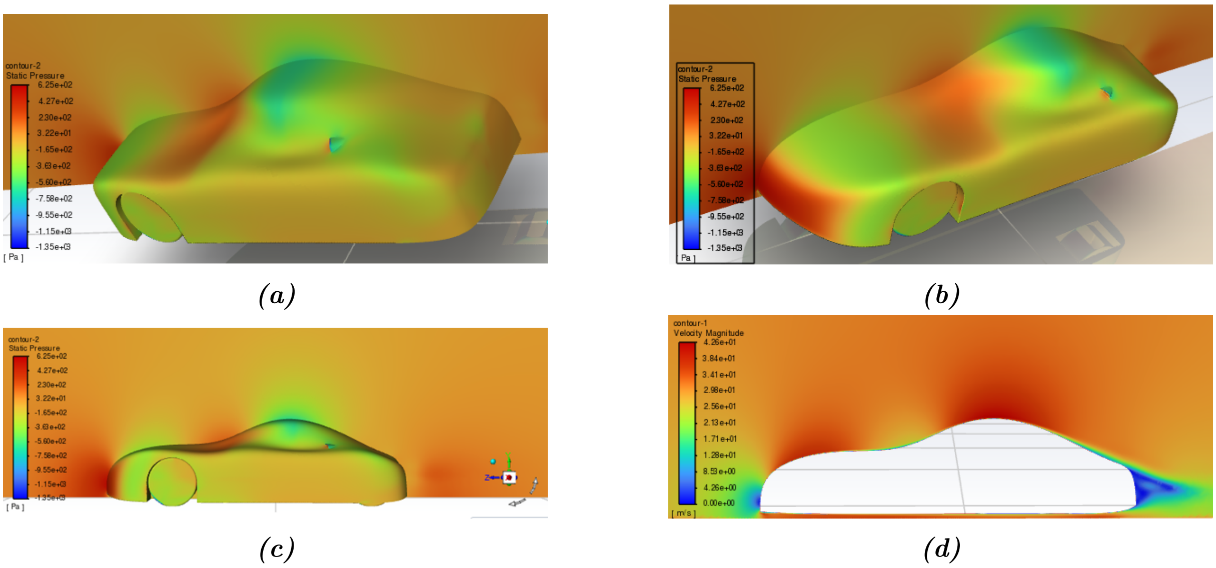

Figure 3.5. Images from the aerodynamic simulation of the first iteration of the car body; showing velocity contour in the lower right corner and pressure contours from different angles on the rest of the images.

Overall, the major drawbacks of the previous design have been eliminated, and the changes made upon it yielded in desirable results; although, the results are lesser in magnitude than desired, as the drag was not notably decreased, and the lift still remained high to a certain extent, despite significant improvement. Yet, this is deemed as satisfactory result, upon which no more reiterations will be performed at this point. This decision has come to fruition due to the fact that the scope of this project is comprehensive and the resources, particularly in terms of time are scarce. Thus, moving on to the other parts of the project being deemed as the right course of action. Notwithstanding, there are a number of improvements that could be done upon the body in order to better its aerodynamic performance. To start off, the undesired geometric features could be fixed. The front of the car could be made longer, thus leaving enough space to shape it so the high pressure stagnation zone is minimized, and perhaps feature an upward slope meant to produce slight high pressure zones on top to produce some downforce, thus offsetting the created lift. Furthermore, the front wheel fender could feature deflective shapes and a narrowing behind the wheel to reduce the air agitation associated with the front wheel well. Apart from that, overall shape and size optimization could be implemented to arrive at shapes, that would approach desired aerodynamic metrics and a reduction in size, particularly the frontal area, which should result in drag and lift reduction, as well as overall effect of the car body on the rest of the car aerodynamics.

Chapter 4
Wing Design

The primary active aerodynamic parts of the car are the front and rear wings, whereas the rear wing is expected to play the most potent role in terms of generating downforce. Therefore, the design will be focused on the design of the rear wing, and the front wing will be practically an altered version of the rear wing, that will also be examined, but to a much lesser extent. The wing has been decided to consist of a single airfoil, as opposed to being a multi-element wing. This decision is due to the fact that a multi-element design would have been much more complicated and more difficult to simulate. Also, the airfoil shape of the wing has been decided to be an existing one, as developing a new wing shape would have been too comprehensible for this project and would not guarantee a better performance than an existing airfoil shape. Thus designing a single element wing based on an existing airfoil shape is stipulated to yield the most satisfying results given the available resources. With that said, by determining the necessary lateral acceleration that the car is wished to withstand and knowing the necessary airfoil data, the wing size can be calculated. After that, the wing can be simulated to check whether it performs as expected. Then, eventual reiterations might occur until the desired aerodynamic performance is obtained. Lastly, the wing should be tested in terms of structural properties in order to ensure that it is capable of withstanding the loads put upon it.

4.1 Airfoil Selection

To start the wing design an airfoil shape should be chosen. Most airfoil data tends to be more tailored towards aerospace applications, being the reason why lift is mentioned in favour of downforce. It should be kept in mind that if an airfoil is inverted about its horizontal axis, the direction of the lift points downwards, effectively acting as downforce. Therefore, lift can practically be regarded as downforce in that sense. The most relevant data for this application are lift, drag and pitching moment coefficients, all of these as a function of angle of attack. At this point it should be clear why lift and drag coefficients are important, and knowing these values as a function of angle of attack provides with notion of magnitude of these values as the wing angle changes, thus being strongly applicable for active aerodynamics. It would be preferential if the lift and drag coefficients are small at low angles of attack, while on the contrary, both values would be large at high angles of attack. This is due to the fact that, this allows for control of these. If these are small at low angles of attack, that setting can be used for low drag and low downforce situation, which would be favourable for achieving high speeds or low energy usage, translating to extended range. Conversely, if these coefficients are large for high angles of attack, that setting can be used for high drag and downforce setting, particularly useful for fast cornering and shortening the braking distance. As of the pitching moment, it informs about the torque being applied by the aerodynamic force vector at the center of pressure around the aerodynamic center of the airfoil. Based on this, it can be stipulated that in order to stop airfoil rotation around its aerodynamic center as a result of aerodynamic forces, a torque that is equal to the corresponding pitching moment must be applied at the aerodynamic center; and the applied torque must be slightly larger than the corresponding pitching moment in order to rotate the airfoil to the desired position. Thus, a lower pitching moment is preferred, as it should require less torque to control the airfoil position, thereby lowering the requirements for the actuation power and resilience. The ratio between drag and lift coefficients is less of a concern for this application, as the wing is going to be changing angles, it does not have to compromise its drag for lift or vice versa. As explained before, having these coefficients correlated is preferential for the settings and scenarios applicable for this case.

To start the selection process, it was found out which airfoil profiles are common and which are known to be used for a car wing design. This is to limit the vast number of airfoils to choose from, thus simplifying and making the selection procedure more effective. Consequently, the choice has been narrowed down to NACA 4412 (26), NACA 6412 (27) and S1223 (28). From these, the NACA 4412 airfoil has been selected, due to its aerodynamic parameters and a seemingly easy to manufacture profile. The NACA airfoils seem to have more linear changes in lift and drag coefficients; a lower coefficient of pitching; lower drag coefficient at small angles; as well as a profile that is more manufacturing friendly and seems to hold more structural integrity. The decision towards NACA 4412 in favour of NACA 6412 was due to a lower pitching moment coefficient of the former.

It is worth mentioning that the provided data cannot be fully trusted, as different sources state different aerodynamic coefficients for the NACA 4412 airfoil. (29) (30) (31) Therefore, once the wing is designed, the NACA 4412 metrics of interest should be simulated, to determine these for this particular case, as it can be inferred that many of these metrics are case dependent, particularly regarding the present conditions (such as Reynolds number or interaction with other objects), wing size, endplates etc. Nonetheless, the AirfoilTools data regarding the NACA 4412 airfoil, (32) will be used as a starting point for obtaining the necessary coefficients; whereby the data for higher Reynolds number will be of greater interest, as these higher Reynolds number values correspond to probable wing size and relative fluid velocity.

4.2 Wing Sizing

Before the dimensions of the wing will be determined, the requirements from which the dimensions will be derived should be found out first. The requirement for whose fulfillment the wing will be dimensioned is the lateral acceleration that the car has to withstand when cornering. The way the wing dimensions relate to that is by the fact that its reference area is proportional to the downforce produced at various velocities, which is described by Equation 2.4, and the downforce aids in pressing the car down to the ground, thus contributing to enhancing grip by increasing the normal force in Equation 4.1, which relates the lateral force F_{grip} that grip should be able to withstand; and normal force N with the tyre friction coefficient μ. The downforce contribution can be noticed in Equation 4.3 as lift F_L being subtracted from the sum. The equation shows contributions to normal force N generation in a car; the first contributor is the weight of the car, which is a product of its mass m and gravitational acceleration g multiplied by the cosine of turn banking angle α_{turn}; the second contributor, featuring a negative sign before it, is the recently brought up lift force, also regarded as downforce, which could be expanded by constituting it with contents of Equation 2.4; the third contributor is centripetal force as a result of ground concavity or sag curve, often experienced when driving through a dip or valley, and is a product of vehicle's mass and velocity squared multiplied by the cosine of turn banking angle divided by the radius of the sag curvature r_{ground}; the fourth contributor is the centripetal force resulting from the banking of the turn, and is a product of vehicle's mass, velocity squared, as well as sine of turn banking angle divided by turn radius r_{turn}. The lateral centripetal force experienced in a vehicle can be described by Equation 4.2, being a product of vehicle's mass and velocity squared divided by the radius of the corner it travels through. If that equation exceeds the magnitude of the lateral force that the grip is able to withstand (Equation 4.1), the vehicle loses grip; one can equate these equations and rearrange them to determine the speed at which the car can corner a turn of specific radius or to determine the necessary downforce to make it through a particular corner of a particular radius.

$$F_{grip} = \mu \cdot N \tag{4.1}$$

$$F_c = \frac{m \cdot v^2}{r_{turn}} \tag{4.2}$$

$$N = m \cdot g \cdot cos(\alpha_{turn}) - F_L + \frac{m \cdot v^2 \cdot cos(\alpha_{turn})}{r_{ground}} + \frac{m \cdot v^2 \cdot sin(\alpha_{turn})}{r_{turn}} \tag{4.3}$$

To determine the desired lateral force that the car would need to maintain grip at, it has been decided to that it should be based on one of the goals wished from the car; namely, the Nurburgring lap record. As necessary telemetry data and other useful information is hard to come by, plenty of information will have to be extrapolated. Knowing the radius of the corner and speed at which the vehicle traveled through it, the lateral acceleration can be extrapolated using Equation 4.2. Then, knowing or presuming the tilt towards the direction of the turn and the transverse concavity of the corner, by rearranging Equation 4.3 the necessary downforce can be found.

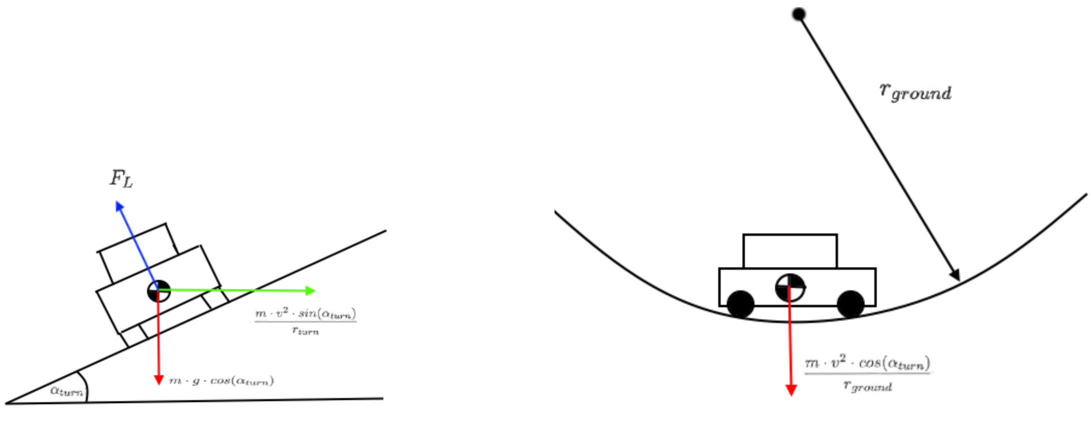

(b)

(a)

Figure 4.1. Illustrations of the different contributions to the normal force in Equation 4.3. The leftmost illustration primarily depicts the vectors from the car's mass in red, turn centripetal force in green and lift in blue. The effects of the sag centripetal force are illustrated in the right image, where it is denoted with a red arrow.

It has been decided the necessary lateral acceleration will be determined based on the amount of lateral acceleration experienced at at a corner where the value of that acceleration peaks around Nurburgring. According to several sources a section known as Foxhole ('Fuchsrohre' in German) is where highest lateral G-forces are experienced. (33) (34) In order to arrive at a specific value of lateral acceleration at that corner, it has been decided that a lap record breaking car should dictate that. For that purpose a video footage of Mercedes AMG One world breaking lap record for a production car at Nurburgring in 2022 is used. (35) It is used due to the fact that it seems to be the most suitable source of information, for this project, as in the video one can see where the car is on the track and at which velocity it is traveling; the vehicle class is appropriate, as the DIS1 car is mainly aimed to compete against other production vehicles; and the car is the most recent lap record holder on the track as of writing this thesis.

For the wing sizing, it has been decided that the wingspan S_{wing} will stretch for the whole width of the car of 1850 mm, thus leaving with the cord length L_c as the only variable to be calculated. To calculate this, what needs to be known is what goes into the normal force acting on the car's wheels, which are included in Equation 4.3 and have been explained previously. All of these contributions are speed dependent, therefore it is the most important thing to be found. In the aforementioned video footage at approximately two minute and 37 second mark the lap record car is going through the supposedly highest lateral acceleration¨corner on the track, with an approximate speed of 280 km/h, converting to a ceiling value of 78 m/s, thus deeming this as the corner velocity v_{turn} for further calculations. In order to obtain the lateral acceleration at that moment, the radius of the driving line at the corner should be approximated. For this, satellite data image from Google Maps of Foxhole turn has been put in use. Then visually approximating the curve of a line a vehicle would be suspected to take around the turn using straight lines and a circle sketch geometry tools in Solidworks, yielded the radius of the driving line around the turn to be 333 m after rescaling the obtained radius value of the sketched circle; this can be observed in Appendix E. Using Equation 4.2 the lateral force is obtained, by dividing it by the car's mass and the earth's gravitational acceleration constant a lateral acceleration of 1.86 G is obtained, which will be represented by G_l.

Before proceeding further the centripetal forces have to be approximated. Due to immensely limited data about corner banking and sag curves on racetracks, it is quite difficult to come up with a sensible value. Initially, the sag curve of compression part of 'Foxhole' was approximated using a cyclist sports data resource (36) which is described in Appendix F; however, with the obtained values the vertical acceleration acting on the car would yield a force deemed too large. Therefore, a different approach has been established; namely, using recommended minimum sag curve radii according to Table 12.1 in Road Planning and Design Manual - Geometric design - Volume 3, Part 3 (37); where a minimum radius of 2700 m is recommended for a velocity of 130 km/h and using the comfort criterion of a = 0.05 G. To proceed, a sag curve radius of 3000 m is used, which yields 0.207 G of additional vertical acceleration, being a more feasible value. As of the banking angle, a value of 2 % is presumed, based on the maximum superelevation rate of four percent for urban roadways. (38) This yields an additional contribution of 0.065 G according to the appropriate contribution in Equation 4.3, resulting in a total of additional contribution of 0.272 G to the normal force. Even though the described geometrical features of the track are likely to be more in favour of contributing even more to the total normal force, the additional normal force contribution will be assumed be even less, ensuring that the design is capable of providing more downforce than necessary, leading to the normal force contribution to equal 0.25 G for further calculations, and will be denoted as G_c. With that in mind the aforementioned contributions in the equation of most interest in this paragraph essentially become a constant, simplifying the further procedure. Thus, rearranging the equations in this chapter will result in the Equation 4.4 for the required cord length to achieve the desired downforce to obtain necessary grip to withstand the stipulated lateral acceleration. The equation is essentially an equation for the necessary wing area divided by its span. It is worth noting that the equation assumes a negligible angle of the turn banking, leading to the exclusion of a cosine term in the equation.

$$L_c = \eta_{wing_r} \cdot \frac{(\frac{G_l}{\mu} - 1 - G_c) \cdot m_{car} \cdot g + \frac{1}{2} \cdot \rho \cdot C_{l_{car}} \cdot A_{f_{car}} \cdot v_{turn}^2}{\frac{1}{2} \cdot \rho \cdot C_{l_{wing}} \cdot v_{turn}^2 \cdot S_{wing}} \tag{4.4}$$

To calculate the necessary cord length of the first iteration of the wing, it has been decided that the wing should generate the necessary downforce to withstand the specified lateral acceleration at a lower velocity. Meaning that in Equation 4.4, G_l will retain its value of 1.86 G, while

v_{turn} will be decreased to 70 m/s. The reason for that is to make the car potentially capable of cornering through sharper at the same velocity by providing even higher normal force, leading to increased lateral acceleration the car can handle before losing grip; as well as again it functions as an additional safety factor. The frontal area of the car A_{fcar} of 1.902 m^2 and its lift coefficient of $C_{l_{car}}$ mentioned in Section 3.3 will be used. As of the wing lift coefficient, a value of 1.51 will be chosen, as this is the value obtained from Airfoil Tools (32) for a NACA 4412 airfoil for an angle of attack of 15 deg, which is close to where the peak downforce is produced according to the source. As it can be noticed, Equation 4.4 features a coefficient η_{wing_r}, representing the percentage of the total downforce generated by the rear wing. The inclusion of this coefficient can be justified by the fact that the car is going to include other aerodynamic elements, while the equation without the coefficient would assume all the downforce needed to supply with necessary normal force would come from the rear wing only. For this computation it has been decided that the rear wing would generate at most 80 % of the total downforce, thus assigning that value to η_{wing_r}. Based on the above, the equation yields a cord length of 381 mm, which has been decided to be rounded up to 400 mm for the design. As of the endplates on the wing, their sizing has been rather arbitrary, mainly based on what seems to be sensible sizing, based on existing wings and their endplate sizing. The enplates have been designed so their portion below the cord line is larger than the one above. This is thought to hold merit due to the fact that the absolute pressure difference between the atmospheric pressure and pressure present at the wing surface tends to be larger at the surface below the cord line than at the surface above it.

4.3 Wing Simulations

As a means to verify that the designed wing will perform as expected and that the available data about NACA 4412 is matching the data of the wing based on that profile; simulations will be performed. The goal of the simulations it to obtain data regarding drag and lift forces and coefficients for different angles of attack, thus providing with sufficient data to approximate the relation between those for the angle of attack range of interest. The simulations are again based on the same ANSYS course as before.(25) However, this time it has been adjusted to match a smaller component, thus resulting in smaller domain and allowing for finer mesh without exceeding the available computational cost that the available resource is able to handle. The simulations have been performed using settings based on assumptions in Section 4.2, therefore deeming the relative fluid velocity as 70 m/s. The simulations have been performed for angles of attack ranging from 0 deg to 15 deg with an increment of 5 deg between each consecutive simulated angle of attack. The results can be seen in Table 4.1, whose content has been converted to graphs seen in Subfigures 4.3a and 4.3b, where the former is showing the relation between angle of attack and coefficient of lift, while the latter does the same, but with the coefficient of interest being drag. The lift to drag ratio in the mentioned table, is absolute in value. This is due to the fact that it is considered more fitting to display that measure in this manner.

Angle Of Attack [deg]	Lift Force [N]	Drag Force [N]	C_l	C_d	$\frac{C_l}{C_d}$
0	-664	43.2	-0.297	0.019	15.6
5	-1486	90	-0.665	0.04	16.6
10	-2260	173.8	-1.013	0.078	13.0
15	-2792	298	-1.251	0.134	9.3

Table 4.1. A table showing the results of the simulations of the first iteration of the wing based on the NACA4412 airfoil, with relative fluid velocity of 70 m/s. The table aims to showcase the relation between drag, lift and the angle of attack. The lift to drag ratio is absolute in value.

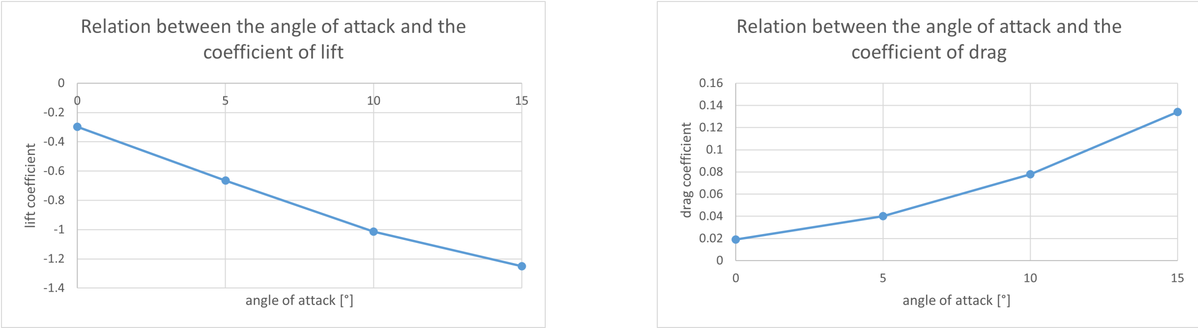

(a) ***(b)***

Figure 4.2. Graphs depicting the relations between the angle of attack and coefficients of lift and drag, shown on the top and bottom graphs respectively. These have been plotted based on values from Table 4.1.

As it can be noticed, the drag and lift coefficients differ significantly from the ones obtained from AirfoilTools (26), particularly the lift coefficient is much smaller, especially at 15 $\circ$ of angle of attack, which is the angle at which maximum lift coefficient is presumed to occur; the simulated value yielded a lift coefficient of 1.25, as opposed to 1.51. This has a potent effect on the downforce generation which is of primary concern at this stage of the design. Meanwhile, for the same angle of attack the drag coefficient obtained in the simulations equals 0.134, being significantly larger than the one predicted using aforementioned source, which would suggest it equaling 0.055. As of the lower angles, the same trend can be observed for both coefficients, where the simulations yield a larger drag coefficient and lower lift coefficient; with their relative discrepancy being larger at lower angles of attack. At lower angles a high drag coefficient works to the detriment of the vehicle performance; however, it being high at higher angles of attack can be a helpful feature, particularly when one attempts to stop the car as quickly as possible. Obviously, since the coefficients of lift and drag differ from the predicted ones, so do the forces acting on the wing, thus yielding an insufficient downforce for the criteria that initially determined the wing size. As a consequence of the considerations above, it has been decided that the wing should be redesigned using the newly obtained wing data and with altered assumptions.

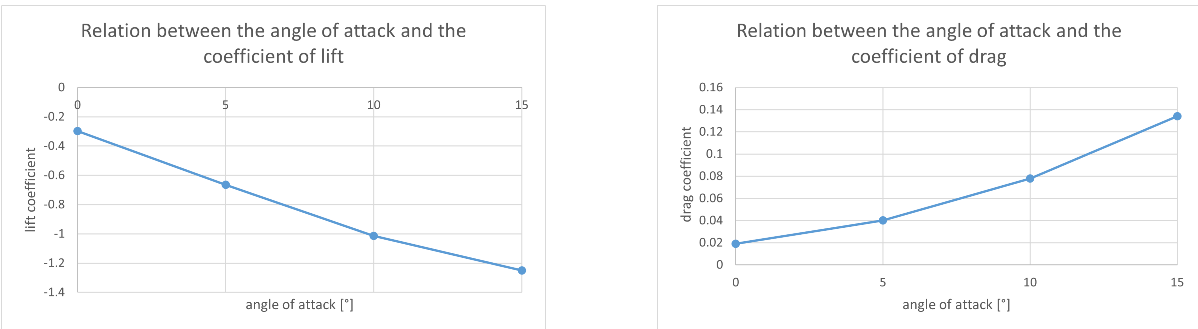

(a) ***(b)***

Figure 4.3. Graphs depicting the relations between the angle of attack and coefficients of lift and drag, shown on the top and bottom graphs respectively. These have been plotted based on values from Table 4.1.

Images obtained from the simulations are displayed in Figure 4.4, where the pressure and velocity contours are shown for the simulations with 0 deg and 15 deg angles of attack. What can be noticed is that the magnitude of the negative pressure is extraordinarily more potent in the upper extreme of the angle of attack, which indicates how strong is the effect of the suction occurring on the underside surface of the wing. Whereas the positive pressure did not experience such a striking difference when looking at the exhibited depictions of the simulations. Even more, it can be observed that the pressure extremes and the largest pressure gradients happen at the front part of the wing surface, which applies both for the negative and positive pressure extremes. This implies that the front part of the wing is the most crucial in terms of lift or downforce production, meaning that this zone is the most important to keep disturbance free when implementing the wing into the design of the whole vehicle. Furthermore, the higher angle of attack simulation seems to indicate that this configuration be more provoking of vortex shedding, which can be noticed on its endplate by the characteristic line there in Subfigure 4.4b and 4.4c and recirculation region behind the wing in SubFigure 4.4d, which can be characterized by a region of of almost stagnant velocity behind the wing.

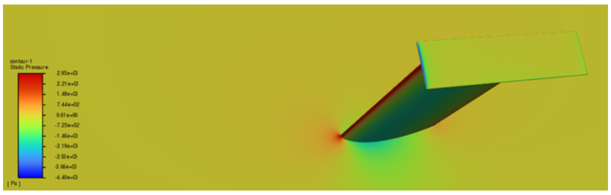

(a)

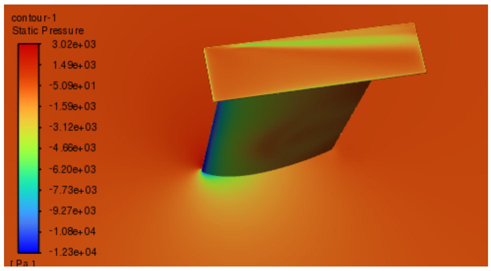

(b)

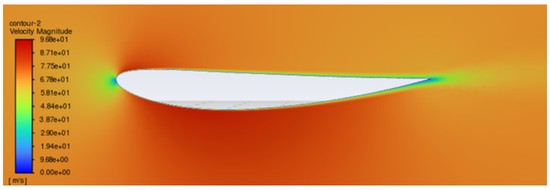

(c)

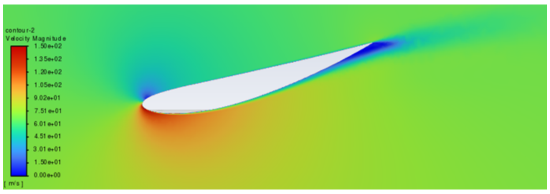

(d)

Figure 4.4. Images from the aerodynamic simulation of the first iteration of the car body; showing velocity contours in the lower images and pressure contours from different angles on the rest of them.

4.4 Reiterations and Validation

As discussed in the previous section, the wing design has to be redone to fulfill the requirements, as according to the recently obtained data and assumed conditions and requirements, the wing would yield an unsatisfying performance. After the new version is designed it should be simulated; firstly, to validate that the aerodynamic performance will be up to par with the expectations; secondly, to validate that it should withstand the forces exerted upon it.

The redesign of the wing is going to be done in the same manner as its initial design, however this time some assumptions will differ. The wing cord length will be chosen according to the same equation (Equation 4.4). Most of the values in the equation will remain the same, the difference will lie in the following: wing lift coefficient C_{lwing} being equal to 1.25, which is based on the lift coefficient value from Table 4.1; the car velocity needed to obtain the necessary downforce v_{turn} is going to be increased to 75 m/s, which is to be a bit more lenient towards the expectations from the car's performance; on that note, the coefficient of rear wing contribution η_{wing_r} has been lowered to 75 % for the same reason. Using these value alterations, along with the previously established values for the remaining variables in the equation dictating the wing cord length, a cord length of 414 mm is obtained. On the basis of that, a cord length of 420 mm is chosen to be used for the design of the second iteration of the wing.

To validate that the newly designed wing will perform up to par with the expectations, a new set of simulations is performed. However, in this case only angles of attack of 0 deg and 15 deg will be simulated, and the fluid velocity in the simulations will be 75 m/s. The reasoning behind doing fewer simulation for this version of the wing is that it is presumed that the coefficients obtained from the simulations of the previous iteration of the wing will remain the same; which again is due to the fact that aerodynamic coefficients are meant to be applicable to a wide range of geometry sizes and fluid velocities, as long as the geometry itself remains the same. The simulation results can be seen in Table 4.2. First of all, it can be observed that the lift and drag coefficients are almost identical, deviating by a bit more than 2 % in the most differing value, which is the lift coefficient at the angle of attack of 15 deg overshooting the value of the previous iteration, thereby yielding a preferable result. Secondly, as expected the values of lift and drag forces are larger in magnitude, thus fulfilling the established downforce criterion upon which the wing size was determined. Therefore, the wing is considered to perform satisfyingly in terms of the aerodynamic requirements towards it, and the further iterations with regards to its aerodynamic performance are halted at this stage of the development.

Simulation results for the second iteration of the wing are depicted in Figure 4.5. The same observations can be made as in the case for the Figure 4.4; however these should not be directly compared. Because of the dynamic nature of aerodynamic simulations, if an image of the simulation is shown, it is solely a snapshot of the whole situation that tends to have an oscillatory behaviour in time. Therefore, one should not conclude too much based on the snapshots of the simulations alone, as some of them might show a vortex forming while another might show an already formed vortex, thus one might mistake it for a constant flow separation if one does not consider the mentioned fact. An example of that can be observed when comparing the velocity contours of the wings at 15 deg angle of attack, seen in Subfigures 4.4d and 4.5f, as in the latter subfigure a clear vortex shedding occurrence with a large recirculation region can be noted behind the wing at the iteration when the simulation ended; whilst the former exhibits a seemingly small recirculation region, which could be deceiving taking into account what has been just stated.

Angle Of Attack [deg]	Lift Force [N]	Drag Force [N]	C_l	C_d	$\frac{C_l}{C_d}$
0	-808	48.8	-0.303	0.018	16.6
15	-3428	352	-1.281	0.132	9.7

Table 4.2. A table showing the results of the simulations of the second iteration of the wing with relative fluid velocity of 75 m/s. The table aims to showcase the relation between drag, lift and the angle of attack.

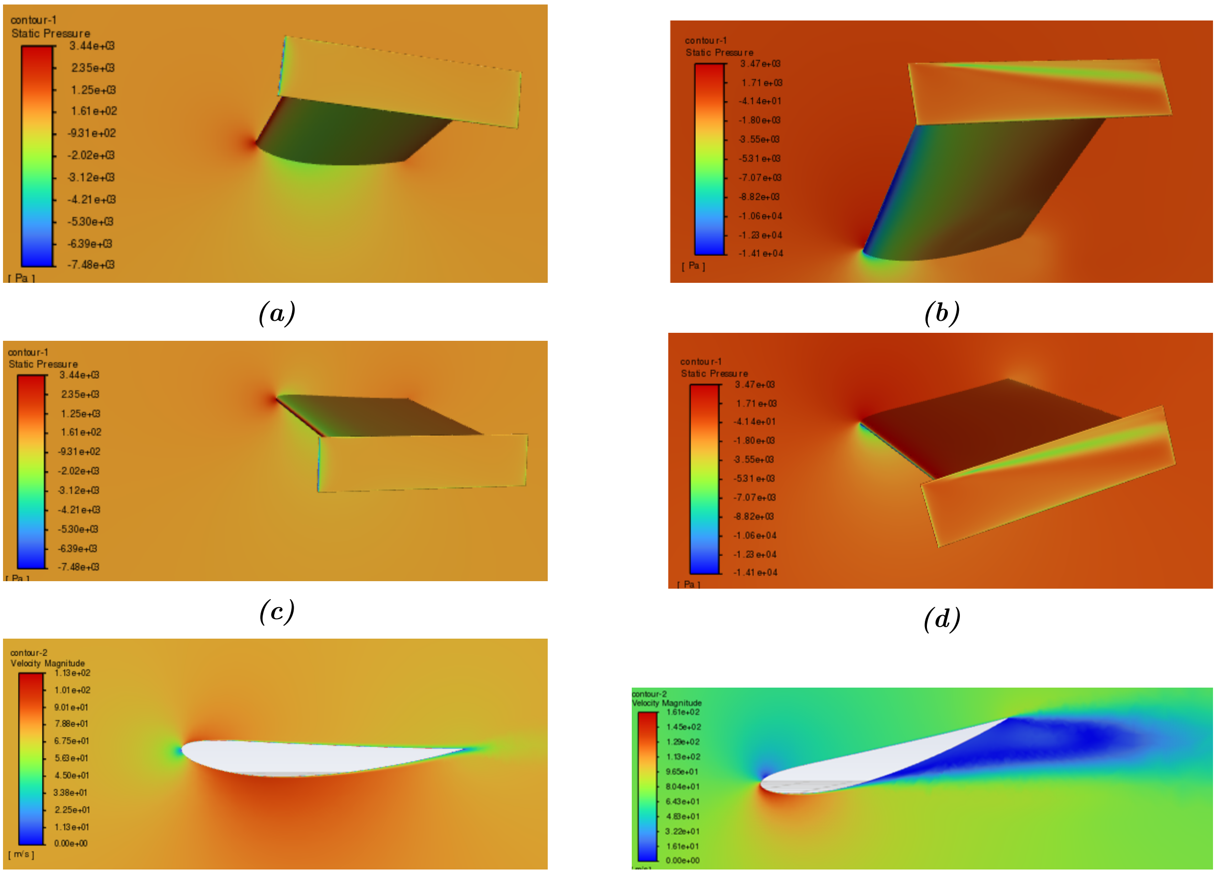

(a) *(b)* *(c)* *(d)* *(e)* *(f)*

Figure 4.5. Images from the aerodynamic simulation of the first iteration of the car body; showing velocity contours in the lower pictures and pressure contours from different angles on the rest of the images.

In order to validate the structural integrity of the wing, a different set of assumptions will be conducted. This is because it is desired that wing were able to handle unfavourable structural conditions. In order to define an adverse scenario the wing would have to withstand, it is envisioned that the wing be tilted to 15 ∘ of angle of attack at the car's maximum velocity on a racetrack, with a headwind classified as a moderate breeze, which should yield very detrimental conditions for the wing's structural integrity. Despite this scenario being quite unlikely to occur, it should still be accounted for and making sure the wing would be able to endure it provides with additional safety factor.

To determine the velocity in the aforementioned scenario, the Mercedes AMG One Nurburgring lap record footage will be used again; this time, however, its maximal speed reached on the longest straight on the track, reaching 308 km/h is about to be used.(35) As previously mentioned a scenario with a headwind categorized as a moderate breeze will be assumed, which yields faster wind speeds than the average wind speed at the Nurburgring during the windiest month of the year. In order to yield a round number for the calculations it will be assumed to be 22 km/h, resulting in 330 km/h of total relative fluid velocity. Knowing that, the area of the wing and other constants, as well as using the drag and lift coefficients obtained in this section; forces acting on the wing can be calculated using Equations 2.3 and 2.4, yielding 5946 N of total force acting on the wing, which will be rounded up to 6000 N to act as an additional safety factor. The obtained value and its lift and drag components will be used for further strength calculations. To initially validate the strength of the wing two structural simulations will be made on one of the wing half split along the symmetry plane; a simulation where the wing has a fixed support in its symmetry plane and the load is applied uniformly on the airfoil surface acting directly downwards is performed; and another where a fixed support is applied on a cylindrical surface within the wing, the load is applied as in the previous case and a rolling support is applied at the surface facing the symmetry plane, which can move only on the symmetry plane itself. The former is meant to simulate the overall flexion of the wing, in a way disregarding the way it would be supported on the vehicle. The latter is meant to simulate it in a way that corresponds to the way it would be supported on the vehicle. It should be noted that the cylindrical support is meant to mimic the wing resting on a shaft, where that support is based on the design described in Chapter 5. The simulations are performed in ANSYS Static Structural module, with mesh refinement in the places on the wing that are thought to need it. The images from the first and second simulations recently described are visible in Figures 4.6 and 4.7 respectively. The material chosen for the simulations is epoxy woven carbon fiber prepreg, meant to mimic the fact that the wing is thought to be made of that material. On that note, it is of grand importance that this is a crude approximation of how that kind of construction would behave, as composite material elements tend to be complex in construction and simulation, as they feature multiple layers of a fibre material laminated and also featuring a filling material, such as a honeycomb, as well as potentially featuring a bracket, reinforcing or skeleton made of another material to further support the structure in its compliance and strength. What is more, there is a significant dependency on the fibre orientation, angle between fibre layers, the way the fibre material is wrapped around the shape etc. affecting the mechanical properties of the structure. In this case it is assumed that the stress and deformation obtained from the default options for the aforementioned material in the software during simulations, provides sufficient approximation to validate the design structurally, considering the fact that the previously mentioned vastness of factors affecting a composite structure strength can be optimized that the structure will perform at least as well as simulated. Also, as mentioned before car wings are not particularly susceptible to damage by aerodynamic means, leading to a rather low emphasis on a in depth structural analysis of the wing itself.

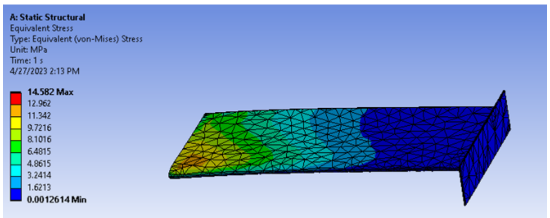

(a)

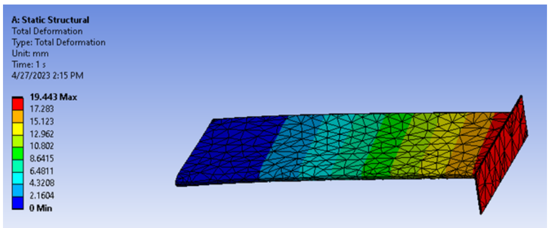

(b)

Figure 4.6. Images depicting simulation results from the structural wing simulation where the wing is fixed with a support at the surface facing the symmetry plane of the wing. The Subfigure on the left illustrates the stress distribution, while the one on the right does it for deformations.

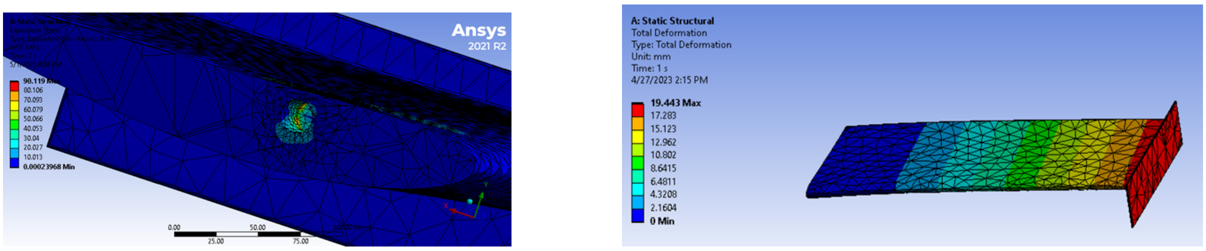

(a) *(b)*

Figure 4.7. Images depicting simulation results from the structural wing simulation where the wing is fixed with a fixed support at the cylindrical surface inside the wing based on the design in Chapter 5. The left picture illustrates the stress distribution at the place where largest stresses occur, which is in the corners of the cylindrical cavity where the wing is supported; while the one on the right shows the deformations.

Looking at the simulation results it can be noticed that the first structural simulation yielded significantly less detrimental stress conditions than the second simulation, which obtained a maximal Von Mises stress of 90 MPa at the corners of the cylindrical surface which supports the wing. Due to carbon fibre strength considerations stated previously, evaluating that result can be difficult; nevertheless, the problem can be simplified by assuming that the compressive stress of carbon fibre epoxy composite of 570 MPa based on the mechanical properties of a 1 mm thick carbon fibre epoxy composite sheet mechanical properties by GoodFellow (39); and that it can be directly compared with obtained stresses in the simulations, considering that the maximal stress seems to of compressive sort. Based on this it can be concluded that there is a meaningful margin between the obtained stress and the strength the material should handle according to the assumptions, yielding a safety factor of more than six; As of the strength of composite materials, it has been decided that if the safety factor surpasses the value of three, the stress level is considered not to cause adverse effects on the material, and the design is considered satisfactory. Regarding the deformations, it can be seen that the deformations are lesser in the second simulation, which is likely to be due to the fact that the wing is supported at a point further away from its center. The maximum magnitude of the deformations is 19 mm at the endplate of the wing in the first simulation, which is considered to be within the tolerance limit. As it can be seen the wing should withstand the presumed load acting upon in without particular issues, thus deeming the design as structurally viable, resulting in the whole wing design to be considered as valid.

Chapter 5
Wing Bracket Design

In order to support the wing in a structurally integral and aerodynamic manner, a wing bracket structure should be designed. The structure will be mounted to the car's body or chassis, the wing will be coupled to it with the usage of bearings and shafts in order to enable controllable rotation of the wing; and these parts will also have to be designed or selected. The design of the structure will be paired with simulations to validate its strength and aerodynamic merit.

It is worth mentioning that the wing bracket design in its initial stage is aimed consist of two supports spaced as closely as viable. This is desired due to the fact that a closely spaced support is thought to be more aerodynamically viable, in the sense that it should have less adverse effects on the drag and lift of the vehicle. This is presumed to be the case due to the fact that the closer the supports are spaced the less they should affect the merging airflow at the rear of the vehicle, as a widely spaced supports are thought to be disturbing the merging process of the airflow earlier, making the zone of that airflow being disturbed larger. Also, by being spaced close together the likelihood of them being in the wake of the airflow behind the car is larger, as aerodynamic wakes tend to occur closer the center of the rear of vehicles. Additionally, there should also be an advantage from the maneuverability standpoint; that is due to the mass of the support being closer to the center of mass in the planes of yaw and roll motions, thus reducing the inertia of the vehicle in these planes. However, the supports are suspected to be susceptible to adverse effects of torque around the wing's center of mass if they are spaced too close together. The mentioned torque can occur due to uneven force distribution around the wing, which again can be caused by phenomena such as airflow fluctuations, airflow incoming at an angle, vehicle roll when turning etc. That torque would be detrimental in the yaw and roll planes, as in these planes the support structure is spaced apart. It is the torque in the roll plane that is of particular concern, as this is where highest forces occur, due to the downforce acting in that plane and being the most potent force acting on the wing. As the process of determining the spacing of the support structure is not of particular relevance to the scope of this project, it will be rather short, as a spacing closely mimicking an already implemented spacing of wing supports will be chosen. Due to extremely limited data regarding swan neck wing support spacing, that has to be approximated using pictures from which the support span would be derived using proportions between it and a known dimension, such as the wing span. For that purpose, a Voltex Racing Type 10, a narrow swan supported wing has been found. (40) Using the aforementioned procedure, its support spacing has been approximated to 200 mm, which will be deemed as the support spacing for the design.

5.1 Shaft Design and Bearing Selection

To start off, the support design will start with designing the shaft and selecting the bearings. This is so the hole in the support structure does not have to be resized after the structure has been designed, which could potentially have an effect on the outcome regarding the strength of the structure; especially considering the fact that the structure will aim to be rather thin in the area where the bearing would be situated, since reduction of that area is expected to be preferential for the aerodynamic performance of the support structure in concert with the wing. The goal of the shaft and bearing design is so these components are compact and light, whilst being structurally sensible; therefore, the shaft will be aimed to be rather short and small in diameter and the bearing will be aimed to be rather narrow and small in outer diameter.

Firstly, it should be determined how the shaft actually will support the wing. It has been decided that there will be two equal shafts, each at its corresponding support structure. This decision came to fruition due to the fact that a single shaft supported by two bearings would experience higher bending stresses, due to the increased moment arm of the force distributed on the shaft. Somewhat arbitrarily the shaft length has been decided to measure 60 mm, assuming that it is long enough to distribute the reaction load acting from the shaft to the wing surface of the cavity where it would be situated, yet short enough to minimize the bending stresses. Secondly, the shaft calculation model is assumed to essentially be modelled as a beam with a fixed support in the middle of its length and with a uniform load pointing downwards being applied on the top part of the beam, as shown in Figure 5.1. This simple model assumes that the load will be uniformly distributed across the shaft and that the bearing will prevent any movement of the shaft apart from its rotation. This also raises the following assumptions about the shaft loading conditions: forces acting along the axis of the shaft are considered negligible; the shaft is expected to have negligible torsional loads applied; the load from the wing onto the shafts is presumed to be almost evenly distributed and is presumed to act in one plane on it; the weight of the shaft is negligible. It should be mentioned that in order to actually insert the shaft into the wing structure, the wing would have to have a detachable part, that would allow the insertion of the shaft. The part would most probably be the top surface of the wing in the area where the shafts are situated, and a bolted coupling between this part and the rest of the wing would probably be the connection of choice.

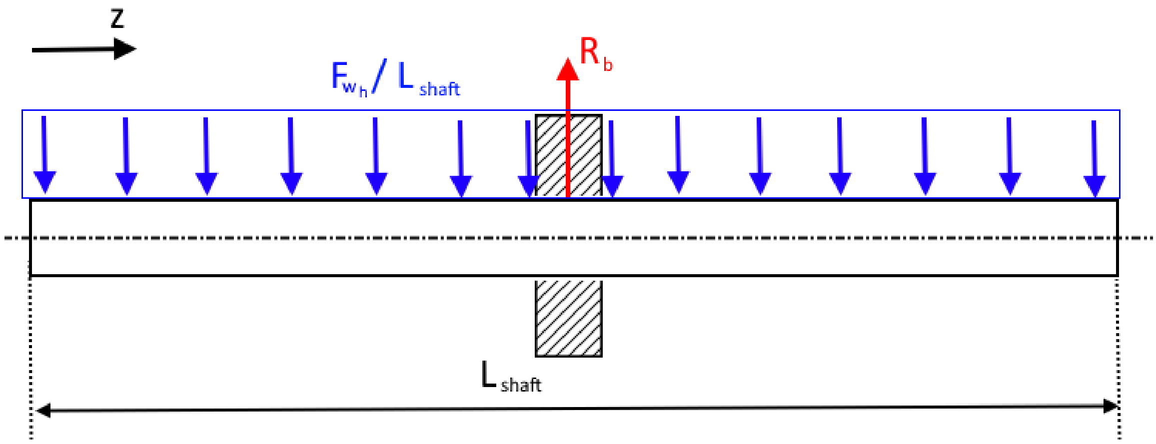

Figure 5.1. A beam model of the shaft loading conditions. In blue, the distributed load coming from the wing is shown and denoted as $\frac{F_{w_h}}{L_{shaft}}$; in red, the reaction force from the bearing is shown and denoted as R_b. The shaft features a fixed support in its center and its length is denoted as L_{shaft}. The distance from the left side of the shaft used in set of Equations 5.3 is denoted as z and an arrow showing the direction of that variable in the equations. The fixed support, marked with a hatch pattern, is supposed to symbolize the bearing.

This leads to the conclusion that it should be sufficient to calculate the necessary diameter of the shaft based on the normal stress and shear stress theories, which can be obtained using Equations 5.1 and 5.2 respectively. Both equations are primarily dependent on the bending moment M_b, the axial torque acting on the shaft T_s, the yield strength σ_y and the safety factor n_s. The axial torque acting on the shaft can be equaled to the pitching moment acting on the wing, as this is the torque the shaft would have to resist. It is assumed that the pitching moment that the shaft would have to resist, is equal to the pitching moment acting at the aerodynamic center of the airfoil. Therefore, it will be assumed that the torsional moment acting on the shaft is half of the total pitching moment acting on the wing, described by Equation 2.5, due to the fact that two shafts would be implemented.

$$d_{NormalStress} = \sqrt[3]{\frac{(16 \cdot (M_b + \sqrt{(M_b^2 + T_s^2)})}{(\pi \cdot \frac{\sigma_y}{n_s})}} \tag{5.1}$$

$$d_{ShearStress} = \sqrt[3]{\frac{(16 \cdot \sqrt{(M_b^2 + T_s^2)}}{(\pi \cdot \frac{\sigma_y}{n_s})}} \tag{5.2}$$

The bending moment is calculated using set of Equations 5.3. These regard one of the two implemented shafts, meaning that the force acting the shaft F_{w_h} is half of the total force acting on the wing. The set of equations changes with the distance from the left side of the shaft z. It is described as a set of equations rather than a single equation, due to the fact that the conditions change at the halfway point of the shaft length L_{shaft}, where the shaft is fixed, as this is where the bearing is supposed to be situated. After that point the bearing reaction force R_b is also affecting the outcome of the equations; that reaction force is equal and opposite in direction to the force acting on the shaft, being the only forces acting vertically, which is the only direction that forces are exerted on the shaft.

$$M_b(z) = \begin{cases} \dfrac{-F_{w_h} \cdot z}{2 \cdot L_{shaft}} \cdot z & \text{z} < \frac{L_{shaft}}{2} \\ \dfrac{-F_{w_h} \cdot z}{2 \cdot L_{shaft}} \cdot z + R_b \cdot (z - \dfrac{L_{shaft}}{2}) & \frac{L_{shaft}}{2} < \text{z} < L_{shaft} \end{cases} \tag{5.3}$$

As it has been mentioned, the shaft length is going to be 60 mm. As of the force acting on the shaft, it is going to be the half of the total force acting on the wing stipulated in Section 4.4, yielding F_{w_h} equal to 3000 N. Using these in the aforementioned set of equations, a graph for the bending moment as a function of the distance from the left side of the shaft is obtained in Figures 5.2. Using the mentioned graph and set of equations, a maximum bending moment of 22.5 Nm is obtained, being of a rather small magnitude, which is to be expected considering the size of the shaft, the magnitude of the forces acting on it and the loading complexity of the shaft. Regarding the torque acting on the shaft, assuming the pitching moment coefficient of -0.1 at 0 deg angle of attack, where it is close to its peak negative value (26); the air velocity of 330 km/h from the previously stipulated unfortunate scenario; and using the dimensions of the wing; the moment yields a value of 82.6 Nm. The shaft is chosen to be made of S355 steel, yielding 355 MPa of yield strength (41). The safety factor n_s is chosen to be equal to two, which is common to use for ordinary materials without severe loading and environmental conditions. Using the recently mentioned values in Equations 5.1 and 5.2, minimum diameters of 14.6 mm and 13.5 mm respectively, leading to the choice of 15 mm as the initial minimal shaft diameter, which might be due to change according to the inner diameter of the selected bearing.

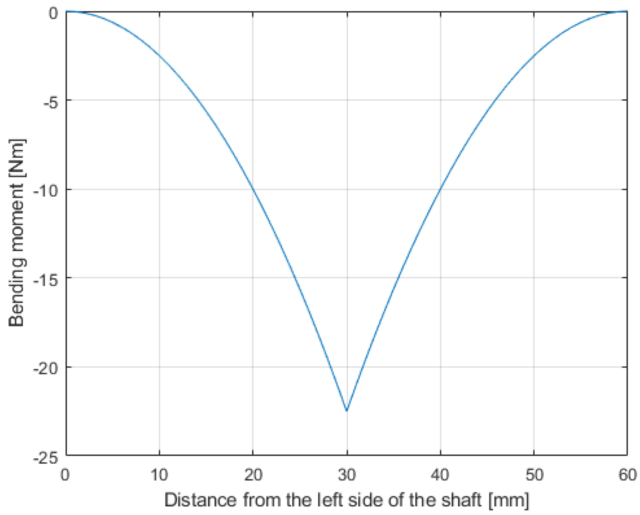

Figure 5.2. A graph demonstrating how the bending moment varies along the length of the shaft, which is based on the set of Equations 5.3.

The selected bearing for this application is SKF 16003 deep groove ball bearing (42), which was chosen based on its minimal dimensions, with its width, inner and outer diameter being 8 mm, 17 mm and 35 mm; as well as based on its basic static loading of 3.25 kN exceeding that of the supposed loading for the shaft calculation.

The shaft has been decided to be situated 10 mm and 5 mm away from the aerodynamic center of the airfoil towards its rear and bottom respectively, as shown in Figure D.1. The reasoning behind this is that the shaft should be near the aerodynamic center so the moments acting on the shaft are changing predictably; yet, it is offset slightly to the rear, which should decrease the moment acting on the shaft, as the aerodynamic forces will acting in the center of pressure will be acting at a shorter arm.Placing the shaft close to the center of pressure has been done due to safety reasons; if the actuation mechanism would fail, the wing would increase its angle of attack until hitting an endpoint, ultimately providing increased drag and downforce, which is safer than the opposite situation, as an increased drag and downforce should act in a manner that would be slowing the vehicle down and providing it with more grip. The downward offset has a primarily a twofold purpose; first is to provide with some additional wing material above the shaft, meant to act in the structural integrity of the wing; second is again diminishing the moment acting on the shaft, as the horizontal center of pressure component will counteract the vertical center of pressure component in terms of moment about the rotational axis. It should be kept in mind that the aerodynamic effects of the shaft center offset from the aerodynamic center are expected to be rather minimal.

5.2 Structural Design and Testing of the Wing Bracket

In order to support the wing a structurally and aerodynamically optimized structure should be designed. There are two main methods of mounting a rear wing in a racecar or a sportscar: direct mounting and swan neck. There is also a method where the rear wing is mounted by its endplates, which is used for instance in Formula One vehicles; however, as stated earlier a different support approach has been decided to go for, where the supports are closer to the center of the vehicle, deeming this mounting method unfeasible. Comparing the direct mounting and swan neck method, most of the available resources point to the fact that a swan neck is favourable in terms of aerodynamics. (43) (44) (45) This is likely because of the underside area being affected by the direct mounting, creating vertices and taking up that useful area, as it is the underside that tends to create the most downforce. The swan wing design mounts on the top, thus not taking any area of the underside, and the support structure is placed at a distance from the underside area of the wing, making the airflow less disturbed in at the underside than a direct mounting. Therefore, it has been decided that the approach of mounting the supports to the wing at its top would be the design approach. This led to the first design being a swan neck design, depicted on Subfigure 5.3a. During the design phase two more mounting ideas using that approach came to fruition. The first one is a reverse swan design, shown in Subfigure 5.3b, where the support curves around the rear of the wing to reach the top where it mounts to the wing. The ideated premise behind this, is that it should not create any disturbances in front of the wing, as an ordinary swan neck mount does, thus essentially leaving the underside wing area clear of any disturbances, thereby maximizing its potential. On the other hand, a larger part of the top side of the wing would be affected by the support; yet, as mentioned earlier, the underside is more crucial in terms of downforce generation, leading to the presumption that the net effect of the reverse swan neck should be rather efficacious in terms of downforce generation. Additionally, the supports are likely to be placed further back than a regular swan neck design, leading to the potential aerodynamic drag reduction, due to a part of the support being in the wake of the vehicle's airflow, or right before the flow separation occurs at the rear of the vehicle; creating turbulent flow at right before the flow separation could delay that process potentially mimicking the effects of vortex generators describe in Section 1.1. What is more, the reverse swan neck design is presumed to be at a structural burden, with the lever arm on which the force is acting on being longer than a conventional swan neck design, leading to potentially larger stresses and deformations, potentially making the design unfeasible. What was later found out, was that this design has in fact been implemented on an Audi RS3 LMS TCR (46) (47) and an aftermarket Lamborghini Huracan rear wing (48).

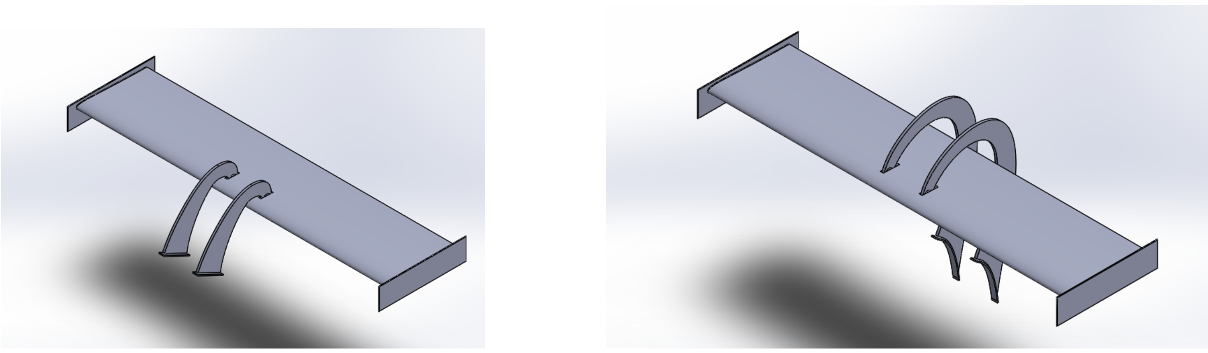

(a) *(b)*

Figure 5.3. A swan neck design and a reverse swan neck design shown on the left and right images respectively. The front is on the left side of the images.

The second wing mounting idea is essentially an evolution upon the reverse swan neck design, and this has been decided to be referred to as 'scorpion tail' wing mount design, which can be seen in Figure 5.4. The main difference lies in the way it reaches the top of the wing from its rear. In this design it has been decided that the support would practically go through the wing to reach the top, in this sense substantially shortening the lever upon which the force from the wing is acting on, thereby significantly reducing the potential stresses that may occur as a result of that. From a structural point of view, it is more reminiscent of a regular swan wing, just turned around so the front of the wing remains undisturbed. From an aerodynamic point of view, it should provide similar benefits to a reverse swan neck design, with the exception that some of the rear area of the underside and the top of the wing would have to be cut out for the support to come through, deeming it useless and potentially causing some disturbances in the area around it. However, it is speculated that since the biggest overall pressures and their gradients occur at the front of the wing, as it can be noticed in Figures 4.4 and 4.5, the areal occupied and disturbed by this design's supports should play rather a minimal role, thus making the detriment negligible. Some more potential drawbacks of that design could include, the complexity of wing design, as it would have to include slots for the supports to fit through; and the inclusion of the slots could affect the wing's structural performance.

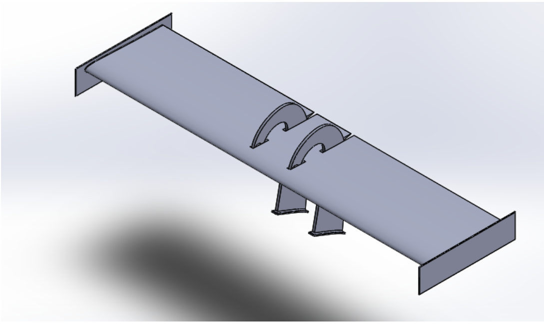

(a)

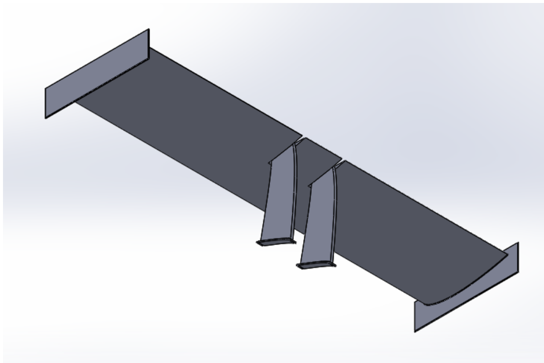

(b)

Figure 5.4. The scorpion tail wing mounting design shown from the top and the underside on the top and bottom images respectively. The front is on the left side of the images.

It has been decided that all three of the aforementioned designs will be attempted to be optimized structurally to a point where the design is satisfactory and the difference in maximal Von Mises stresses and maximum total deformations is negligible between the subsequent iterations. Thereafter, once all the designs are finalized structurally, these will be simulated aerodynamically, and based on their performance in both domains, as well as other considerations, a design will be chosen. The designs are going to be structurally simulated using ANSYS Static Structural module, with mesh refinements in the appropriate spots. The surface of the base of the bracket will be subdued to a fixed support, as this is to simulate as if the bracket would be mounted either to the car body or chassis. The load applied will be a bearing load applied to the cylindrical surface of the bracket, where the bearing is supposed to be placed. The load will consist of two components, horizontal and vertical, corresponding to drag and force components of the unfavourable load scenario stipulated in Section 4.4, with its respective drag and lift components of 158 N and 5958 N. This has been obtained through calculations, particularly by using the velocity at the unfavourable scenario applied to the Equations 2.3 and 2.4, where the area of reference is the plan area of the designed wing in the referred section; and the drag and lift coefficients obtained from the AirfoilTools source. This load has been chosen to be used for the simulations, as in the initial strength simulations it produced more detrimental results than if the coefficients obtained from simulations would be used, or if a vertical load of 6000 N would act on the bracket. Clearly the forces are halved, as there are two brackets over whom the forces are distributed. It has been chosen to simulate the brackets as if they would be made of epoxy carbon woven prepreg and structural steel materials available in ANSYS material library. The stress criterion for the epoxy carbon woven prepreg has decided to be achieving a maximal Von Mises stress value of below 190 MPa, which would yield a safety factor of at least three in relation to the ultimate compressive strength for the material equaling 570 MPa, as mentioned in Section 4.4. The reason for the inclusion of structural steel simulations is the fact that they are more likely to be accurate than the simulations for a composite material, due to numerous considerations regarding a composite material stated in Section 4.4. Also, structural steel serves as a meaningful reference material, whose results can be extrapolated to other materials. Moreover, the structural steel strength simulations can serve as a first step towards designing a steel skeleton or truss of the bracket, that could later be encapsulated in a composite material body. The criterion for the structural steel is a maximal Von Mises stress of below 100 MPa, yielding a safety factor of more than 2.5 for a yield strength of 250 MPa, being the yield strength of the structural steel material in ANSYS. An additional structural requirement for the bracket design is the total deformation being less than 40 mm for the composite material and 5 mm for steel. Furthermore, during the structural optimization it will be aimed to reduce the volume and drag inducing characteristics of the brackets. It is important to note that all bracket designs have the same thickness of 12 mm, which is to have sufficient space to accommodate the selected bearing, whose width is 8 mm and accessories to secure it in place. The simulation results are summarized in Table 5.1, featuring maximal Von Mises stresses and total deformations for epoxy carbon woven prepreg and structural steel bracket material, as well the volume occupied by all the three simulated bracket designs.

Wing Bracket Type	Swan Neck	Reverse Swan Neck	Scorpion Tail
Maximum Von Mises Stress (Epoxy Carbon Woven Prepreg) [MPa]	178.2*	184.9*	189.3*
Maximum Von Mises Stress (Structural Steel) [MPa]	67.4*	94.4	86.3*
Maximum Total Deformation (Epoxy Carbon Woven Prepreg) [mm]	8.0	34.8	5.8
Maximum Total Deformation (Structural Steel) [mm]	0.39	2.09	0.34
Volume [L]	0.627	1.210	0.902

Table 5.1. Table showing the results of the structural analysis of the wing bracket designs. *These stress values were observed in almost the same spot on the analyzed structures, which should not differ substantially between the designs. Therefore, these values are not advised to be directly compared between the designs.

Firstly, the swan neck bracket was about to be designed. The material area around the bearing cavity is meant to be rather small, as some of its volume would coincide with the one of the wing, and minimizing the wing's volume reduction is crucial for its structural and aerodynamic performance. This design feature led to stress concentrations being the largest in that area in the final design. Another design feature being aimed for is placing the necks preferably far from the wing itself, this is to reduce the airflow disturbances caused by the support necks interacting with the airflow around the wing by letting these disturbances occur far from the wing. To reduce the volume of and viscous forces acting on the bracket, the necks are aimed to be designed to be narrow. Each subsequent iteration was changed with these aims in mind, as well as improving upon the criteria established in an earlier paragraph. One very noticeable change that had too be made, was the inclusion of a plate by who's means the bracket would be mounted to the vehicle. This is due to the fact that during initial simulations, when the plate was not included there was a stress concentration point as a result of a boundary condition, which can be seen in Figure 5.5; and the inclusion of the plate got rid of that stress concentration point, proving the cause of the issue.

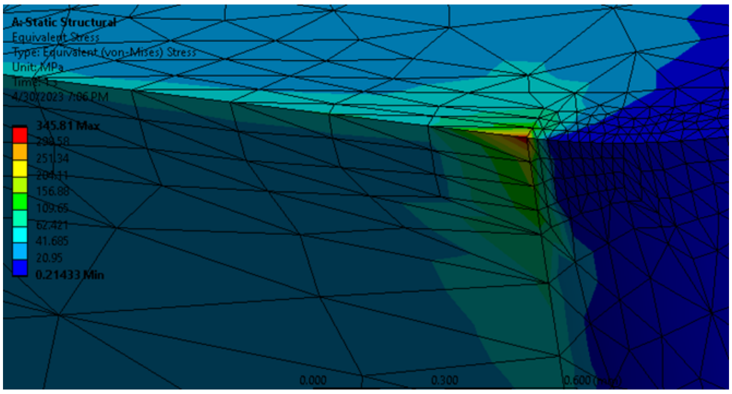

Figure 5.5. An image illustrating one of the structural simulations of the swan neck design where a stress concentration point occurred right at the boundary where the bracket was mounted. This led to the inclusion of a support base, eliminating the stress concentration point.

As it can be seen the maximum stresses occur in the cavity for the bearing, showcased in Subfigure 5.6b. Other significant areas of stress can be observed at the curved surfaces and where the inner curve meets the plate, depicted in Subfigure 5.6a. The maximal Von Mises stresses and total deformations, which are listed in Table 5.1 are well within the tolerance limit, deeming the design structurally satisfactory. The stresses achieved by this design are of the lowest magnitude out of the designed brackets; however, this should not be too conclusive, as these occur in an area that is common with the other designs. Volume-wise this design achieves the lowest value, which is likely due to its short moment arm and the fact that the bracket base being in front of the wing, has the shortest distance to the wing, due to the vehicle's rear curvature.

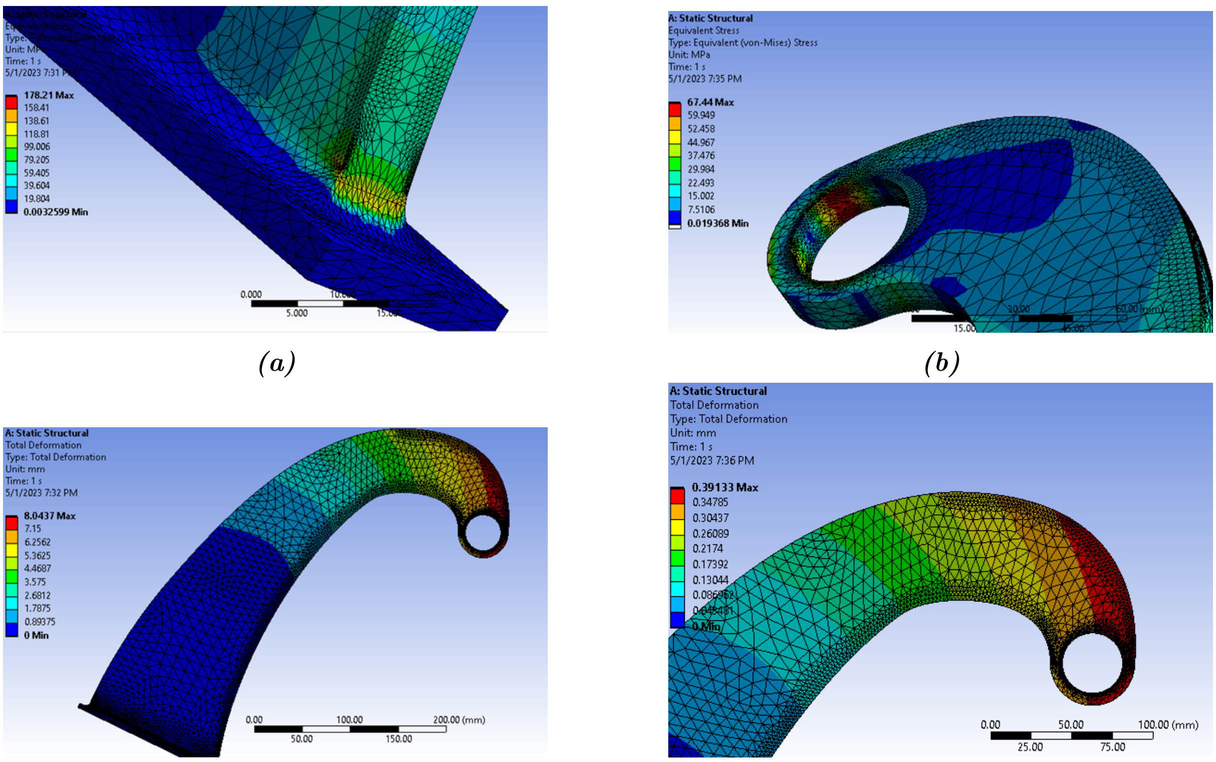

(a) *(b)*

(c) *(d)*

Figure 5.6. Visualizations of the structural simulations of the swan neck bracket design. The simulations were done for epoxy carbon woven prepreg and structural steel as materials for the bracket, shown on the left and right respectively. Von Mises stresses are shown in the upper images, while the total deformations are shown on the lower ones.

Secondly, the reverse swan neck was designed. Most of the considerations and aims were common with the swan neck design. Nevertheless, some of them differed; the plates through which the bracket would be mounted to the vehicle, just had to be close enough to the front so they do not stick out of the rear of the vehicle, and to reduce the volume of the bracket associated with it; the bracket neck was aimed to be just far enough from the wing to not notably interfere with it in terms of the structure and aerodynamics. One additional consideration was making the curvatures so the curvature gradient is minimal, while reducing the moment arm at which the bearing force would act on. Everything considered, after several iterations of the optimizing procedure, the final design was obtained, whose resultant stresses and deformations are listed in Table 5.1 and shown in Figure 5.7. In this case it should be noted that the maximal stresses occur both at the bearing cavity and the inner curvature for the composite material simulation, while the inner curvature is the sole zone of maximal stresses in the steel simulation, as it can be noticed in Subfigure 5.7d. This indicates that this design has an additional structural flaw in comparison to the other ones. Also, the deformation is much larger than in the other designs; this might have additional implications in terms of aerodynamics, as this leads to a geometrical change. The design is considered satisfactory as it passes the criteria posed upon it; however, the results of this design's simulations should encourage additional cautiousness around its structural integrity. Moreover, this design is the most sizeable, making it the least feasible in terms of weight and potentially having a detrimental effect on drag.

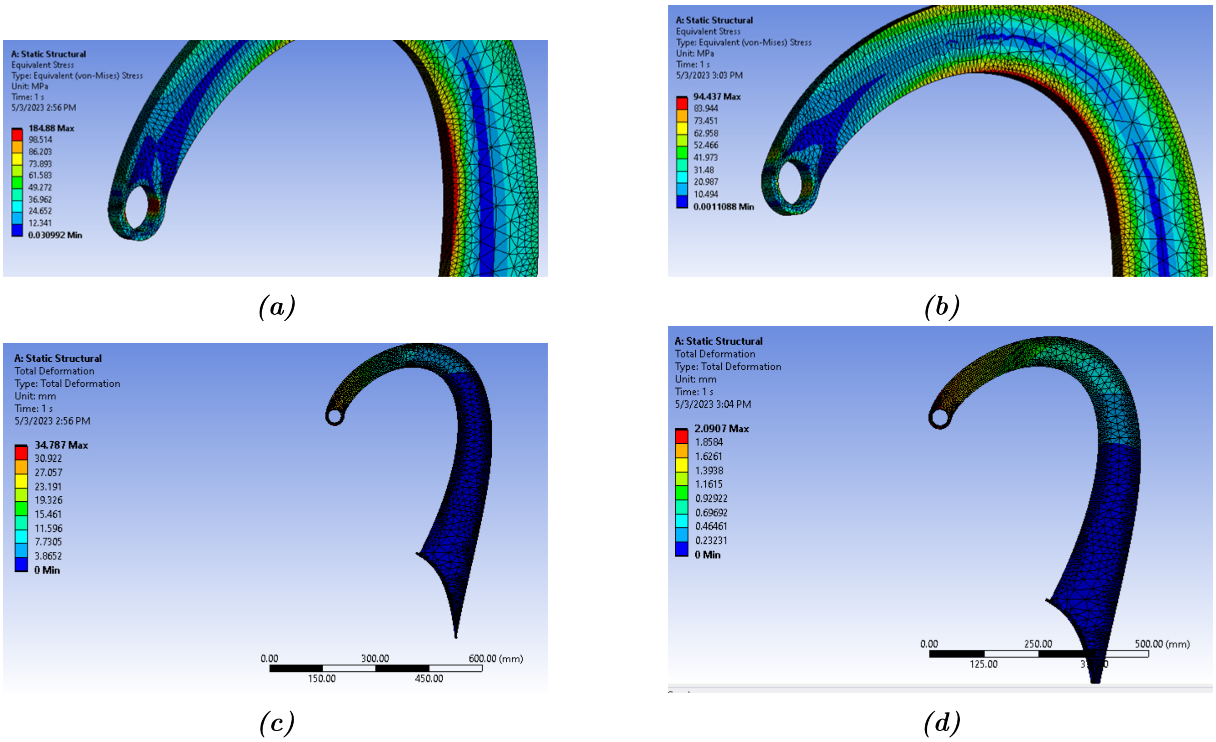

(a) *(b)* *(c)* *(d)*

Figure 5.7. Depictions of the structural simulations of the reverse swan neck bracket design. The simulations were done for epoxy carbon woven prepreg and structural steel as materials for the bracket, shown on the left and right respectively. Von Mises stresses are shown in the upper images, while the total deformations are shown on the lower ones.

Thirdly, the scorpion tail design was developed with significantly less iterations than the previous designs. This is due to the fact that the conclusive reasonings from the previous designs paved the way to a quicker achievement of the final design. Again, many of the objectives were common with the previous designs, such as maintaining a certain minimal curvature gradient to reduce the the stress concentrations; reducing the volume of the bracket; keeping the lever arm on which the forces from the wing are acting as small as feasible. On that note, the lever arm could not be too short either, as a lever arm that is too short would mean that the bracket and the wing would start interfering further to the front of the wing; and it should be aerodynamically advantageous for the interference to occur further rearwards, as it would lead to retaining a larger portion of the wing, and less of the wing surface closer to its front would be affected by the bracket. Just like in the case of the swan neck design, the largest stresses occur in the bearing cavity in the bracket as seen in the upper images of Figure 5.8. As of the composite material simulation, the maximal stress is the largest of the presented designs, yet this should not be particularly conclusive as this occurs in a zone that is common to all designs, and a slight change of the design of that zone should mitigate the stress occurring there. The second area of stress concentrations is the inner curvature of the bracket, however these stresses are of much lesser magnitude and are not of concern at this point. As of the total deformations, it achieved the smallest out of the presented designs, proving that this design yields the highest rigidity, as well as how significant structural advantage is achieved by shortening the lever arm in comparison to the reverse swan neck design. Regarding the volume occupied by the bracket, it is somewhat larger than the swan neck design, yet smaller than the reverse swan neck design. Its volume increase in comparison to the swan neck design, is primarily due to the increased distance between the base of the bracket and the wing, which again is a result of the car body's rear curvature. This distance could perhaps be shortened by repositioning the wing, however in order to keep the comparison consistent to a certain extent, it has been decided the wing be positioned on the same horizontal line in relation to the car body, making the vertical positioning the same between the designs. Nevertheless, the horizontal position of this design in relation to the others is offset slightly forward, this is due to the fact that if this would not have been done, the base of the bracket would be positioned in a very inconvenient position.

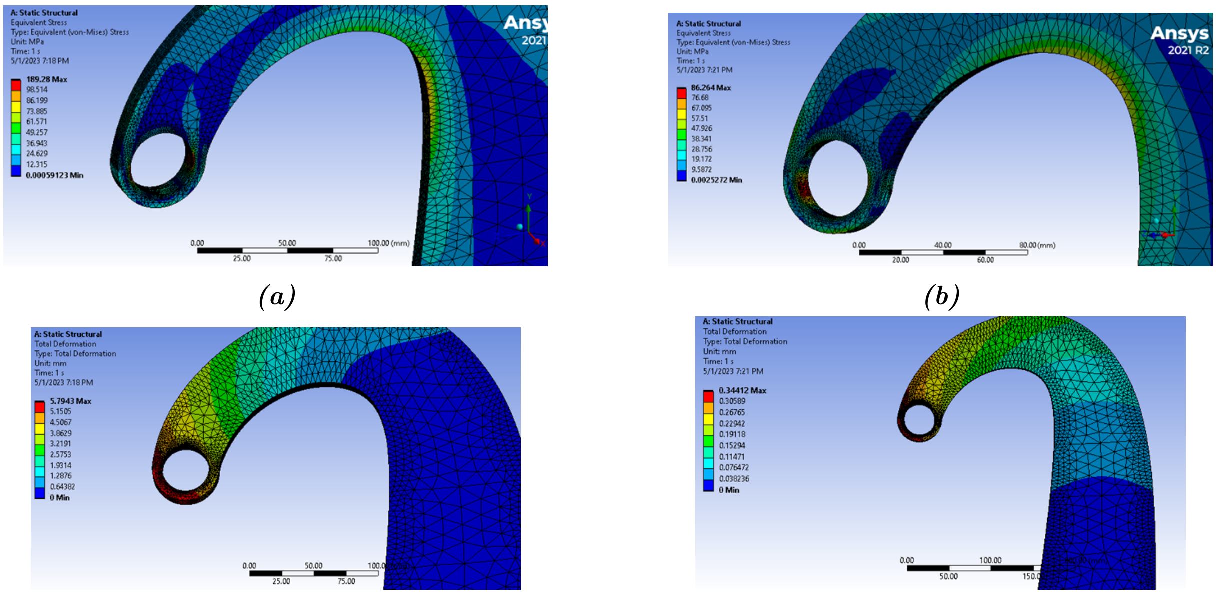

(a) *(b)* *(c)* *(d)*

Figure 5.8. Depictions of the structural simulations of the scorpion tail bracket design. The simulations were done for epoxy carbon woven prepreg and structural steel as materials for the bracket, shown on the left and right images respectively. Von Mises stresses are shown in the upper images, while the total deformations are shown on the lower ones.

Moving on, as the wing had to be modified for the scorpion tail bracket, it has been decided that it should be structurally analyzed with the usage of the same simulation procedure as for the wing with the cylindrical fixed support. As it can be seen in Figure 5.9, the simulation results are almost identical to the first one done on the wing with cylindrical support, seen in Figure 4.7; with the maximal stresses and deformations occurring in the same spots; and yielding slightly larger maximal Von Mises stress and total deformation of 94 MPa and 14.9 mm respectively.

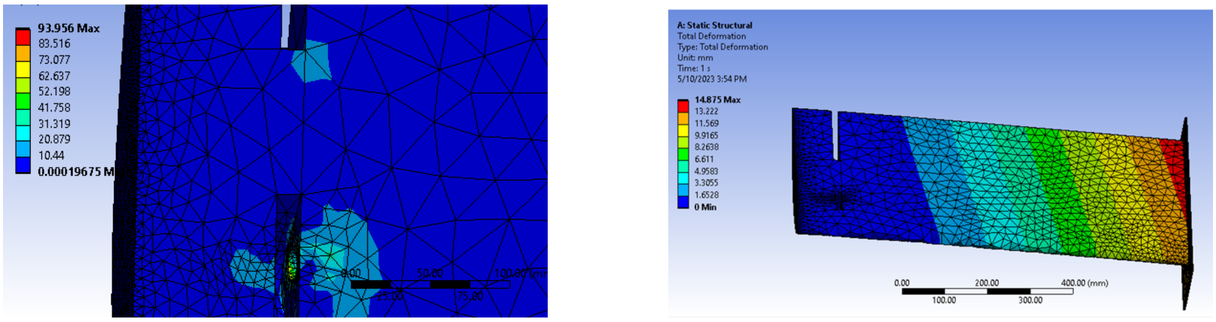

(a) *(b)*

Figure 5.9. Depictions of the structural simulations of the wing modified for the scorpion tail bracket, with Von Mises stresses and total deformations shown in the left and right pictures respectively.

5.3 Aerodynamic Validity of the Wing Bracket

As stated previously all the finalized designs from the previous section are going to be analyzed aerodynamically, by the means of aerodynamic simulations in ANSYS. The simulation settings and procedure will be similar to the one where the wing was simulated, with the relative fluid velocity of 75 m/s and 30 m/s.Nonetheless, two sets of simulation types will be performed; the first set of simulations will feature the shape of the rear of the vehicle with the exclusion of the gap between the body's underside and the ground, which can be seen on the simulation fluid body encapsulation shown in Figure 5.10; the reasoning behind that is that there is a substantial aerodynamic dependency between the car's body, rear wing and its brackets. This is due to the fact that the rear of the body dictates the fluid flow encountering the bracket and the wing, which are placed on and in a particular relation to the body. Consequently, the simulations feature a moving ground and a stationary no slip surface body in addition to the bracket and the wing, whereas these are regarded as a single entity in the simulations. The cord lines of the wings will be parallel to the ground, which may not necessarily be the same as an angle of attack equal to zero degrees. This is due to the fact that the vehicle's rear curvature is likely going to change the direction of the the airflow, potentially increasing the angle of attack, as the airflow may be deflected downwards, thus 'attacking' the wing at a positive angle. At this point, however, the airflow deflection angle at the rear is unknown. The simulation enclosure is vastly simplified, so the ground effects and airflow deflections caused by the front of the car are omitted in the simulation, as these are suspected to have a minimal effect on the rear wing. This set of simulation has been decided to be performed only for the higher of the mentioned velocities.

The second set of simulations was performed for both of the mentioned velocities, and the vehicle geometry is much simpler, as it consist solely of a geometry whose all surfaces are perpendicular to the inlet surface. This geometry is a solution to a problem related to negative drag that occurred in the first set of simulations, as after numerous simulations with different geometries imitating the rear of the car, this one yielded a positive drag. It is thought that this geometry is still representative of the rear of the vehicle, as the wing is likely going to be placed in proximity of a surface in the same manner as it is in this case, with the major difference lying in the surface's curvature relative to the axis of the inlet surface. Clearly, this set of simulations is unlikely to induce any disturbances similar to those occurring at the rear of a car, which is probably the reason why these simulations did not result in negative drag and converged much better, in the sense that the results converged in a small amount of iterations and the results practically did not differ from iteration to iteration after the mentioned amount of iterations. It is worth mentioning that the geometry in this case covers parts of the brackets that would otherwise be exposed due to the downwards curvature of the car. This is both a limitation and a convenience; the former is due to the fact that the way the brackets interact with the curvature of the car is one of their characteristic attributes; the latter is the case due to the isolation of the way in which the wing is interacting with the bracket, being the primary characteristic of each of the brackets. Apart from the geometry and the velocities, this set of simulations was set up in the same manner as the first one. The first set of simulations was not discarded, as it was thought that it should provide useful insights, that should be analyzed with caution.

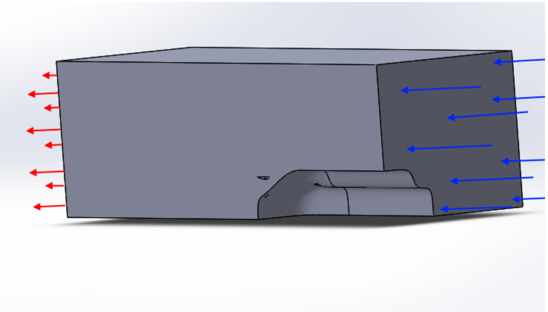

(a)

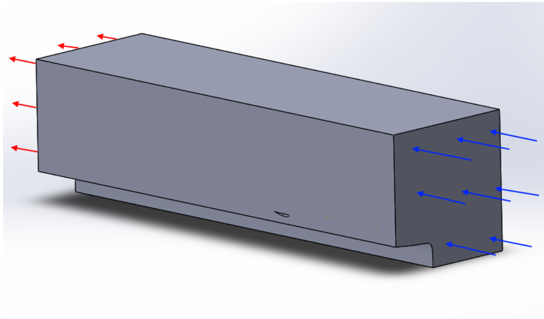

(b)

Figure 5.10. Illustration of the bracket simulation fluid body enclosures, with arrows indicating inlet and outlet in blue and red respectively. The cavities in the encapsulations are the car's body; and the wing and bracket entity, which are barely visible as they occur primarily inside the encapsulation. The encapsulations are shown from the symmetry wall side, the wall on the bottom is the ground and the rest of the walls are tunnel walls. The left subfigure represents the first set of simulations, while the right does it for the second set.

The final results of the aerodynamic simulations are summarized in Tables 5.2 and 5.3, for the first and second set of simulations respectively. It has been decided that it is the aerodynamic forces that are going to be displayed rather than coefficients, being due to the fact that the reference area varying between the bracket type and wing assemblies. What should be mentioned with regards to the first set of simulations is that throughout the iterations the obtained values varied, and they have been averaged between iterations where the values started oscillating around a seemingly average value; and it was made sure that the iteration range across which the averaging was applied, started and ended at approximately the same value, as well as a similar rate of change; for instance if the range started at a downward slope, it had to end at the same value occurring at a downward slope. It is important to mention that the value variation and oscillation regularity differed between different bracket design simulations; the swan neck had its values of interest oscillating in the most regular manner and were smallest in magnitude; the scorpion tail performed slightly worse in those terms, as its values were differing in less regular manner and variation was slightly larger; the reverse swan neck design simulation featured very irregular variation of the monitored values and their variation was also the biggest; therefore the trustworthiness towards the simulation results should be in the respective order, whereas the first two designs can be regarded as trustworthy, while the third should be interpreted with caution. It is also substantial to mention that the selection of the averaged iteration region is a somewhat subjective process, which could have an effect on the obtained data. The first set of simulations resulted negative drag, meaning they would suggest that the wing and bracket assemblies generated thrust, which is deemed to be impossible given the conditions taking place. Therefore, data from this set of simulations will be approached with caution and the drag data will be dismissed, due to its absurdity. As of the lift, it has been decided to take these into consideration, as their values seem to be reasonable based on the values from previous simulations, given the fact that the angle of attack is likely to be above zero, due to the airflow being deflected downwards at the rear of the car. The pressure and velocity contours also seem sensible, contributing to the confusion regarding attaining negative drag from these. The second set of simulations featured a significant variation in the magnitude of aerodynamic forces between different bracket types, leading to the encouragement towards a cautious analysis of the results. Regardless, since data from these sets of simulations is the only available data for the bracket comparison, it will act as an aid in guiding towards choosing the thought to be the best bracket type. An important remark is that the negative lift generated by the wing bracket assemblies in the simulations, cannot be fully attributed to the additional downforce acting on the vehicle as a result of the wing. This is because of the fact that due to the wing's close proximity to the car's surface, a fast moving air flows in the zone between the wing and the car's surface, creating low pressure or suction there, which will obviously generate downforce on the wing, since the suction occurs under the wing; as well as it will likely also create lift on the car's body, as a result of the suction occurring above it.

Wing Bracket Type	Swan Neck	Reverse Swan Neck	Scorpion Tail
Lift Force [N]	-2446	-2421	-2531
Drag Force [N]	-328	-292	-338

Table 5.2. Table summarizing the results of the first set of aerodynamic simulations of the wing brackets.

Wing Bracket Type	Swan Neck	Reverse Swan Neck	Scorpion Tail
Lift Force [N] at 75 m/s	-1065	-927	-1514
Drag Force [N] at 75 m/s	73	87	128
Lift to Drag Ratio at 75 m/s	14.58	10.61	11.83
Lift Force [N] at 30 m/s	-162.6	-143.4	-236.0
Drag Force [N] at 30 m/s	12.6	14.8	21.2
Lift to Drag Ratio at 30 m/s	12.90	9.68	11.13

Table 5.3. Table summarizing the results of the second set of aerodynamic simulations of the wing brackets.

As it can be seen in the Table 5.2 and 5.3, the scorpion tail obtained the largest values of lift and drag in both sets of simulations, with the lift being the most prominent outlier compared to the rest. This could be in some measure caused by the fact that its wing is situated slightly further forwards than for the other bracket designs in the first set of simulations. It can be inferred that this is essentially increasing the angle of attack of the wing, as the airflow is more inclined to follow the declined curvature of the body the closer it is to it, while it is more prone to be horizontal the further it is from the body. It is also stipulated that the rearward bracket placements provides the benefit of keeping the air clean and undisturbed and the front part of the wing, which generates the most downforce. The drag is likely the largest due to the fact that the brackets are obstructing the flow in a region close to where the flow has the highest velocity, that is nearby the suction zone under the wing. The depictions of the simulation results for the scorpion tail bracket design are displayed in Figure 5.11. It is worth mentioning that as in the case of wing simulations, aerodynamic simulation images provide a single frame of a dynamic circumstance that is taking place, thus making comparisons, especially in terms of recirculation regions, should not be peculiarly conclusive. This is inferring that the depictions of the aerodynamic simulations serve more as a general overview of the aerodynamic behaviour, rather than a comparison tool.

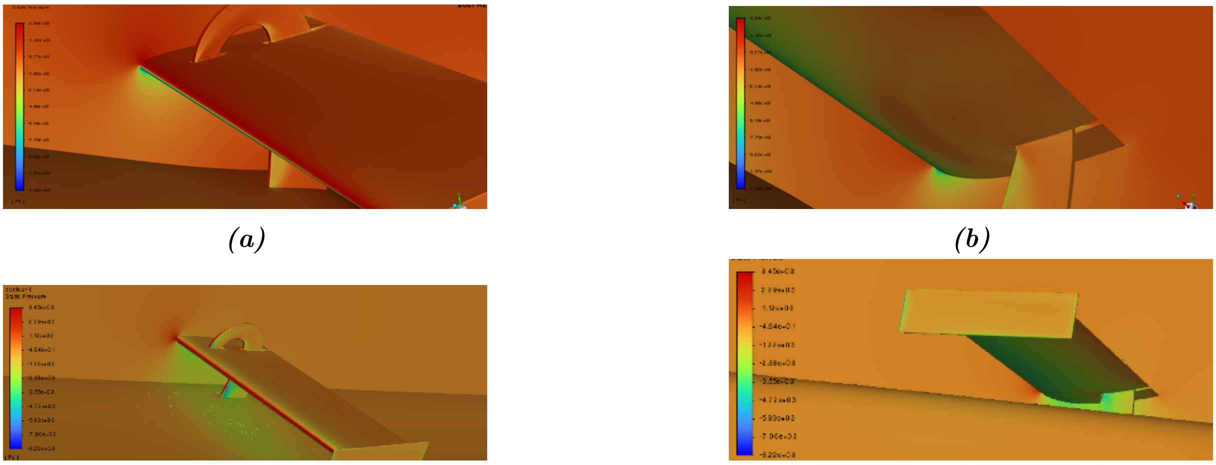

(a) *(b)*

(c) *(d)*

Figure 5.11. Depictions of the aerodynamic simulations of the scorpion tail bracket design, with static pressure contours from the first set of simulations in the top two pictures, and from the second set in the bottom.

As of the reverse swan neck bracket wing assembly, the low downforce value in both sets of simulations is a particularly surprising part, as beforehand it has been presumed that this configuration will, in fact, produce the most downforce. What could be at play in this case, is that the bracket itself might be generating positive lift, counteracting the advantages that have been stipulated for this design. Its drag being lower than the scorpion tail design is presumed to be as a consequence of it being further away from the region where the airflow is the fastest; the drag being higher than the swan neck design, can be attributed to the fact that the reverse swan neck bracket has more surface area. Its simulation results are displayed in Figure 5.12.

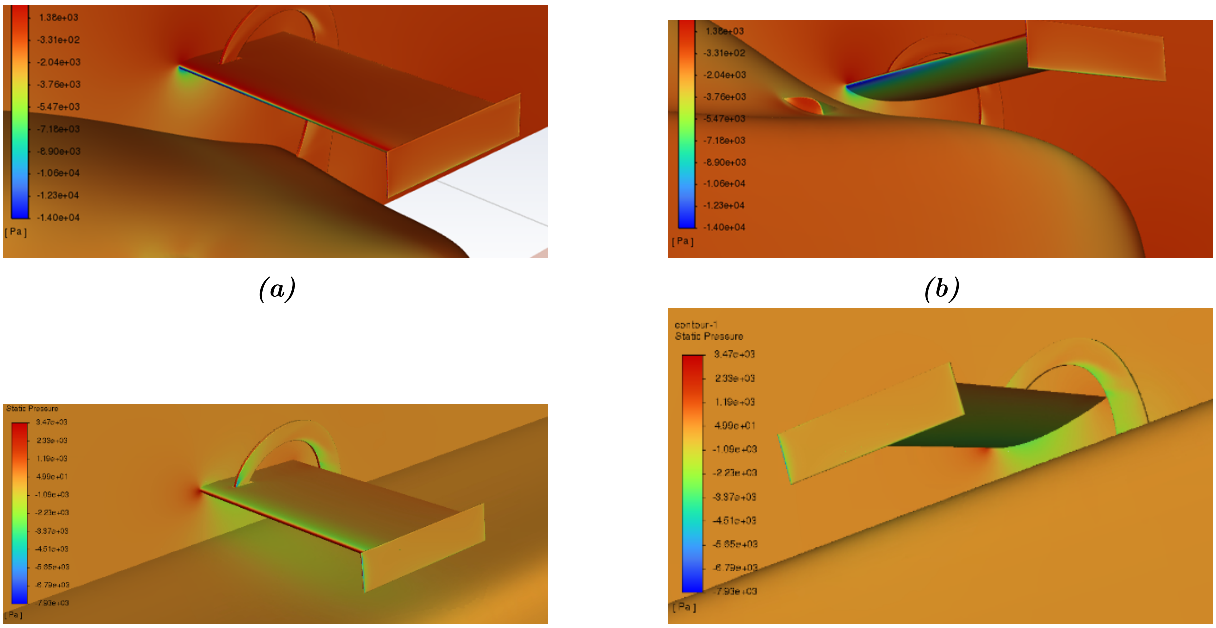

(a) *(b)*

(c) *(d)*

Figure 5.12. Depictions of the aerodynamic simulations of the reverse swan neck bracket design, with static pressure contours from the first set of simulations in the top two pictures, and from the second set in the bottom.

The swan neck design obtained lift values that fall between the ones of the other designs. This could be due to the presumed disadvantages of having the bracket in front of the wing, where the brackets being in front of the wing disrupt the airflow encountering the front part of the airfoil, being the part that generates the most downforce. Its low drag value can be explained by the fact that this design has the smallest surface area and the brackets are placed far from the the region where the air is moving the fastest. The simulation outcomes of this design are shown in Figure 5.13.

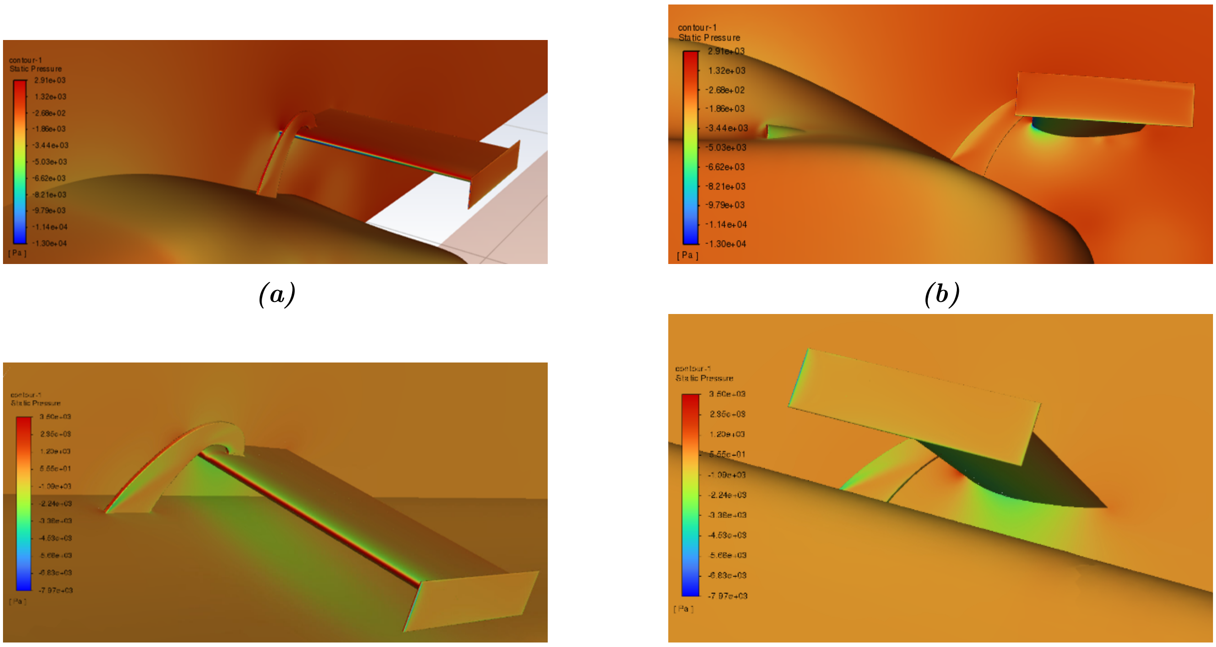

(a) *(b)* *(c)* *(d)*

Figure 5.13. Depictions of the aerodynamic simulations of the swan neck bracket design, with static pressure contours from the first set of simulations in the top two pictures, and from the second set in the bottom.

Subsequently, the scorpion tail design has been deemed as the bracket design of choice for this application. First of all, its downforce production is the largest in both sets of simulations, demonstrating a significant advantage over the other designs in that domain. Its drag, however, was demonstrated to be the largest according to the simulations, as well as its lift to drag ratio was inferior to the swan neck design. Nevertheless, it has been decided that the downforce generation is of the highest importance. Thus, given its downforce superiority, the scorpion tail passes the most important criteria to proceed in the design process. Yet, as stated previously, these simulations should be approached with caution, and the results cannot be fully trusted, thereby deeming the obtained results inconclusive to an extent. Secondly, mechanically it performs up to par with the swan neck design, without significant stress concentration regions that differ from the other designs. It has a slight volume disadvantage in comparison to the swan neck design, as well as the fact that the wing has to be altered in a major way; however, these are considered as rather small hurdles. Last but not least, this is an innovative design that has not been implemented before. As the DIS-car is meant to be a demonstration of engineering innovation, the scorpion tail bracket design is a compelling invention to exhibit a pioneering development.

Chapter 6
Final Remarks

Since the primary active aerodynamic components and the car body are designed, the next step would be to apply them to the whole assembly of the car, as well as develop the necessary supplementary components. As the aerodynamic and other parameters of the design are known, the design should be benchmarked, to obtain data regarding the performance of the car in different configurations. When the active aerodynamic parts of concern for this project are designed and their performance implications known, a control scheme should be developed.

6.1 Final Assembly

As it has been stated before, the front wing design is based on the rear wing design. The same airfoil and size have been decided to be used, with the main difference lying in the top view shape of the wing, as the wing has been decided to be simply cut out in the area that it would coincide with the car's body, both from the top view and when changing angle of attack. Another difference lies in the endplate design, as the endplates have been made smaller to account for the fact that the wing is much closer to the ground, and a certain clearance should be ensured, even when the wing is tilted. Unlike the rear wing, since the front wing practically encounters air that is not substantially disturbed by other objects, its true angle of attack is assumed to be equal to the angle it has relative to the ground. Therefore, simulations that were done for the rear wing will be omitted for the front wing; although, it can be stipulated that the front wing can have a potent effect on the aerodynamics of the rest of the vehicle. Also, due to the already extensive amount of performed wing simulations, it has been decided that front wing simulations will be omitted completely. The shafts and bearings holding the wing are going to be the same as for the rear wing, as the front wing is expected to generate less downforce, due to its reduced wing area. The front wing design can be seen in Figure 6.1.

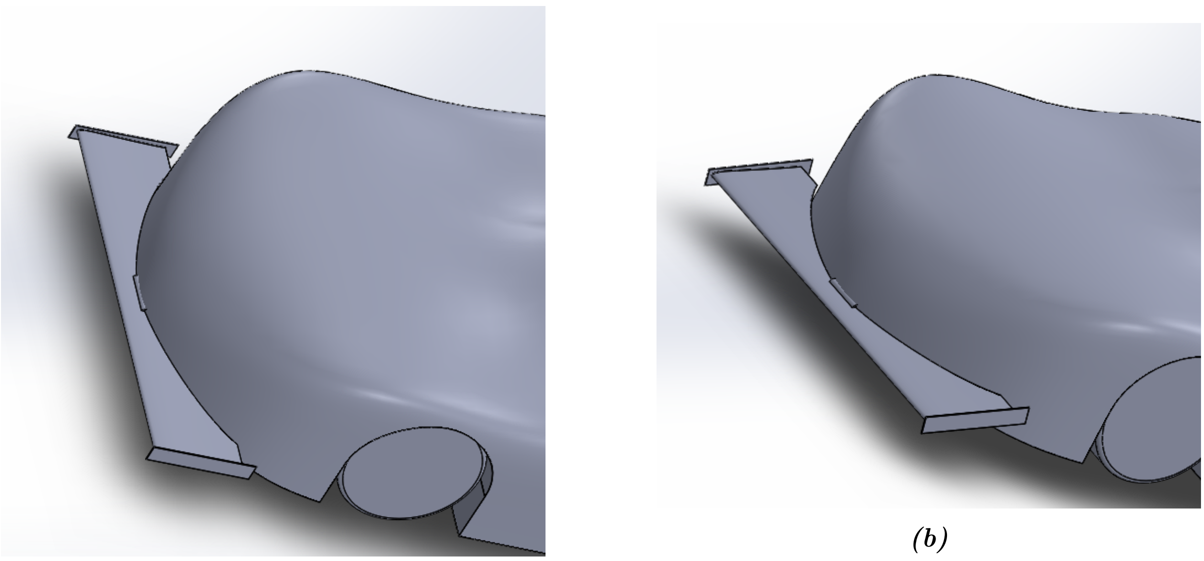

(a) *(b)*

Figure 6.1. Depictions of the front wing design positioned at 0 deg and 15 deg angles of attack on the upper and lower image respectively.

It can be seen that when looking at the final car body design from the side, in Subfigure 6.2b, that its area facing that plane is larger behind the center of mass than in the front, increasing the likelihood of its sideways center of pressure being placed behind the center of mass, which is a desirable trait. As mentioned in Section 2.3 it should make the car more yaw stable, as sideways airflows should not increase the car's probability of increasing the steering angle caused by the sideways airflow, when the car is moving forwards. Since the rear wing generates more downforce than the front one, it is likely that the car's longitudinal center of pressure is shifted backwards, biasing it towards understeering.

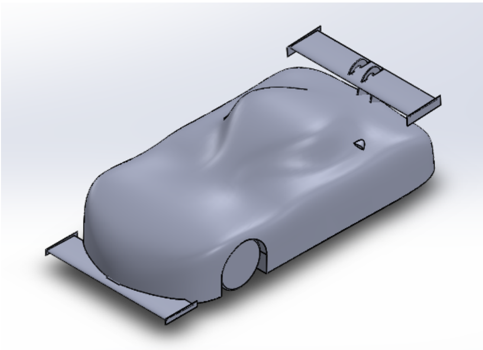

(a)

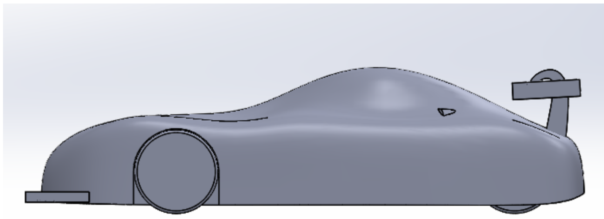

(b)

Figure 6.2. Images of the whole car design, with the left image showing the car in isometric view, while the right one shows it from the right side.

It has been decided that the wing would be actuated by the means of a servo motor. This is due to the fact that servo motors are electric motors whose position can be simply, accurately and quickly controlled, which are the desired characteristics demanded from the wing actuation. Additionally, these motors tend to be compact and low in weight, as well as their utilization finds its place in domains such as robotics or radio controlled model airplanes and cars, whose control might be reminiscent that of an active aerodynamics device. In order to determine what motor will be selected, the actuation mechanism should be developed.

In most known active aerodynamics, the actuation tends to occur through the usage of linear actuators, whose movement is driven either mechanically or hydraulically. However, in the former case the geometry between the motor placement to the actuated component, has to be rather simple, so the linearly moving components can move freely, in the latter case the mechanism tends to be rather heavy; leading to the conclusion that developing an alternative way of active aerodynamics actuation might be an apt attainment. One of the primary challenges is the shape of the wing bracket, as it features almost a u-turn, making force transfer and actuation difficult. To overcome this, a solution using a worm gear drive to power the shaft, to which the motor is providing power via a flexible shaft was invented. The reason a worm drive appears to be a suitable solution, is that it provides plenty of flexibility in terms of how much reduction can be achieved and it should not have a significant impact in terms of additional forces caused by the implementation of the mechanism. More, a worm drive tends to be non/reversible in most cases, this provides with the benefit of the lack of necessity of transmitting any torque to the worm screw in order for the wing to be stationary. Drawbacks of worm drives include decreased efficiency of the transmitted power, relatively high wear and cost; notwithstanding, these are not considered concerning for this application, since the mechanism is not expected to operate for loads of cycles, nor are cost and efficiency concerning. A flexible shaft was chosen, due to its flexibility in terms of of shapes it can transmit power through, thus making it magnificently befitting solution to the problem. The primary problem of a flexible shaft for this application is the fact that a torsional angle proportional to the applied torque becomes a factor, which can have a considerable effect on the position control of the wing, as well as might potentially add a delay between the applied position of the motor shaft and the position of the worm gear. These flaws can potentially be mitigated with proper modelling of these phenomena, to then utilize these models in the control scheme of this device.

The components for the described arrangement have been selected based primarily on the torque that needs to be transferred from the motor to the worm drive. This can be determined by the amount of torque needed to turn the shaft after the reduction from the worm drive. However, the gear ratio has to be determined first, which again is dependent on the desired torque input from the motor and its rotational speed. Therefore, the gear ratio, as well as motor and flexible shaft selection happened concurrently. The gear ratio has been determined to be 42:1; assuming 82.6 Nm needed to turn the shaft under the previously speculated unfortunate conditions, it would yield 1.97 Nm necessary to turn the worm screw in the worm drive. An additional requirement is to be able to turn the wing quickly enough; as a result of this it has been stipulated that the a 30 deg angle change should occur in less than quarter of a second, yielding the necessary motor speed of at least 210 RPM. For this purpose a Wittenstein servo actuator with the order code of ARSQ038B030C8C1BSHM1PSNBUN was selected, offering a rated torque of 2.4 Nm with a permanently permitted speed of 408 RPM and weighting 0.89 kg (49). The flexible shaft selected for this application is a FIAMA TR with a diameter of 6 mm (50), whose length is expected to be between 500 mm and 800 mm. It should be acknowledged that there will be two of these setups, each on its corresponding bracket, driving its own shaft. The actuation design assembly can be seen in Figure 6.3.

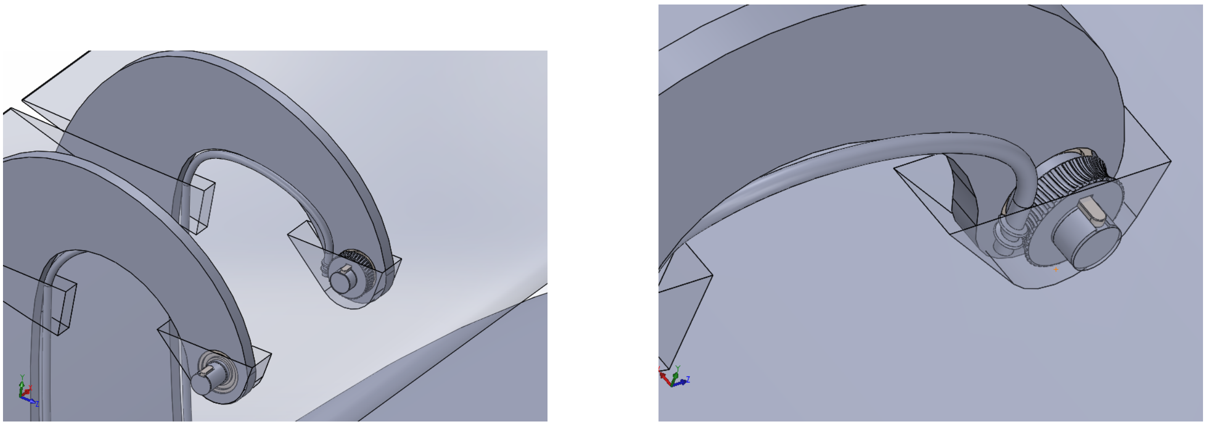

(a) *(b)*

Figure 6.3. Images of the actuation mechanism of the wing. The object resembling a pipe or a tube following the curvature of the bracket is the flexible shaft, which is coupled to a worm screw, which is then driving the worm gear coupled to the shaft transferring the torque to the wing via keys present on it.

The depicted illustration of the solution is there to provide an overview, the details remain to be determined, for example the flexible shaft would probably need mounting clips to maintain its shape. As of the shaft and its assembly with the worm gear and the bearing, it is depicted in Figure 6.4. There it can be seen that the worm gear would transfer its torque to the shaft via a key, and its axial position would be held in place by a set screw, whose hole can be seen in Subfigure 6.4b. The bearing would be held in place by an external retaining ring on one side and a shaft shoulder on the other, preventing it from moving axially. The same concept could be applied to the way the bearing, thus also the shaft would be held in place relatively to the bracket; with the exception being that the retaining ring would be of the internal type, and the shoulder would be replaced by its hole equivalent, a counterbore that is. Another important remark in the shaft assembly would be the inclusion of endstops, preventing the wing from rotating too much in either direction in case the existing actuation mechanism would get damaged. This is simply implemented in the wing design by having the cavities that allow the ends of the brackets where the bearing is situated to be within the side profile of the wing airfoil. These cavities are shaped in a way that allows the wing to rotate within a certain angle range, which when exceeded will cause the wing to come in contact with the brackets, thus preventing it from rotating any further.

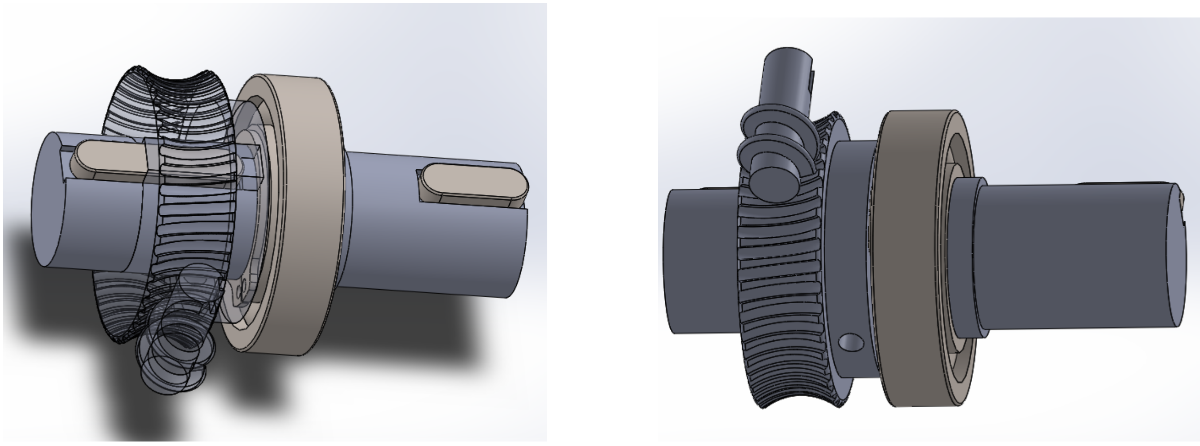

(a) *(b)*

Figure 6.4. Images of the shaft assembly, where the worm gear, keys, mounting clips and bearing are situated on the shaft.

6.2 Benchmarking

In order to evaluate the performance of the design, benchmarking should be performed. Firstly, aerodynamic simulations of the car body with its active aerodynamic components in their two characteristic positions should be performed; minimum drag position and maximum downforce position. However, when attempting these simulations, they yielded results that were deemed invalid, due to yielding negative drag on certain parts and magnitude of the aerodynamic forces that hardly corresponded with previously performed simulations. Consequently, it has been decided that the necessary aerodynamic characteristics would be extrapolated based on the available data so far. Then, knowing the aerodynamic attributes of the car in these positions, along with its total weight, the car's potential performance statistics can be calculated, giving an educated prediction of its performance and thus allowing to examine whether the initially set goals are obtainable. It should be mentioned that the obtained benchmarked characteristics are foreseeing an optimistic scenario and are not considering many aspects that may occur in real conditions, thus these should not be perceived as the ultimate capabilities of the vehicle.

As already mentioned, due to invalid whole car simulations, its aerodynamic attributes will be extrapolated from the available data. The drag of the car will be estimated based on Equation 2.4, where the reference area and the drag coefficient, will be those of the car body itself, yielding $1.902\,\mathrm{m}^2$ and 0.28 respectively; to that the doubled drag of the scorpion tail design at $30\,\mathrm{m/s}$ from Table 5.3 will be added, adding additional $42.4\,\mathrm{N}$ of drag force, denoted as $F_{D_{add}}$. The reasoning behind doubling the force obtained in the mentioned table, is that there are two wings that are implemented, and despite the fact that the front wing is likely to generate less drag as a result of its decreased wing area and lack of brackets; the doubling is meant to offset the potential detrimental drag effects resulting from the airflow being disturbed by the wings when flowing around the car body. As of the downforce, it is assumed that what the whole car assembly will generate will be the sum of the lift generated by the car body itself and the wings, which together are presumed to generate 125 % of the rear wing downforce listed in Table 4.2 at 15 deg angle of attack. The same will be assumed for the drag in when the car operates in that setting. The wing downforce being enlarged by 25 %, is a consequence of the assumption that the rear wing would produce 80 % of the total downforce of the active aerodynamic components. Likewise, corresponding drag values from the same table will be used when accounting for it in that setting.

The cornering abilities of the car will be evaluated in its high downforce and drag setting, that is wings with an angle of attack of 15 deg. The resulting downforce at any speed will be a sum of the equations for car's lift, as well as the rear wing's lift multiplied by the aforementioned enlargement; where each equation will feature a corresponding lift coefficient, being a form of Equation 2.4. Using the mentioned assumptions and the assumptions from Section 4.2, Equation 6.1 can be attained for the required speed to generate sufficient downforce for he car to handle the specified lateral acceleration G_l of 1.86 G, being the speculated peak of the current production car record holder at Nurburgring. All the constant stay the same as in the section where the wing sizing was being determined, with the exception that the car mass m_{car} is now larger. Also, taking the mentioned magnification of the rear wing downforce to account for the front wing is done by the usage of the coefficient η_{mag}, equaling 125 %, being multiplied by the lift coefficient of the wing $C_{l_{wing}}$ and its reference area A_{wing}. Everything considered, the equation yields a required velocity v_{req} of 86.6 m/s, being almost 9 m/s more than Mercedes AMG One achieved at that turn and more than 11 m/s faster than the speed at which the wing was calculated to generate sufficient downforce. The reason why the active aerodynamic seem to underperform in this instance is that the rear wing contribution has been changed compared to what has been assumed in Section 4.4 and the mass of the vehicle has increased in the current calculation. If the downforce magnification coefficient η_{mag} would equal 133 %, which would correspond to 75 % rear wing contribution to the total active aerodynamics dowforce production; then the required speed around the corner would equate to 77.6 m/s. To evaluate the vehicle handling from another perspective, the lateral acceleration the car should be able to handle on a flat surface at a specified velocity can be calculated using Equation 6.2, where the normal force N is a sum of the car's weight and the net lift aerodynamic forces acting on it, which in this case would be lift from the car's body and the downforce from the active aerodynamics. For the velocities of 75 m/s and 30 m/s the lateral accelerations would equate to 1.48 G and 1.33 G respectively. Based on that it can be inferred that at lower velocities, such as the latter of the recently mentioned, the active aerodynamics does little to no difference in terms of car handling.

$$v_{req} = \frac{(\frac{G_l}{\mu} - 1 - G_c) \cdot m_{car} \cdot g}{\frac{1}{2} \cdot \rho \cdot (\eta_{mag} \cdot C_{l_{wing}} \cdot A_{wing} - C_{l_{car}} \cdot A_{car})} \tag{6.1}$$

$$G_{flat} = \mu \cdot \frac{N}{m_{car} \cdot g} \tag{6.2}$$

The car's range will be estimated based on Equations 6.2, 6.2 and 6.2. The range distance d_{range} is obtained by dividing the vehicle's total energy capacity E_{tot} of 58.3 kW obtained from Table 2.1, by the total resistive force F_{res} acting on the vehicle. This force is described by Equation 6.2, and is a sum of the rolling resistance F_{rr}, drag force F_D acting on the car's body and the drag force $F_{D_{add}}$ acting on the active aerodynamic components. Equation 6.2 describes the rolling resistance as a product of the tyre rolling resistance coefficient C_{rr} and normal force N.

The tyre rolling resistance coefficient is attained from Table 2.1, yielding a value of 0.013. The normal force is assumed to be solely affected by the car's mass, which is due to the fact that the car in that setting is not expected to produce substantial downforce. Nonetheless, the car is more massive than before, as the bodywork and active aerodynamics, along with the actuation components should be taken into account as well. Using Solidworks' evaluation tool the volume of the aforementioned additional components can be obtained, yielding 97.5 L. Assuming all of these are made of the same carbon fiber composite that was evaluated in the previous chapters, and that the whole volume is occupied by material, with the density of 1.6 kg/L (39), it results in an additional weight of 156 kg. The actuation components are presumed to weigh 6 kg in total based on the fact that four motors will be implemented with necessary cabling, as well as supplementary components such as shafts and bearings; this gives rise to the total car mass to be estimated as 862 kg. An average velocity of 20 m/s (72 km/h) will be assumed for the drag force equation, being a speed that is close to one that one may experience when driving on the road. With these in mind, the vehicle's range is calculated to be 749 km, which considerably overshoots the 400 km range set as a goal for this car. This could be attributed to the fact that the car is relatively light, has a low overall drag and its total energy capacity is high for its weight. Also, the range distance equation does not take into account mechanical and electrical losses in the car itself, neither does it consider factors such as elevation changes, acceleration and deceleration. Yet, the car can be quite surely assumed to be able to exceed the range goal set for it, as the mentioned considerations should not cause a range loss of a magnitude leading to it falling below the specified goal. Concerning the goal of 50 km track range, the problem is going to be vastly simplified by assuming that the car is driving at a constant speed of 75 m/s around a one mile oval track, which is just above the average speed on such a track for NASCAR vehicles (51). Additionally it will be assumed that the car is in the high downforce and drag setting for the whole duration, thus taking into account its contribution in Equation 6.2. With these in mind, the estimated track range is 89 km. Again, as in the previous case many considerations have been omitted, therefore the actual range is likely to be lower; yet again the range exceeds the track range goal to the point, where it should be reached despite the setbacks associated with these.

$$F_{rr} = C_{rr} \cdot N \tag{6.3}$$

$$F_{res} = F_{rr} + F_D + F_{D_{add}} \tag{6.4}$$

$$d_{range} = \frac{E_{tot}}{F_{res}} \tag{6.5}$$

The maximum car speed is going to be obtained using the same assumptions as when calculating the potential range of the vehicle, with the difference lying in the wing drag contribution, as it will rather be based on the drag coefficient attained from Table 4.2 at 0 deg angle of attack. To attain the maximum velocity the principle that power is a product of force and velocity is used. In this case the force is the sum of resistive forces, being the drag and rolling resistance forces; the velocity is the maximum velocity; and the power is the total continuous power of the motors present in the car equaling 384 kW as stated in Table 2.1. On that basis Equation 6.2 is obtained, which is not the final form of the equation to obtain the maximum velocity, but rather a form that is meant to be solved computationally. This is due to the fact the drag being a part of the resistive force in this equation, constitutes partially of the maximal velocity squared itself, making the equation considered to be too complex to solve analytically, thus leading to deciding to resolve it using MATLAB solve function. With the aid of this tool, one real number solution has been obtained, resulting in the maximum vehicle velocity to be 105 m/s or 378 km/h. Nevertheless, it is unlikely that the car would be able to achieve that speed in a straight line, as inefficiencies, cooling, gear ratios and other phenomena have not been taken into consideration.

$$v_{max} = \frac{P_{cont}}{F_{res}} = \frac{P_{cont}}{F_{rr} + \frac{1}{2} \cdot \rho \cdot (C_{l_{car}} \cdot A_{car} + C_{l_{wing}} \cdot A_{wing}) \cdot v_{max}^2} \tag{6.6}$$

6.3 Control

One of the primary premises of active aerodynamics is the fact that it can be controlled. The simplest control schemes could be either manual, or based on a simple proportionality between the steering angle and the shaft position of the servo motors. However, these are unlikely to yield an optimized performance, therefore a more sophisticated control should be developed. Yet, it is important to keep in mind, that the control scheme developed here is just to showcase the principles of how a developed controller would work, thus omitting plenty of details and nuances.

The control of the active aerodynamics will occur by the means of receiving necessary inputs, that will then dictate the output to the servo motors, by being transformed using necessary blocks in the control scheme. The primary input to the control system would be the reference signal, which in this case would be the steering wheel angle. In simple terms, the steering wheel angle represents the desired corner radius the driver intends to make. The second input to the system would be the vehicle velocity, based on which in combination with the intended corner radius the lateral acceleration experienced by the car would be calculated. This can then be used to obtain the necessary normal force to provide grip for the car to handle the corner, which again can be translated into the resulting suspension compression of the car. This calculated suspension compression can then be compared with the measured suspension compression, that would then yield an error, or rather the deviation from the desired value. This error would dictate how much the angle of active aerodynamic components would need to change, which again could be translated to the shaft position of servo motors.

The steering wheel angle input could be measured with a dedicated sensor, which many vehicles are equipped with by default; alternatively, the front wheel steering angle could be measured directly by measuring the movement of the steering rack. The car's velocity input, could simply be read from the speedometer data, which is oftentimes data from sensors measuring the vehicle's wheels rotational speed. The suspension compression could be measured using proximity sensors, or other sensors capable of measuring short distances in a confined space; these would be placed within each suspension's coils springs center. The data from these used to generate the error could be used in several manners, yet two methods are considered the most sensible; using the averaged data from all the suspension springs or using data from the least compressed spring. At the first glance the former seems to be the most representative of what is happening with the car in terms of suspension compression; however, it could overlook the fact that some wheels would not be pressed to the ground with sufficient normal force to provide them with the required grip to make the corner. The latter would try to make sure that every wheel is pressed to the ground with at least the required normal force to make the corner, as the least compressed wheel would dictate the error to be corrected by the controller. This is a much more reassuring way of providing grip to the wheels, but on the other hand it is likely to provide an abundance of grip, producing more downforce and drag than necessary as a result. Concerning the output, it could be a single change in angle of both wings adjusted for mapping. What is meant here is that it might be the case that for every degree of angle change of the rear wing, the angle change of the front wing would be a fraction of that.

A simplified control scheme is presented in Figure 6.5 constructed using Simulink; there the steering wheel angle denoted as $steer_ref$ along with the velocity input v squared enter a Mux block, where these are combined into a virtual vector, thus permitting to enter two vectors into the first transfer function block, marked as $Transfer_Function1$. There, the mentioned inputs get converted into a desired suspension compression output des_susp_x, which then gets compared with the actual measured suspension compression, yielding an error signifying the difference between the measured and desired suspension compression. That difference is then processed by a controller, which in this case could be a simple PID controller. The output from that controller would then enter another transfer function block $Transfer_Function2$, to be translated to the required motor position $motor_pos$ to tilt the wings to an angle that would induce the necessary downforce to exhibit the desired suspension compression.

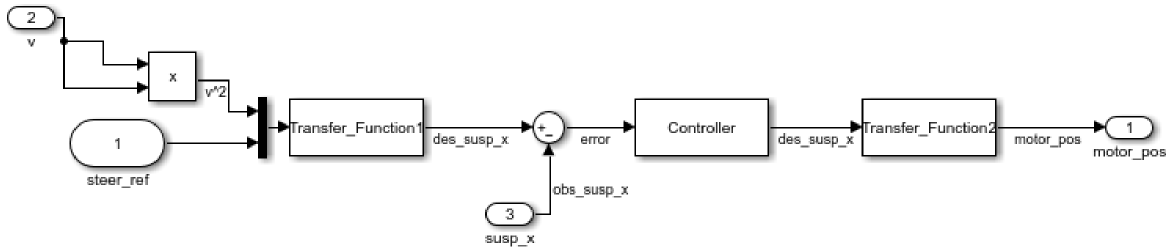

Figure 6.5. A simplified block diagram showing the control scheme for the active aerodynamic components.

Alternately, a multiple-input-multiple-output (MIMO) scheme could be implemented, where the suspension compression data would be divided between front and rear suspensions, as well as the outputs to the servomotors to the front and rear wing would be separated. Clearly, the coupling between the rear suspension compression data and rear wing angle would be much stronger than a contrary coupling; yet, it cannot be discarded that there is a meaningful coupling between the opposing sides. On that basis, a diagonal relative gain array may not be be the optimal control solution for that case; although it would be the simplest, as then the rear wing angle would only be directly coupled to the rear suspension compression in terms of control, with an analogous situation for the front wing angle, thus keeping the control loops separated.

Concerning the braking control loop, it is thought that a simple open loop gain based control could be applied, where both wings would be tilted proportionally to the brake pedal, perhaps including some deadzones close to the operating range ends of the pedal. Additionally, a slight bias towards the rear wing could be implemented to counteract the forwards balance change when the car is decelerating. As of the wing angle as a function of speed in a straight line, what could be done is that the wings would tilt sufficiently to counteract the lift generated by the car body, when the car velocity surpasses certain velocity value.

Chapter 7
Discussion

This chapter will focus on discussing the overall results of this project. This is to gain an overview over the whole project and aid in evaluation and later conclusion.

7.1 Simulations and Accuracy

As it has been mentioned before negative drag has been obtained in some aerodynamic simulations, particularly ones where the wing was simulated in an enclosure domain, which included only the rear of the vehicle and the bracket wing assembly. Also, simulations of the whole car with active aerodynamic components have been performed, these also yielded negative drag on the rear wing, but not on the front; in fact the results were reminiscent of those where only the rear of the vehicle was included in the domain. The whole body simulations due to their invalidity were deemed to be excluded from the analysis in this project. This leads to the conclusion that there is some phenomena occurring at the rear of the vehicle in the simulation domain triggering these seemingly invalid results. Therefore, in Section 5.3 another set of simulations was performed, which featured essentially a highly defeatured version of the first set of the rear wing bracket simulations. This set of simulations was, in fact, one of many rear wing bracket simulation types that led to this particular one. All of these differed in the enclosures tested, which were alterations of the enclosure from the first set of simulations, being depicted in Figure 7.1.

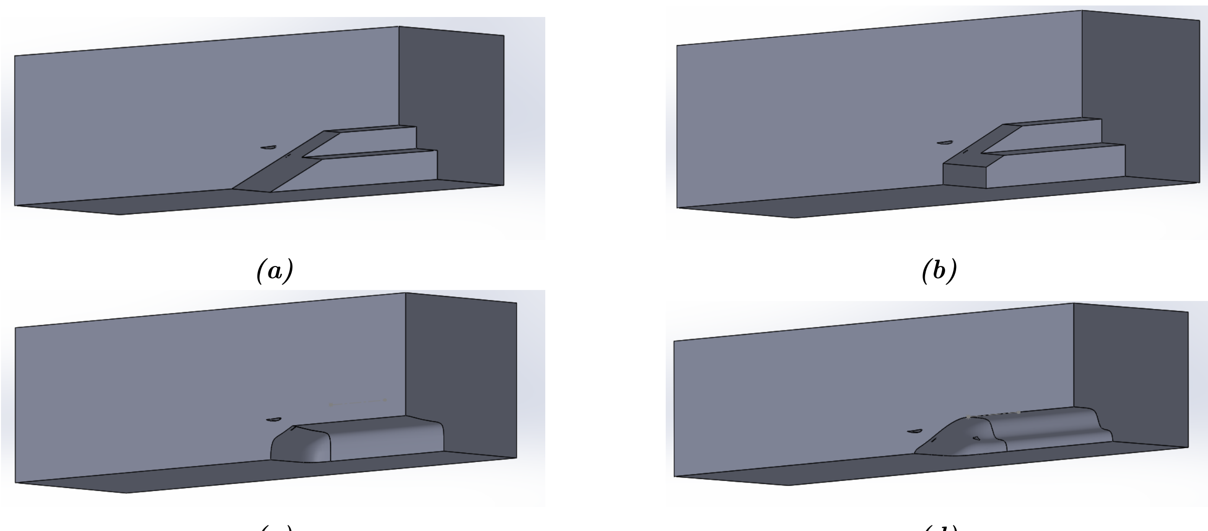

(a) *(b)* *(c)* *(d)*

Figure 7.1. Depictions of some of the developed enclosures to determine features that could be the culprit behind the attained negative drag in the first set of simulations in Section 5.3.

Each of the altered versions of the enclosures altered in a way to get rid of a certain feature that could be the cause of the negative drag. In Subfigures 7.1a and 7.1b the initial enclosure had its shape vastly simplified, getting rid of any round edges and making the geometry as simple as possible, yet still resembling the shape of the designed car body. The former of the enclosures features a constant slope at the rear, which was to see whether it is the change in curvature that has to do with obtaining a negative drag in simulations; while the latter is primarily testing the geometry complexity effect on it. The Subfigures 7.1c and 7.1d are meant to simulate which part of the rear curvature is the culprit of the drag simulation issue. All of these enclosures were simulated for one of the bracket designs, and all of them exhibited negative drag during simulations, leading to the conclusion that none of the tested features in isolation was the culprit. Based on that fact and that the enclosure used for the second set of wing bracket simulations in Section 5.3 did not yield a negative drag, can lead to the verdict saying that the change in curvature, geometry complexity, lower part or upper part of the rear of the vehicle are not the cause of negative drag in simulations in isolation; it is rather implying that the negative drag may be due to a downwards curvature being present at all in a close proximity of the wing, as this is the primary lacking feature in the enclosure used in the second set of the aforementioned simulations.

More profoundly, the root cause behind the negative drag is even more difficult to determine based on the available results. There could be several causes at play, including ill constructed mesh, wrongly configured simulation settings or faults in post-processing. These have also been attempted to be tested by for instance applying different meshes or changing simulations settings. Yet, since these can be configured in a tremendous number of ways, it does not seem like much can be concluded from it. Alternatively, it can be inferred that perhaps the negative drag has a physical merit; by for example being caused by the lowered pressure behind the vehicle or fast moving air slightly in front and below the wing due to the suction occurring underneath the wing. However, these particular causes are thought to not make much sense, considering the fact that these should be negated by the high pressure being a consequence of the air encountering the wing at the front; or considering that simulations with a very low velocity have been performed and yielded a negative drag as well. Therefore, at the time of writing this the root cause of negative drag in the simulations is unknown.

Apart from that, many aerodynamic simulations have had a lot of variance in the results suggesting that these should be taken with caution. The most accurate aerodynamic simulations were those of the wings in isolation, as these were very consistent and featured little variance. One could say that the variance was significant once higher angles of attack were tested; however, the variance was predictable, as the results varied between iterations in a predictable oscillatory manner, most probably being a result of vortex shedding phenomenon. Some of the other aerodynamic simulations featured less consistency, had unpredictable result pattern between iterations or simply presented surprising results. An example of that was the mentioned second set of wing bracket simulations, where the differences between bracket designs yielded much larger differences than expected. Consequently, the values obtained from aerodynamic simulations apart from the wings in isolation, should be approached with caution and should not be claimed to be the ultimate aerodynamic characteristics of the components. Yet, these were used to extrapolate data as this was the only source to provide educated information about the designed components. It should also be stated that the mesh in some of the simulations was quite coarse as a result of limited computational resources available to work on this project. A more detailed description of the performed aerodynamic simulations can be read in Appendix B. As of the structural designs, these are considered to be more trustworthy, as the complexity of these simulations was much lower, and they did not feature particular signs of concern. One specific remark was stress concentrations at a boundary condition, yet this was fixed promptly and it did not pose issues later on.

It should also be stressed that the components have not been evaluated in terms of fatigue. To start, this is due to the fact that this is difficult to simulate or obtain any other useful data in that regard for complex geometries. It is assumed that the static simulations or calculations done with for a particular component, incorporating a safety factor, ensures that during the usage of the component the likelihood of it failing is rather small. Furthermore, components for a demonstrative or race-car do not tend to be long lasting components, these usually last a few races, and the car itself is not used extensively.

7.2 Design Procedure

The project involved designing numerous components, whose design premise, criteria and evaluation varied. The components were designed in the following order: car body, rear wing, rear wing bracket, front wing and wing actuation. This design order took place based on the premise that the car body should be as streamlined as possible, so the active aerodynamic components are responsible for all downforce and drag manipulation. A streamlined body should create as little disturbances to the other components as possible, therefore making these components dictate the aerodynamic behaviour of the car. This approach assumes that the added components will not have a potent effect on the flow around the car body itself, which may not be necessarily applicable.

One considerable flaw of the body design as it turned out later, was that it produced a significant amount of lift according to the simulations. At the time of finishing the design, it was thought that the produced lift will be easily overcome with the active aerodynamic components; and the fact that the lift was significantly reduced between the two performed iterations of the design, was deemed satisfying. However, the lift generated by the car's body caused the active aerodynamic components to be designed so a compensation for this is taken into account. Which again made them larger, bearing more loads and potentially causing more drag. In turn, making the rest of the design process more complicated. Perhaps, it would of be of benefit to rather design a body that produces less lift in the first place, which could cause the car to potentially generate more drag and airflow disturbances. Nevertheless, the active aerodynamic components could then be designed with less compensation for the generated lift in mind, and their placement could then be optimized with the created airflow disturbances taken into account. It is worth mentioning that the decision to move on from the body design at the second iteration was driven by the time constraints put on the project, as well as the satisfaction by the improvement upon the first car body iteration. The magnitude of the problem became more prevalent at a later stage of the design, which in a scenario where time constraints relative to the scope of the project's content would play a lesser role, would prompt reverting to the stage of body design, so it can be reiterated to then proceed further in the design. Preferably, each stage of the design would be performed in an reiterative manner, and then if the subsequent stage encounters problems with the previous stage, then that stage should be revisited and reiterated. It is presumed that sort of design scheme would be much more promising in terms of yielding an optimized result; however, it would be potentially more time consuming, which could pose a serious thread to the project's time constraint.

Chapter 8
Conclusion

The scope of the project encompassed the design and evaluation of a body with active aerodynamics for a DIS1 racecar, where the foremost focus was the rear wing. The motivation behind this was the incorporation of electro-mechanical system design in the design of aerodynamic components, as well as demonstrating multidisciplinary competences when approaching a complex problem.

To initiate the process of fulfilling the scope of this project, the problem has been introduced along with the car in question and theoretical framework. Thereafter, the car body has been designed based on the premise of being streamlined and undisruptive for the airflow. After two iterations it has been deemed satisfactory, as it yielded a substantial improvement over the first iteration. Afterwards, the wing design has started with determining its sizing based on lateral acceleration the car would have to handle to drive through the Foxhole compression corner at Nurburgring where the largest lateral G-forces are experienced; as fast as the current lap record holder. The wing sizing underwent two iterations, as the simulations for the first wing iteration proved that a NACA4412 airfoil when implemented in this instance, yields different relations between aerodynamic coefficients and angle of attack. Next, the support for the wing was design. The development started with structurally designing and simulating three different wing bracket designs, which then underwent aerodynamic simulations to aid in determining which design would be implemented. The 'Scorpion Tail' bracket type was elected as the ultimate design; this is an inventive design, which exhibited excellent structural and aerodynamic performance. Later, the remaining part of the design was performed, which included the front wing and the actuation mechanism. The actuation mechanism was another innovative solution consisting of a servo motor, flexible shaft and a worm drive. Subsequently, the design underwent a benchmarking process, where the data needed to determine the performance of the car was extrapolated from the data generated in this project, yielding promising results that would indicate the car achieving the goals set by DIS as plausible. Then, a simple control scheme was developed. Lastly, the project has been discussed in terms of obtained design and results. What has been concluded there was that the design process could be less linear and aspects such as the car body design should perhaps be revisited. What is more, simulations and their accuracy have been discussed, with the key stress on investigating the negative drag problem that occurred in some simulations. There it has been figured that it is likely that the negative drag on the rear wing was related to the downward curvature of the rear of the car; however, the root cause has not been identified.

In conclusion, it can be inferred that the objective has been achieved, as the car body and active aerodynamics have been designed, as well as analyzed to the extent that should satisfy the project scope. In doing so, innovations have been made and some results indicated promising outcome regarding achieving the goals that DIS set for the car.

Chapter 9
Reflections

The purpose of this chapter is to reflect upon what design work could be done further in the project to yield significant improvements and maximize learning outcomes, if the project were to be continued.

9.1 Wing Improvements

The wing itself could be improved in a number of ways, as its design was very simple in principle. Its improvements could be done on several different fronts. Firstly, its airfoil type could have been chosen to be different, as due to the vastness of the existing airfoil shapes, only a small fraction of them has been investigated. Secondly, the wing itself could consist of multiple airfoils as it often does in instances such as Formula One vehicles. Moreover, the wing placement and wing shape could be further developed as described in the following subsections.

9.1.1 Wing Placement

The wing placement was chosen arbitrarily to a large extent; its placement was simply assumed to be in a zone behind the car body, where the airflow is minimally disturbed and where the deflection angle is not too steep. Upon reflections after the fact, it has been concluded that a more optimal approach would be to determine a close to optimal wing placement before the wing brackets would be designed. The criteria for the wing placement would be to for the wing to minimize drag in its angle attack of 0 deg, maximize downforce at 15 deg of angle of attack; while being placed within a feasible distance from the car body and the potential bracket placement. This would yield an optimized result in terms of aerodynamics, allowing to exploit a far greater potential from the wing than otherwise. Additionally, it is possible that a cleaner airflow over the wing and less interaction with car body would be less problematic in terms of performing the simulations. Again, a significant flaw of this approach would be its time consumption and the extensiveness of the scope of this project, as well as it could yield a more complicated and comprehensive bracket if the feasible region would not be defined correctly at the start. However, as a future work development that would be worth investigating.

9.1.2 Wing Shape

Since the car shape at the rear varies from the front view, the angle of attack on different wing sections along its span varies, as the airflow is deflected more downwards by the slope of the rear in the middle of the rear of the vehicle, than in the regions away from the middle. In fact, closer to the edges of the wing span, the airflow is likely barely disrupted, thus being nearly parallel to the ground. This angle of attack discrepancy decreases the effectiveness of the wing. For instance, if its angle of attack produces minimal downforce and drag in the middle of the wing, being at 0 deg of angle of attack, at the edges of the wingspan it is likely to have a negative angle of attack, due to the airflow hitting the wing at a different angle than in the middle. Therefore, to combat this discrepancy, the wing should be twisted along its pitch axis; where the twist would occur so the wing has a lower angle of attack in the middle than on its edges. The twist angle should be investigated, which could be done by performing simulations that would determine the angle of attack of 0 deg along the distance from the middle of the rear of the car where the wing is placed. Alternately, the wing could consist of three sections with two different angles of attack, where the middle region of the wing would have a lower angle of attack than the regions on the sides. Again, the size of each region and their corresponding angles of attack would have to be determined.

9.2 Car Body Improvements

Because the car body went only through two iterations, it can be said that plenty could be improved. The primary improvements are discussed in detail in the subsections below.

9.2.1 Overall Shape

The overall car shape of the car could perhaps yield better conditions for downforce generation if a few more things would be kept in mind. Firstly, the front of the car being one of the major drag generating regions of the vehicle, is likely also responsible for generating some lift as well. It could be stipulated that if the front would feature a more prominent upwards slope, it would generate some downforce, without a significant increase in drag, although it would probably require to extend the bodywork length wise to be able to accommodate the slope. Secondly, the rear of the car could be shaped so the airflow deflection is lesser than currently, making the conditions at the rear wing more favourable. Perhaps extending the rear of the car so the wing could be placed further away from the downwards slope of the rear of the car, again yielding better conditions at the rear wing, as well as enabling more flexibility when it comes to rear diffuser design. Lastly, minor geometric fixes mentioned in Chapter 3 should be done, such as the rear wall of the front wheel fenders should be reshaped and other undesired geometric features.

9.2.2 Underfloor

One impactful aerodynamic area of the body is the underfloor, which has not been attempted to be optimized. Mainly the underfloor of the existing body design was meant to be undisruptive and feature some upward slope at the rear to mimic some of the diffuser effects. If investigated further the underfloor make use of ground effects to produce downforce to counteract the lift that the body generates, without substantial drag penalties. A forceful device to be implemented would be a diffuser, which could have a meaningful impact on the overall downforce generation. However, its development is a comprehensive task in itself, likely requiring as much investigation as wing design. Moreover, a diffuser could also be developed so it is an active aerodynamics device. Additionally, skirts could be implemented on the sides of the car to enhance the suction occurring at the car underfloor.

9.2.3 Other components

The air intakes in the design have been designed somewhat arbitrarily. If the car development be continued these should be designed properly, that is making sure that they provide sufficient airflow to the radiators, yet they cause minimal drag and other undesired aerodynamic effects.

The car would likely need to be equipped with mirrors, which have been omitted from the aerodynamic design of the car. The mirrors would likely need to be placed in a manner that would create the least airflow disruptions affecting the rest of the car, as well as to minimize drag associated with their inclusion.

Bibliography

[1] Paul Niedermeyer. Automotive History: An Illustrated History Of Automotive Aerodynamics – Part 1 (1899 – 1939). 26/01-2012. URL: https://www.curbsideclassic.com/automotive-histories/automotive-history-an-illustrated-history-of-automotive-aerodynamics-part-1-1899-1939/.

[2] Paul Niedermeyer. An Illustrated History Of Automotive Aerodynamics: Part 2 (1940 – 1959). 26/01-2012. URL: https://www.curbsideclassic.com/automotive-histories/an-illustrated-history-of-automotive-aerodynamics-part-2-1940-1959/.

[3] Paul Niedermeyer. An Illustrated History Of Automotive Aerodynamics: Part 3 (1960 – Present). 26/01-2012. URL: https://www.curbsideclassic.com/automotive-histories/an-illustrated-history-of-automotive-aerodynamics-part-3-1960-present/.

[4] René Fagnan. The first appearance of wings on Formula 1 cars. 31/01-2018. URL: https://us.motorsport.com/f1/news/1968-first-wings-f1-1000902/1389076/.

[5] Blake Z. Rong. Jim Hall and the Chaparral 2J: The Story of America's Most Extreme Race Car. 23/01-2017. URL: https://www.roadandtrack.com/motorsports/a32350/jim-hall-chaparral-2j-history/.

[6] Mark Hughes, Giorgio Piola. Tech tuesday: The lotus 79, f1's ground effect marvel. *formula1.com*, 15/02-2022. URL: https://www.formula1.com/en/latest/article.tech-tuesday-the-lotus-79-f1s-ground-effect-marvel.sAD9PXt7mC8iMSwwe6CCw.html.

[7] S. McBeath. *Competition Car Aerodynamics 3rd Edition*. Veloce Publishing Ltd, 2017. URL: https://books.google.dk/books?id=RIP4DQAAQBAJ.

[8] Mercedes-Benz. Mercedes-Benz T80 world record car. URL: https://www.mercedes-benz.com/en/art-and-culture/museum/mercedes-benz-t-80/.

[9] WOUTER MELISSEN. Porsche 550 Spyder "Michael May"l. 15/02-2022. URL: https://www.collierautomedia.com/porsche-550-spyder-michael-may.

[10] Vlad Radu. Lancia Thema 8.32: The Forgotten Italian Sleeper With a Ferrari-Sourced V8 Under the Hoodl. 15/02-2022. URL: https://www.autoevolution.com/news/lancia-thema-832-the-forgotten-italian-sleeper-with-a-ferrari-sourced-v8-under-the-hood-197915.html.

[11] evo staff. The original McLaren F1 press release in full - Every detail of the incredible V12 supercar - McLaren F1 design concept. 31/05-2016. URL: https://www.evo.co.uk/mclaren/f1/17794/the-original-mclaren-f1-press-release-in-full-every-detail-of-the-incredible-v12/page/0/6.

[12] Bugatti. BUGATTI Veyron Technology. URL: https://www.bugatti.com/models/veyron-models/technology/.

[13] Janusz Piechna. A review of active aerodynamic systems for road vehicles. *Energies*, 14(23), 2021. URL: `https://www.mdpi.com/1996-1073/14/23/7887`, `doi:10.3390/en14237887`.

[14] Thomas Wolf. Rear-end diffuser arrangement for a motor vehicle, Apr 2017.

[15] Bugatti. Bugatti Dimple Airscoop – a new invention for enhanced aerodynamics, 10/12-2020. URL: `https://www.bugatti.com/media/news/2020/bugatti-dimple-airscoop/`.

[16] Ollie Marriage. Don't Panic! 08-2018. URL: `https://zenvoautomotive.com/wp-content/uploads/2018/02/TG_Uk_Aug18.pdf`.

[17] Zac Bowman. how the lamborghini huracan performante's active aerodynamics system works. 21/04-2017. URL: `https://www.motorauthority.com/news/1110070_how-the-lamborghini-huracn-performantes-active-aerodynamics-system-works`.

[18] Lamoborghi San Francisco. Lamborghini Huracán Performante. URL: `https://www.lamborghinisf.com/lamborghini-huracan-performante.htm`.

[19] EMRAX. *EMRAX 228*. URL: `https://emrax.com/wp-content/uploads/2022/11/EMRAX_228_datasheet_A00.pdf`.

[20] EMRAX. *EMRAX 268*. URL: `https://emrax.com/wp-content/uploads/2022/11/EMRAX_268_datasheet_A00.pdf`.

[21] Michelin. The Tyre; Grip, 2001. URL: `http://docenti.ing.unipi.it/guiggiani-m/Michelin_Tire_Grip.pdf`.

[22] Reid Harrison. Lecture 1: Why is low power circuit design important?, 2001. URL: `https://picture.iczhiku.com/resource/eetop/sHKhfAULkfdHqbcn.pdf`.

[23] Ezhil Vendhan R.Sharavanan. PERFORMANCE ANALYSIS OF HIGH EFFICIENCY PETROL ENGINE. 116, 2017. URL: `https://acadpubl.eu/jsi/2017-116-13-22/articles/14/84.pdf`.

[24] Barrie S. H. Royce. Stability and control. URL: `https://www.princeton.edu/~maelabs/hpt/mechanics/stability.htm`.

[25] ANSYS. Aerodynamics of an FSAE Car. URL: `https://courses.ansys.com/index.php/courses/aerodynamics-of-an-fsae-car/`.

[26] Airfoil Tools. NACA 4412 (naca4412-il). URL: `http://airfoiltools.com/airfoil/details?airfoil=naca4412-il`.

[27] Airfoil Tools. NACA 6412 (naca6412-il). URL: `http://airfoiltools.com/airfoil/details?airfoil=naca6412-il`.

[28] Airfoil Tools. S1223 (s1223-il). URL: `http://airfoiltools.com/airfoil/details?airfoil=s1223-il`.

[29] Mayurkumar Kevadiya and Hemish Vaidya. 2d analysis of naca 4412 airfoil. *International Journal of Innovative Research in Science, Engineering and Technology*, 02:1686 –1691, 05 2013.

[30] Genç, Mustafa Serdar, Koca, Kemal, Açikel, Halil Hakan, Özkan, Gökhan, Kiris, Mehmet Sadik, and Yildiz, Rahime. Flow characteristics over naca4412 airfoil at low reynolds number. *EPJ Web of Conferences*, 114:02029, 2016. doi:10.1051/epjconf/201611402029.

[31] Dr. Van Treuren David Heffley.

[32] Airfoil Tools. NACA 4412 (naca4412-il) Xfoil prediction polar at RE=500,000 Ncrit=9. URL: http://airfoiltools.com/polar/details?polar=xf-naca4412-il-500000.

[33] Overtsteer48.com. Nurburgring Foxhole – the Scariest Corner on the Ring? URL: https://oversteer48.com/nurburgring-foxhole/.

[34] Herman Liesemeijer. Fuchsrohre - The most G-forces at the Nurburgring. URL: https://www.circuitsofthepast.com/fuchsrohre-nurburgring/.

[35] nuerburgring.de. NEW RECORD TIME ON THE NORDSCHLEIFE: MERCEDES-AMG ONE IS FASTEST PRODUCTION VEHICLE. URL: https://nuerburgring.de/news/neue-rekordzeit-auf-der-nordschleife-mercedes-amg-one-ist-schnellstes-serienfahrzeug?locale=en.

[36] Strava. Nürburgring Nordschleife. URL: https://www.strava.com/segments/5539685.

[37] *Road Planning and Design Manual: Guide to road design. Intersections and crossings - general. Supplement*. Number vb. 3. Department of Transport and Main Roads, 2020. URL: https://books.google.dk/books?id=vDkQzgEACAAJ.

[38] Azad Abdulhafedh. Design of superelevation of highway curves: An overview and distribution methods. 1:35–40, 09 2019. doi:10.12691/jcd-1-1-6.

[39] GoodFellow. Carbon Fibre Reinforced Epoxy Sheet 1mm thick. URL: https://www.goodfellow.com/p/c-42-sh-000100/carbon-fibre-reinforced-epoxy-sheet.

[40] LGC Legacy Racing. Voltex Racing Type 10 Swan-Neck 1500mm GT Wing - 2020+ Toyota Supa (A90). URL: https://lgcracing.com/products/voltex-racing-type-10-swan-neck-1500mm-gt-wing-2020-toyota-supa-a90.

[41] Corus Construction Industrial. European structural steel standard EN 10025 : 2004. URL: https://www.tf.uni-kiel.de/matwis/amat/iss/kap_9/articles/en_steel_standards.pdf.

[42] SKF. 16003. URL: https://www.skf.com/uk/products/rolling-bearings/ball-bearings/deep-groove-ball-bearings/productid-16003.

[43] Pablo Fernández. Aerodynamics of rear wing mountings. URL: https://theansweris27.com/aerodynamics-of-rear-wing-mountings/.

[44] Michael J. Fuller. The Rise of the Swan Neck. URL: http://www.mulsannescorner.com/rearwingLMPCFD2009.html.

[45] Richard Smith. CFD Study Comparing Racecar Wing Mounts. URL: https://www.symscape.com/blog/cfd-study-comparing-racecar-wing-mounts.

[46] Lawrence Butcher. Audi launches RS3 LMS TCR . URL: https://www.pmw-magazine.com/news/new-competition-car/audi-launches-rs3-lms-tcr.html.

[47] Alex Misoyannis. 2021 Audi RS3 LMS racer revealed, previews next-gen RS3 road car. URL: https://www.drive.com.au/news/2021-audi-rs3-lms-racer-revealed-previews-next-gen-rs3-road-car/.

[48] Euro Bahn Dynamics. Lamborghini Huracan Evo Swan Neck Wing. URL: https://eurobahndynamics.com/products/lamborghini-huracan-evo-swan-neck-wing.

[49] Wittenstein. Industrial small servo drive system The second generation. URL: https://cyber-motor.wittenstein.de/fileadmin/06-Downloads/WITTENSTEIN-cyber-motor/Kataloge/small-servo-drive-system-gen2-en.pdf.

[50] Fiama. TR flexible shafts. URL: https://www.fiama.it/en/trasmissioni-flessibili-e-supporti/171/tr-trasmissioni-flessibili.html#tab6.

[51] motorracingsports.com. How Fast Does A NASCAR Go? URL: https://motorracingsports.com/how-fast-does-a-nascar-go/.

Appendix A
Full list of the goals for the DIS racecar

DIS has presented ambitious goals for the racecar, which are following:

- 3 seats
- 4-wheel drive
- Low weight
- Low center of gravity
- Low moment of inertia
- Be build on innovative solutions
- HP / Kg bigger than 1:1
- Accelerate 0-100 in less than 2,0 sec
- Accelerate and decelerate 0-200-0 in 10 seconds or less
- Range of 50 km on the racetrack
- Range of 400 km for road use
- Focus on performance rather than comfort
- Be the fastest car ever on the TopGear test track
- Be the fastest car around the Nürburgring – Nordschleife
- Be able to achieve the above mentioned on road legal tires

Appendix B
Notes About Performed Simulations

The aerodynamic simulations are performed based on the 'Aerodynamics of an FSAE car' course by ANSYS. (25) All simulation procedures performed in this project have been based on this because of a close resemblance of the aerodynamic problem to be solved. A car of similar size with aerodynamics features is analyzed with regards to drag, lift and airflow. The car and its features are essentially no slip walls in a moving fluid domain, which is created based on enclosing the body of interest and subtracting it from the domain. All simulations are done only on one of the symmetric sides of the simulated object in question, thus the wall being the plane of symmetry, is a symmetry wall in the simulations. In the front of the domain there is a velocity inlet wall, where the fluid velocity vectors are pointing in a direction perpendicular to the wall. At the rear of the domain a pressure-outlet wall is present, whose backflow direction is normal to boundary and which has a gauge pressure of 0 Pa. The walls above and to the side opposing the symmetry wall; are tunnel walls, which are free slip walls, as they feature a specified wall shear stress of 0 Pa in all of its components. The wall below the object of interest is a ground wall, which in all the simulations is a no slip moving wall. All the simulations were performed using k-ω SST turbulence model with curvature correction.

The first simulations were performed for the car body, its mesh was done in the following manner and the mesh in other simulations was done equally with pointed out differences. The mesh generation occurs in two primary stages; surface and volume mesh generation. The surface mesh featured local sizing options for bodies of influence and the curvatures present on the main bodies in questions, which in this case is the car body. Two bodies of influence were present in encapsulating the main object in question during the surface mesh generation, differing in their size and their target mesh size. The near-field body of influence was about larger enough to encapsulate the whole body of interest and in this case had a mesh target size of 32 mm; meanwhile, the far-field body of influence was enlarged by 500 mm in each dimension in relation to the near-field body of influence, and its rear dimension was extended all the way to the rear end of the fluid domain, and had a mesh target size of 64 mm. The car surface was meshed using a curvature size control type, with its local minimum and maximum sizes being 1 mm and 24 mm respectively. The overall surface mesh size was configured with its minimum and maximum size of 1 mm and 256 mm, as well as three cells per gap. The volume mesh generation utilized last ratio as boundary layer offset method type, with 10 layers, a transition ratio of 0.2 and first height of 5 mm situated around the car body. The volume mesh generation occurred by filling the domain with poly-hexcore, one peel layer, minimum and maximum cell lengths of 4 mm and 512 mm. As the last step of each mesh generation process, the mesh underwent mesh improvement procedures.

To showcase the mesh size differences in the wing simulations with reference to the previous; the near-field body of influence has its mesh target size of 16 mm; the wing curvature minimum and maximum sizes of 0.5 mm and 12 mm respectively; overall surface mesh minimum and maximum sizes of 0.5 mm and 256 mm respectively; boundary layers' first height of 0.5 mm; volume mesh with cell minimum and maximum lengths of 0.5 mm and 512 mm respectively. As of the mesh size differences between the wing bracket assemblies and the previous; the near-field body of influence has its mesh target size of 24 mm; the wing curvature minimum and maximum sizes of 1 mm and 16 mm respectively; the car body curvature minimum and maximum 1 mm and

32 mm respectively; overall surface mesh minimum and maximum sizes of 0.5 mm and 256 mm respectively; boundary layers for the wing bracket assembly first height is 0.5 mm, while for the car body it is 1 mm; volume mesh with cell minimum and maximum lengths of 0.5 mm and 512 mm respectively.

Appendix C
Sketch of the Second Car Body Iteration

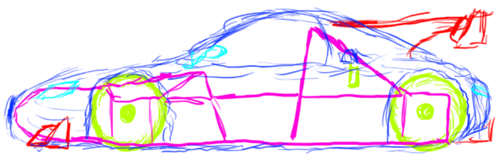

Figure C.1. The right view of the second iteration of the body design sketch. This view showcases the major differences between sketches of the first and second iteration of the car body.

Appendix D
Shaft positioning

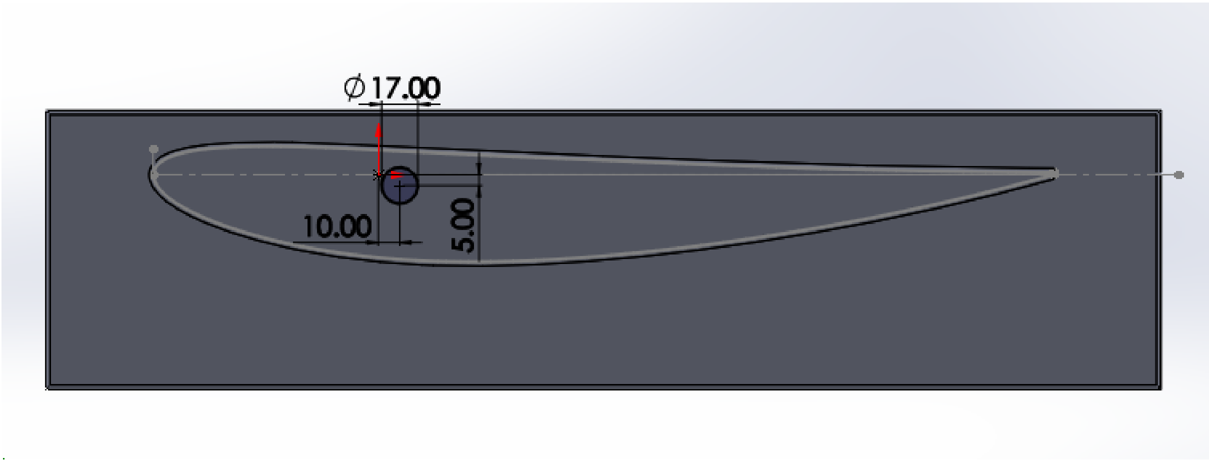

Figure D.1. An image showing how the shaft is positioned within the wing.

Appendix E
Foxhole Driving Line Radius

To approximate the driving line around the corner with the highest lateral acceleration at Nurburgring, satellite data image from Google Maps of Foxhole turn has been put in use, where the curbs have been measured as a reference, which can be seen in Subfigure E.1b. Then visually approximating the curve of a line a vehicle would be suspected to take around the turn using straight lines and a circle sketch geometry tools in Solidworks was drafted, which is depicted in Subfigure E.1a. In the same subfigure, it can be observed that the curbs and the radius of the circular portion of the drafted assumed driving line were measured. Using the measured curb lengths from both of the aforementioned subfigures, a ratio between the lengths from satellite data and the drafted lines in Solidworks was attained. This yielded the radius of the driving line around the turn to be 333 m after rescaling the obtained radius value of the sketched circle of 447.58 mm, by multiplying by the $\frac{70.23\,\text{m}}{94.31\,\text{mm}}$ ratio.

(a) *(b)*

Figure E.1. Images used to illustrate how the driving line radius around the compression region of the 'Foxhole' section around the Nurburgring was obtained. The left image shows the sketched driving line in blue, along with its dimensions. The right image is a picture from Google Maps with the curbs measured.

Appendix F
Foxhole Sag Curve

The turn at the Nurburgring, where the highest lateral acceleration occurs is at the compression portion of the 'Foxhole' section of the track. A cyclist sports data resource (36) has been utilized to obtain the slope angle before and after the turn of interest, yielding approximately 5.7 deg for both; as well as the distance between the slopes of 200 m. In Solidworks, these were used to draw two symmetrical lines of the described slope, with whom a drafted circle coincided tangentially with at a point on each of the lines spaced 200 mm apart in the drawing. This constructed a fully constrained circle of radius equalling 1007 m of sag after rescaling. This draft can be seen in Figure F.1.

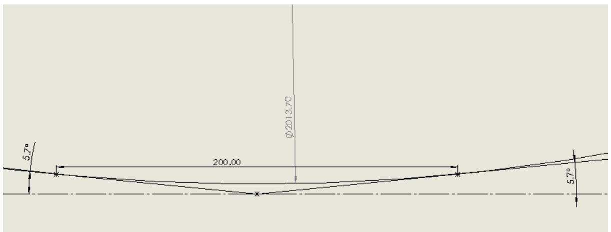

Figure F.1. A Solidworks sketch showing how the sag curve radius was obtained.

However, using the centripetal force due to sag curve contribution of the normal force described by Equation 4.3, after correct derivations would yield more than 0.6 G of vertical force, deeming downforce useless for sufficient grip generation for the required lateral acceleration. Consequently, this radius has been discarded in the process of arriving at a sensible value for the normal force contributions.